DEVELOPMENT AND VALIDATION OF A BOND GRAPH TENDON MODEL OF THE HUMAN FINGER WITH THE ANATOMICALLY CORRECT TESTBED (ACT) HAND

by

Raymond J. King

A dissertation submitted to the faculty of
The University of Utah
in partial fulfillment of the requirements for the degree of

Doctor of Philosophy

Department of Mechanical Engineering

The University of Utah

May 2015

The University of Utah Graduate School

STATEMENT OF DISSERTATION APPROVAL

The dissertation of **Raymond J. King**

has been approved by the following supervisory committee members:

Stephen A. Mascaro	, Chair	**12/15/2014** Date Approved
Sanford G. Meek	, Member	**12/15/2014** Date Approved
Ashish D. Deshpande	, Member	**12/23/2014** Date Approved
K. Kenneth Foreman	, Member	**12/15/2014** Date Approved
Andrew S. Merryweather	, Member	**12/15/2014** Date Approved

and by **Timothy A. Ameel** , Chair/Dean of

the Department/College/School of **Mechanical Engineering**

and by David B. Kieda, Dean of The Graduate School.

ABSTRACT

Modeling the human hand's tendon system can bring better understanding to roboticists trying to create tendon based robotic hands and clinicians trying to identify new surgical solutions to hand tendon injuries. Accurate modeling of the hand's tendon system is complex due to the intricate nature of how tendons route and attach to each other and the skeleton system. These tendon complexities have restricted previous tendon models to single finger models with limited anatomical accuracy and no ability to depict fingertip contact force with external surfaces. This dissertation outlines the use of bond graph modeling to create and improve upon previous tendon models of the single finger. This bond graph tendon model of the single finger is the first model to incorporate many anatomical features, including tendon interconnections and anatomical stiffness, of the tendon system. A graphical user interface is presented to visually explore the relationship between tendon input and finger posture.

The bond graph tendon model is validated using cadaver and *in vivo* experiments, along with the Anatomically Correct Testbed (ACT) Hand, which is a biologically inspired robotic hand that accurately mimics the bone structure, joints, and tendons of the human hand. Comparisons of the bond graph tendon model to *in vivo* data on finger joint coupling and fingertip pinch force, and cadaver data on the tendon system showed strong correlation in trends and magnitudes. A motion experiment, comparing the joint angle results of tendon excursions of the bond graph tendon model and the ACT Hand, and a force experiment, comparing the fingertip force generation of the two systems, were devised to validate the

bond graph tendon model. The results of the motion experiments showed close agreement between the two systems (< 8° joint angle error), while the results of the force experiments showed a larger range correlation between the two systems (8-42% difference).

The result of the validation experiments showed that the bond graph tendon model is able to accurately represent the tendon system of the finger. The model is also the first tendon model to allow for exploration of the effects of fingertip contact on the tendon system.

TABLE OF CONTENTS

CHAPTER 1

INTRODUCTION

The human hand is capable of both grasping objects greater than 100 lb. and manipulating small objects between and around fingertips. This broad range of ability has been an area of interest for both roboticists and clinicians. Over the past decades many roboticists have attempted to recreate the abilities of the human hand by mimicking its structure [1-6]. This movement has led more robotic systems to incorporate bio-inspired tendon based actuation, where actuators are placed in the forearm of the robot and connected to the hand/end-effecter through a tendon system for driving the robot's finger motion. Placing the actuators in the forearm also helps to reduce the size and bulk of robotic fingers. As more robot hands integrate tendon based actuation, roboticists have become more interested in understanding the biomechanics of the human hand's tendon system. Clinicians have also become interested in better understanding the intricacies of the human hand's tendon system for estimating tendon motion and tension during various tasks [7-11]. A better understanding of the human hand's tendon system can help clinicians identify new surgical solutions to hand tendon injuries. Roboticists can improve future robotic devices and clinicians can improve tendon repair surgeries through the use of tendon models that accurately mimic human hand biomechanics.

Modeling any human biomechanical system is a challenging task due to the complexity

of the human body, and the tendon system of the hand is no exception. The intricate relationship between hand motion and tendon excursion is difficult to model due to the many complexities of tendon modeling; a full description of these complexities are discussed in Chapter 2. Due to these complexities there are limited tendon-driven models in the literature, there are only models that produce grasping and motion without respect to the tendon system [12-14]. Currently, only single finger tendon models are available to represent the relationship between finger motion and tendon excursion [15-21]. However, none of these models can accurately explore the effect of finger contact with the environment on tendon tension because they do not include the joint or tendon stiffness of the human finger in their models. Very few tendon models attempt to include many of the complexities of tendon modeling or validate their models with experiments.

Validating tendon models with the human system is also challenging, as validation with either *in vivo* or cadaver experiments have disadvantages. *In vivo* experiments cannot accurately measure internal tendon parameters, and often use imprecise techniques for measuring tendon excursion. Cadaver experiments allow for more accurate measurement of internal tendon stiffness and tendon excursion, but obtaining these parameters can be difficult without prolonged testing, which can lead to specimen degradation. With few publications over the last decade on tendon modeling and validation, new methods for both are required to continue to expand our understanding of the tendon system of the human hand.

This dissertation presents a new tendon model, created using bond graph modeling, to accurately represent the kinematics of the human hand's tendon system. This model includes all achievable tendon modeling complexities and is validated using the Anatomically Correct

Testbed (ACT) Hand. The ACT Hand is a proven tool for studying the human hand, due to its unique mimicking of the hand's anatomical structure, and does not have the disadvantages of *in vivo* or cadaver experimentation [22-24]. This work will present previous tendon modeling research, the development of a new tendon model and two experiments using the ACT Hand for model validation. In addition, a Graphical User Interface (GUI) finger simulation is presented for visualizing the kinematic results of the tendon model.

1.1 Motivation

As robotic and prosthetic hands attempt to approach human-like capabilities, researchers and designers are including tendon driven systems to reduce bulk around the fingers. Since very little has been published on human hand tendon kinematics in over a decade, the development of tendon driven robotic hands has been limited to tendon models made before 2000 [9]. The current tendon models are limited in scope and lack several tendon intricacies that keep them from accurately modeling the human hand's tendon system. Clinicians hoping to use tendon models to develop new surgical techniques are also limited by current tendon models.

This work presents vast improvements over previous tendon models by being the first tendon model to incorporate anatomical stiffness, which allows for the exploration of the effects of fingertip contact on the tendon system. Using this new tendon model, future work could create an anatomically accurate tendon model of the entire hand, which could have great impact in the areas of understanding of human motion, tendon repair surgery, and tendon driven robotic hands, exoskeletons and prosthesis.

1.2 Contributions

The major contributions of this dissertation are:

- A new finger tendon model developed using bond graph modeling.
- A Graphical User Interface (GUI) of the tendon system of the finger for visualizing the tendon model.
- Validation of the bond graph tendon model with cadaver and *in* vivo experiments.
- Validation of the bond graph tendon model with the ACT Hand's index finger during motion experiments.
- Validation of the bond graph tendon model with the ACT Hand's index finger during fingertip force experiments.

1.3 Dissertation Outline

This dissertation is organized into six chapters. This chapter provides the introduction and motivation for this research in human hand tendon modeling and lists the contributions of this work.

Chapter 2 provides the relevant anatomy knowledge and background on tendon kinematics. The anatomy of the hand and the kinematics of the finger's tendon system are outlined. This chapter also provides an overview of the basics of tendon modeling and presents previous tendon models. Lastly, additional features required for creating an anatomically accurate tendon model are presented.

Chapter 3 presents the development of a new tendon model using bond graph modeling. This chapter also introduces a custom finger GUI for visualizing the bond graph tendon

model. Lastly, comparisons are presented between the bond graph tendon model and human tendon experiments.

Chapter 4 presents the experiments used to validate the motion of the bond graph tendon model. First, The Anatomically Correct Testbed (ACT) Hand is introduced and described. Second, a joint friction model is added to the bond graph tendon model to match the friction of the ACT Hand. Finally, an experiment for recording the ACT Hand's index finger motion is developed, and a discussion comparing the experimental results and the bond graph tendon model is presented.

Chapter 5 presents the experiments used to validate the fingertip force of the bond graph tendon model. In this chapter, a fingertip force element is added to the bond graph tendon model, and a new fingertip force experiment involving the ACT Hand index finger is developed. Both the results from the ACT Hand experiment and *in vivo* experiments presented in the literature are compared to the bond graph tendon model.

Chapter 6 contains a summary of the major contributions of this work and suggests future extensions to improve the bond graph tendon model.

CHAPTER 2

FINGER ANATOMY AND KINEMATICS

This chapter is arranged into three sections: basic hand and finger anatomy, background of finger tendon modeling, and the features necessary for making an anatomically accurate tendon model. The anatomy section will present general anatomical terminology of the hand for the bones, muscles, and tendons. The background on tendon modeling will illustrate the progression of finger tendon models and highlight its current stagnant state. The final sections will present several different anatomical features needed for the development of an anatomically accurate tendon model.

2.1 Finger Anatomy

2.1.1 Bones of the Fingers

There are twenty-seven bones in the hand: fourteen phalanx bones (five proximal, four intermediate/middle, and five distal), five metacarpal bones, and eight carpal bones (Figure 2.1) [25]. The phalanges make up the structures of the fingers and thumb. The metacarpals connect the phalanges to the carpal bones of the wrist, and the carpal bones connect the wrist to the radius and ulna arm bones. The metacarpal and carpal bones make up the structure of the palm of the hand.

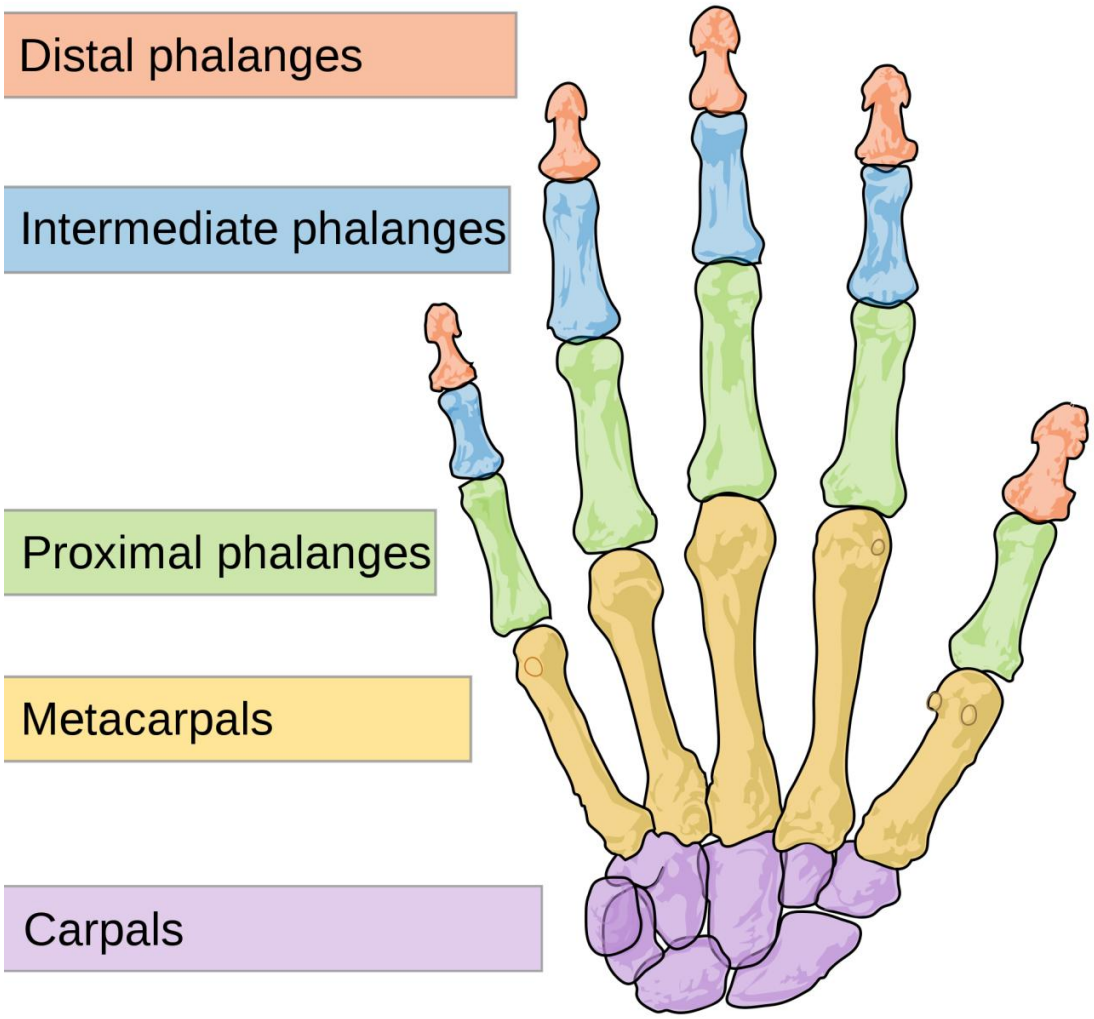

Figure 2.1. Bones of the human hand. Adapted from [26]

2.1.2 Joints of the Hand

The index, middle, ring and little fingers all contain three joints: the metacarpophalangeal joint (MCP), the proximal interphalangeal joint (PIP), and the distal interphalangeal joint (DIP) (Figure 2.2) [27]. The thumb contains only the MCP and PIP joints. The MCP joint joins the metacarpal bone to the proximal phalanx and is commonly referred to as the knuckle. The PIP joint joins the proximal phalanx with the intermediate phalanx and is the first joint past the knuckle. The DIP joint joins the intermediate phalanx with the distal

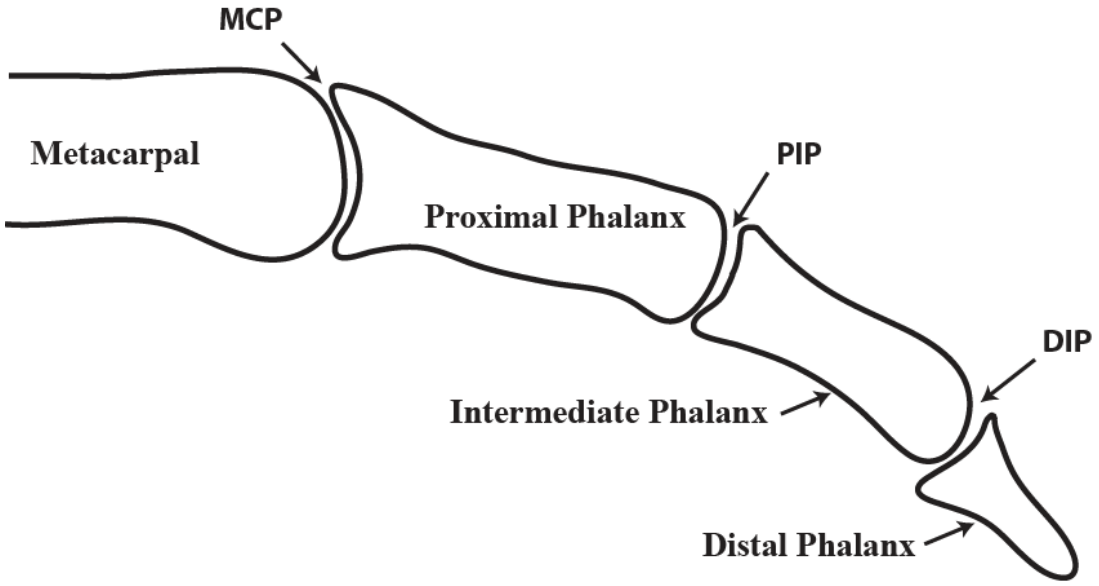

Figure 2.2. Bones and joints of a single finger.

phalanx and is the final joint on the fingers. The MCP joint allows for flexion-extension (flex-ext) and abduction-adduction (ab-ad), while the PIP and DIP joints only allow for flexion-extension.

2.1.3 Muscles and Tendons of the Hand

The muscles that facilitate motion in the hand are separated into two types: intrinsic and extrinsic. Intrinsic muscles are muscles that begin and end in the hand, while extrinsic muscles are muscles that begin in the forearm and end in the fingers. Figure 2.3 shows the posterior and anterior sides of the hand and forearm. The figure highlights the complexity of the extrinsic and intrinsic muscles and tendons that make up the hand [25]. The three central fingers of the hand (index, middle, and ring) have similar tendon and muscle structures while the medial and lateral fingers (thumb and little finger) have different tendon and muscle structures. The muscle and tendon structure of central fingers will be described first and the

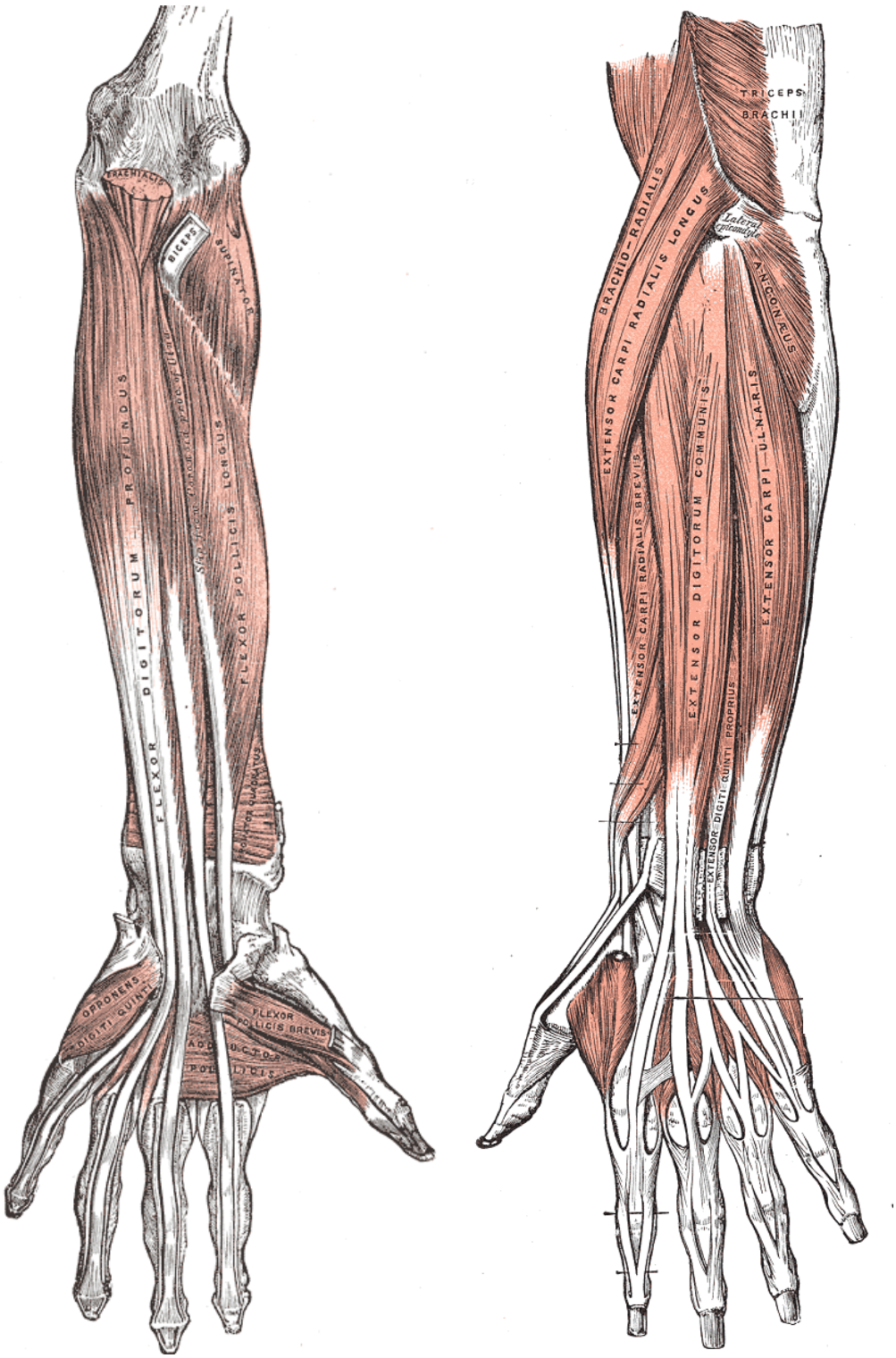

Figure 2.3. Posterior and anterior view of the forearm muscles and tendons. Adapted from [25].

structural disparities of the thumb and little finger will be detailed in a following section. This section only describes the names and connections of the muscles and tendons, the following section discusses the motions caused by the contraction of these muscles.

2.1.3.1 Muscles and Tendons of the Central Fingers

The middle and ring central fingers each have six muscles, three extrinsic and three intrinsic, which are responsible for their individual motion (Figure 2.4). The index finger has seven muscles, four extrinsic and three intrinsic. The extrinsic muscles that reside in the forearm are the flexor digitorum profundus (FDP), the flexor digitorum superficialis (FDS), extensor digitorum (ED), extensor indicis (EI) [27]. These four muscles have tendons that travel over or through the wrist and insert into the fingers. The FDP, FDS and

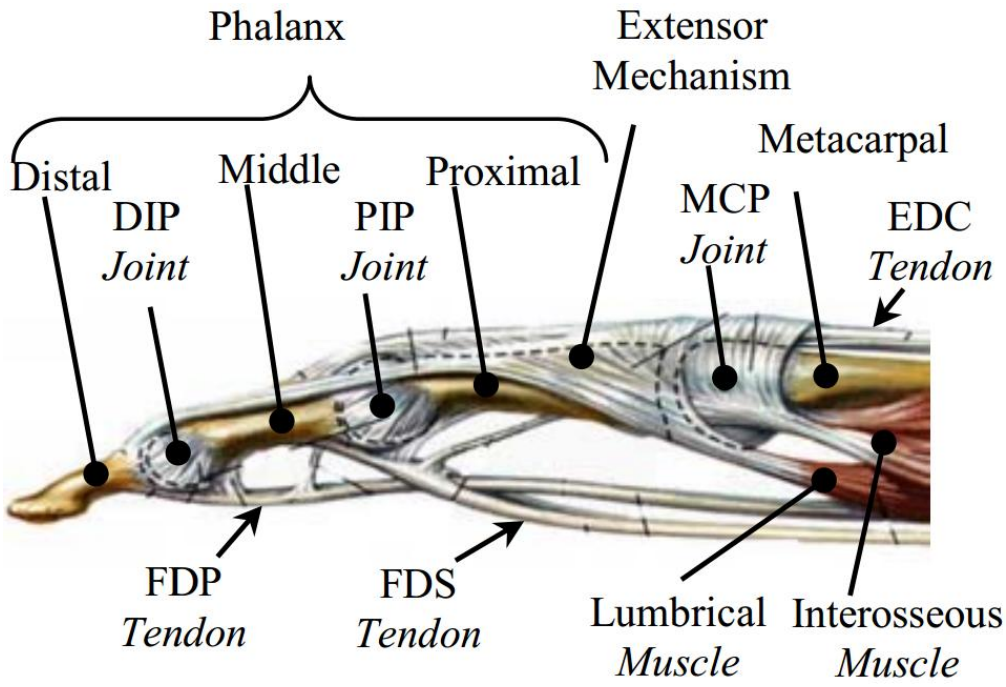

Figure 2.4. The anatomical structure of a central finger, note that this figure shows the dorsal interosseous (DI) muscle but not the palmar interosseous (PI) muscle, which is located on the other side of the finger. Adapted from [27].

ED muscles split into four tendons, with each tendon inserting into one of the four fingers of the hand. The FDP's tendons insert on the anterior side of the distal phalanx. The FDS's tendons insert on the anterior side of the middle phalanx. The ED's tendons both insert on the posterior side of the middle phalanx and the extensor mechanism of each of the four fingers [28]. The extensor mechanism will be explained in greater detail after the intrinsic muscles are introduced. The EI's tendon is only found in the index finger and inserts only on the index finger's posterior side of the middle phalanx and the extensor mechanism.

The intrinsic muscles responsible for the motion of a central finger are, the lumbrical (LUM), the dorsal interossei (DI), and the palmar interossei (PI) [27]. The DI and PI muscles originate from the metacarpal bones of the hand and insert into the extensor mechanism. All the fingers and the thumb have either one or both interossei muscles, and they are anatomically numbered based on their position in the hand (Figure 2.5). The LUM muscle originates from the FDP tendon and inserts into the extensor mechanism. The LUM muscle is one of the only muscles in the body that has an origin on a tendon instead of an origin on a bone [29].

The extensor mechanism (also called the dorsal aponeurosis or extensor hood) is a fusion of tendon material that multiple extensor tendons insert into, each finger has its own extensor mechanism [28]. The extensor mechanism is divided into two sets of bands, the lateral bands and the median band (Figure 2.6). The lateral bands are comprised of the ED, LUM, DI, and PI tendons traveling down the sides of the finger; their insertion point is the anterior side of the distal phalanx. The median band is also a combination of the ED, LUM, DI, and PI tendons and its insertion point is the posterior side of the middle phalanx.

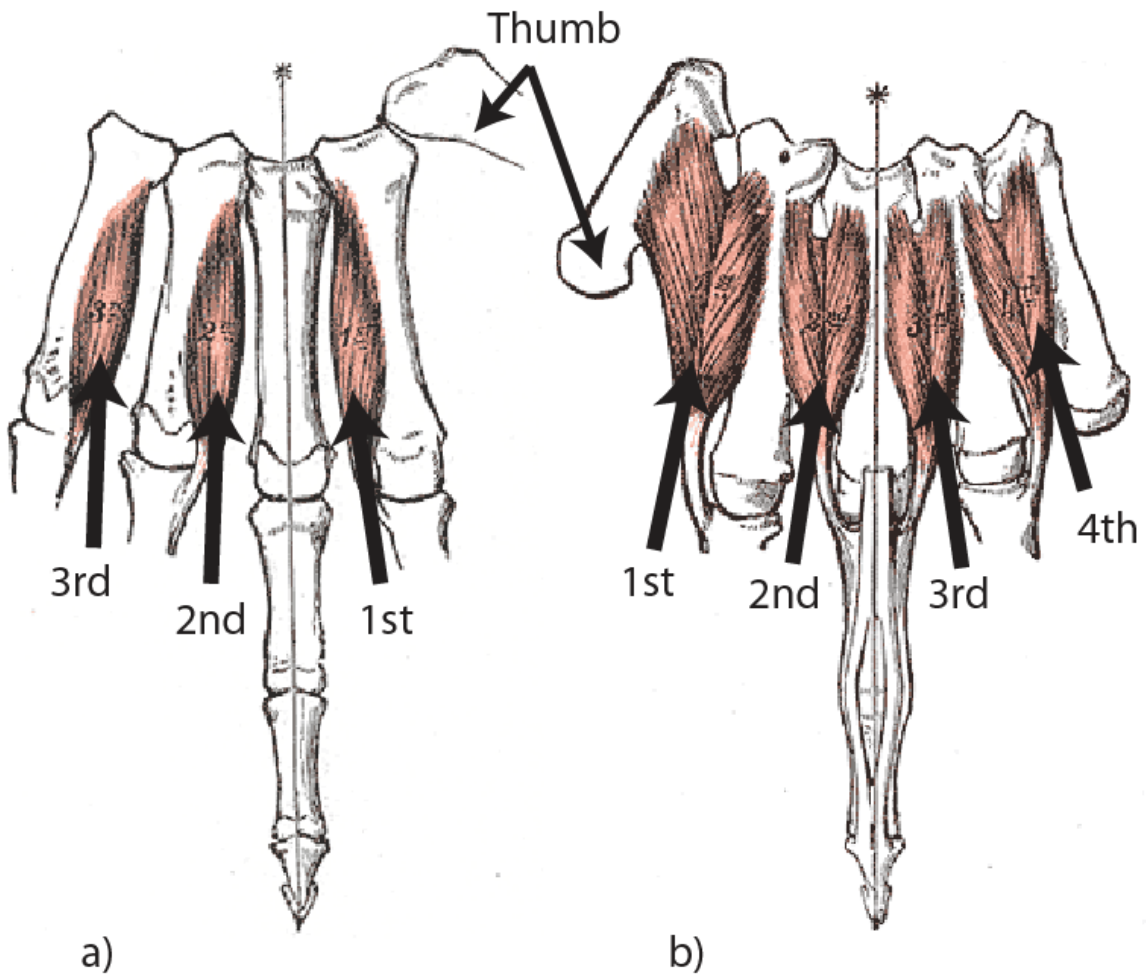

Figure 2.5. The number system for the PI and DI muscles and tendons. *(a)* Palmer interossei. *(b)* Dorsal interossei. Adapted from [25].

2.1.3.2 Muscles and Tendons of the Thumb and Little Finger

In contrast to the structure of the central fingers, the structures of the thumb and little finger are more unique. The thumb has nine muscles responsible for its motion, four extrinsic and five intrinsic [27]. The four extrinsic muscles that are contained in the forearm are the abductor pollicis longus (APL), extensor pollicis brevis (EPB), extensor pollicis longus (EPL) and the flexor pollicis longus (FPL). The APL's tendon inserts on the radial side of the thumb's metacarpal bone. The EPB's tendon inserts on the posterior side of the proximal

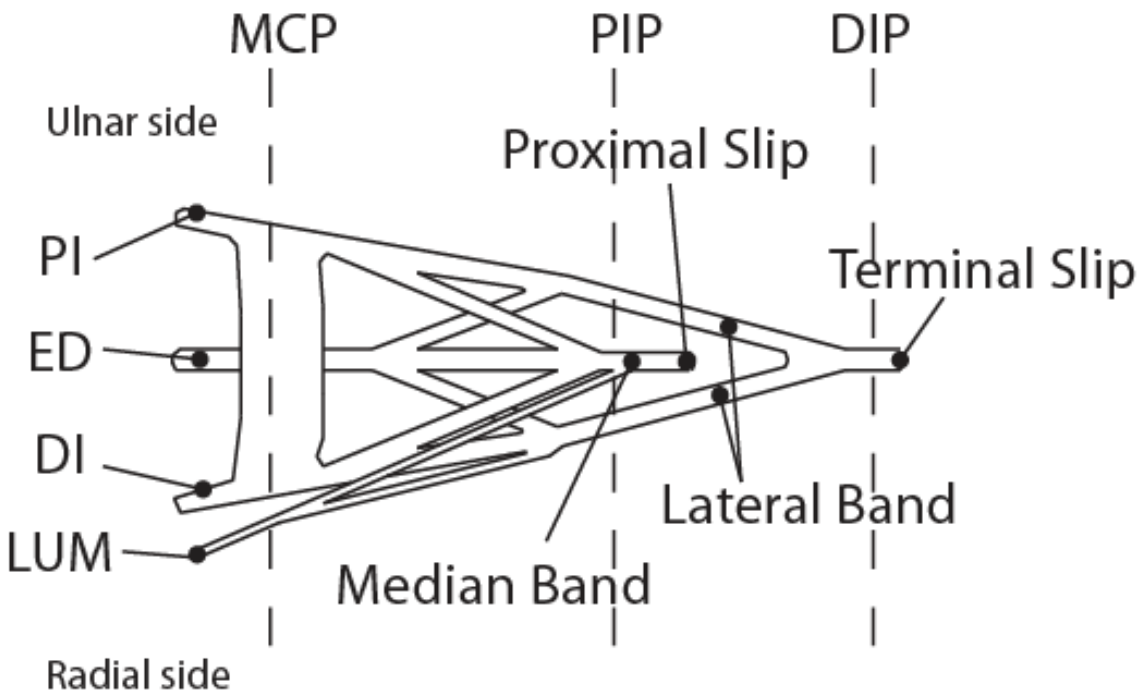

Figure 2.6. A simplification of the connections of the extensor mechanism, referred to as Winslow's Rhombus. Adapted from [30].

phalanx. The EPL's tendon inserts on the posterior side of the distal phalanx. The FPL's tendon inserts on the anterior side of the distal phalanx. The thumb's intrinsic muscles are the abductor pollicis brevis (APB), the adductor pollicis (AP), the first dorsal interosseous (DI), the flexor pollicis brevis (FPB), and the opponens pollicis (OP). The APB originates from the carpal bones of the wrist and inserts on the radial side of the proximal phalanx. The AP originates from both the metacarpal of the middle finger and carpal bones and inserts on the ulnar side of the thumb's metacarpal joint. The first dorsal interosseous originates from both the metacarpal of the thumb and index finger and inserts on the extensor mechanism of the index finger. The FPB originates from three carpal bones and inserts on the radial side of the thumb's metacarpal joint. The OP originates from the carpal bones and inserts into the radial side of the thumb's metacarpal bone. In addition to having a very different tendon

structure, the thumb also has a saddle joint at the proximal end of its metacarpal bone [31]. This allows the metacarpal bone of the thumb to have a much higher level of mobility than the other fingers.

The little finger has eight muscles responsible for its motion, four extrinsic and four intrinsic [27]. The little finger is similar to the central fingers and has the FDP, FDS, and ED extrinsic muscles, however, it has an additional extrinsic called the extensor digiti minimi (EDM). The FDP, FDS, and ED's tendon insertions are the same as the central fingers. The EDM's tendon inserts on the posterior side of the little finger's middle phalanx and extensor mechanism. The little finger's intrinsic muscles are the PI, the opponens digiti minimi (ODM), the abductor digiti minimi (ADM), and the flexor digiti minimi brevis (FDMB). The PI muscle's origins and inserts are the same as for the other central fingers. The ODM muscle originates from the carpal bones and inserts on the ulnar side of the little finger's metacarpal bone. The ADM muscle originates from the carpal bones and inserts into the extensor mechanism of the little finger. The FDMB muscle originates from the carpal bones and inserts into the ulnar side of the little finger's proximal phalanx.

2.2 Central Finger Kinematics

The muscles and tendons responsible for the motion of the fingers and thumb have been presented above. The first part of this section will specify how the tendons are routed around the finger joints and the anatomical motion caused when the attached muscles are activated. Since modeling the entire intricate tendon system of the hand is an extensive undertaking, the scope of this dissertation is limited to modeling the tendon system of a single central finger. The second part of this section will present early tendon models and their

identification of several modeling complexities associated with tendon systems. The last section will illustrate the progression of finger tendon models and highlight its current stagnant state.

2.2.1 Central Finger Anatomical Tendon Routing

The anatomical routing of a central finger can be seen in Figure 2.7. The FDP tendon routes anterior to the MCP, PIP and DIP joints, and during FDP muscle contraction all three joints are flexed. The FDS tendon routes anterior to the MCP and PIP joints, contracting the FDS muscle causes flexion of only these two joints. The ED tendon routes posterior to the MCP joint before combining with the extensor mechanism, the extensor mechanism then continues to route posterior to the PIP and DIP joints. Contraction of the ED muscle results in extension of all three joints of the finger. The LUM tendon routes anterior and radial to the MCP joint before connecting to the extensor mechanism. Contracting the LUM muscle

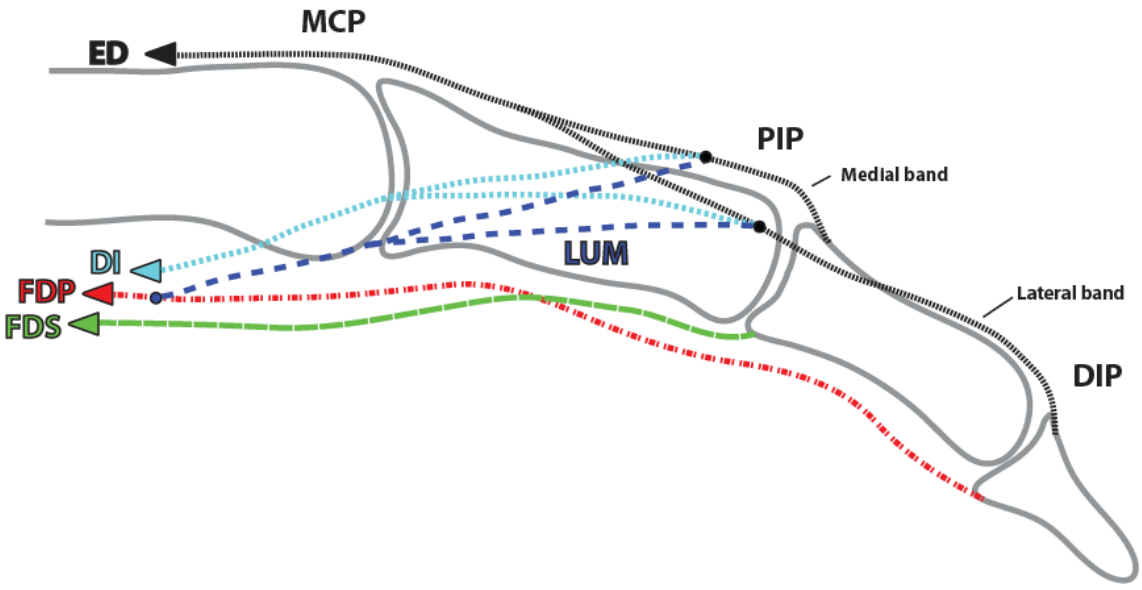

Figure 2.7. A side view of the tendons of the middle finger. The second interossei tendon is not visible from this side.

causes flexion and adduction of the MCP, and extension of the PIP and DIP joints. The DI and PI tendons always route anterior to the MCP joint, however, depending on the number designation of the PI or DI they can route either radial or ulnar to the MCP joint before connecting to the extensor mechanism. In general, contraction of a DI muscle causes finger abduction, while contraction of a PI muscle causes adduction. All DI and PI tendons cause flexion at the MCP and extension at the PIP and DIP joints.

There are a few important kinematic characteristics caused by tendon routing in the finger: (ab-ad) motion caused by the FDP, FDS and ED, kinematic coupling of the PIP and DIP, independent control of MCP (flex-ext), and the unique origin the LUM tendon. The FDP, FDS, and ED tendons primarily contribute to flexion and extension, however, they also cause adduction and abduction around the MCP joint. Their contribution is small compared to the LUM, DI, and PI tendons and is dependent on finger posture, as they can contribute to MCP abduction in one finger posture or MCP adduction in another [23]. Another kinematic characteristic of the presented tendon routing is the coupling between the PIP and DIP joints. There is no combination of tendons that will allow independent function of the PIP and DIP joints, either both joints flex together or extend together [8]. In contrast to the coupled motion of the PIP and DIP joints, the MCP joint can be controlled independently. Since the LUM, DI, and PI are routed to cause flexion on the MCP and extension on the PIP and DIP joints, the MCP can move independent of the position of the other joints [31]. The final kinematic characteristic is the origin of the LUM tendon. As mentioned in the anatomy section, the LUM originates from the FDP tendon. Since this proximal attachment of this small muscle is so unique, the complete function of the LUM is unknown and still debated [29, 32, 33].

2.2.2 Early Modeling of Central Finger Kinematics

Finger kinematics were first investigated by Landsmeer in 1949 [28]. Landsmeer produced several papers investigating different areas and parts of the hand and forearm and hypothesized their possible function [28, 34, 35]. Landsmeer never created any kinematic models of the fingers but he did produce three models for estimating tendon excursion in relation to changes in joint angle. These three models are referred to as Model I, Model II and Model III, each for estimating the tendon excursion relationship in different situations (Figure 2.8) [35]. Landsmeer's models are still used in tendon models, including the one in this dissertation.

Landsmeer's Model I is used for estimating tendon excursion when a tendon is wrapped around the outside of a finger joint (e.g., the ED tendon over the MCP joint as the MCP joint flexes). Model II and Model III are both used to estimate tendon excursions when a tendon routes under an articulating joint (commonly called "bowstringing") during motion, usually

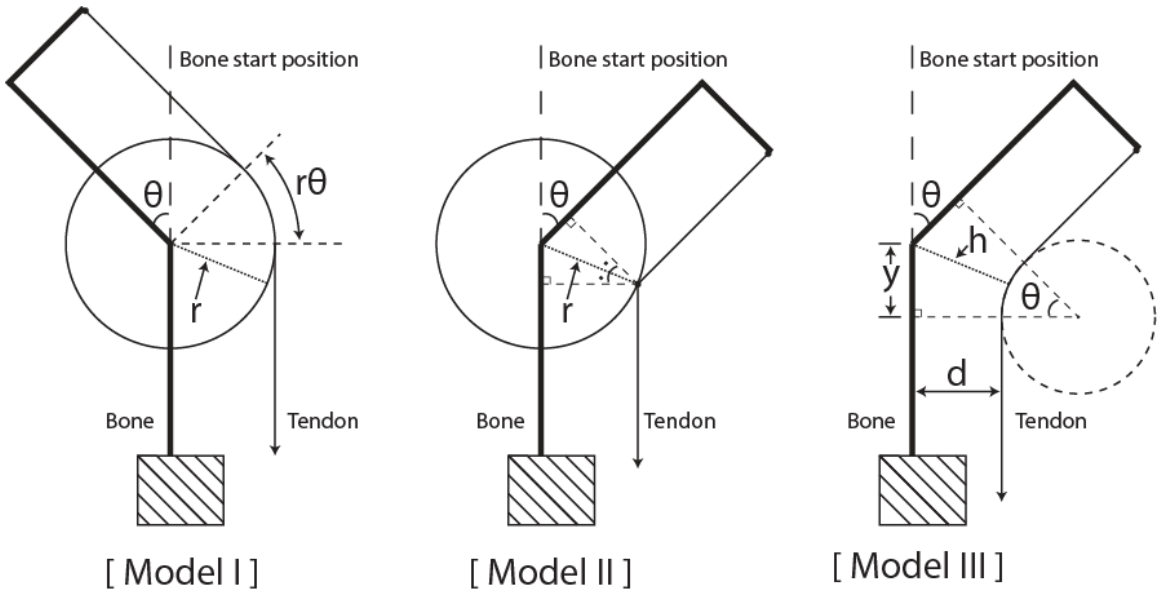

Figure 2.8. Landsmeer's models for estimating tendon excursion. Adapted from [35].

during flexion (e.g., FDP tendon at the PIP joint as it flexes). The difference between Model II and Model III is complexity. Model II is a simpler model that allows the tendon to bend at a single point, while Model III does not allow the tendon to bend at a point but instead keeps the tendon curved during bowstringing. All three of Landsmeer's models require finger joint anthropomorphic data to calculate the relationship between tendon excursion and joint angle change. Models I and II only require the distance from the center of rotation of the joint to the tendon of interest; this distance is commonly referred to as the moment arm of the tendon [36]. Model III does not require knowledge of the tendon moment arm, but instead requires different anthropomorphic data including bone thickness, the distance from the bowstringing tendon to the apex of the joint, and the distance from the joint apex to where the tendon touches the bone. Model III is very rarely used in tendon models since it requires much more anatomical data than Models I and II. Models I and II are common in kinematic models since many researchers have previously investigated the tendon moment arms for all the tendons around all the joints of the fingers [23, 37, 38].

Using early tendon moment arm data, along with other anthropomorphic data, the first few kinematic models were developed [17, 39]. The earliest model described the rotation matrices necessary to estimate finger position with known joint angles [39]. These models did not attempt to relate tendon excursions to joint angles but they are considered the earliest kinematic finger models. A model created by Leijnse et al. was the first kinematic model to address the relationship between tendon excursions and joint angles [17]. Using Landsmeer's Model I and a central finger, Leijnse et al. explored the transformation between the tendon "excursion domain" and the "movement domain" of the finger (Figure 2.9). The transformation between the two domains is limited by both constraints on allowable tendon

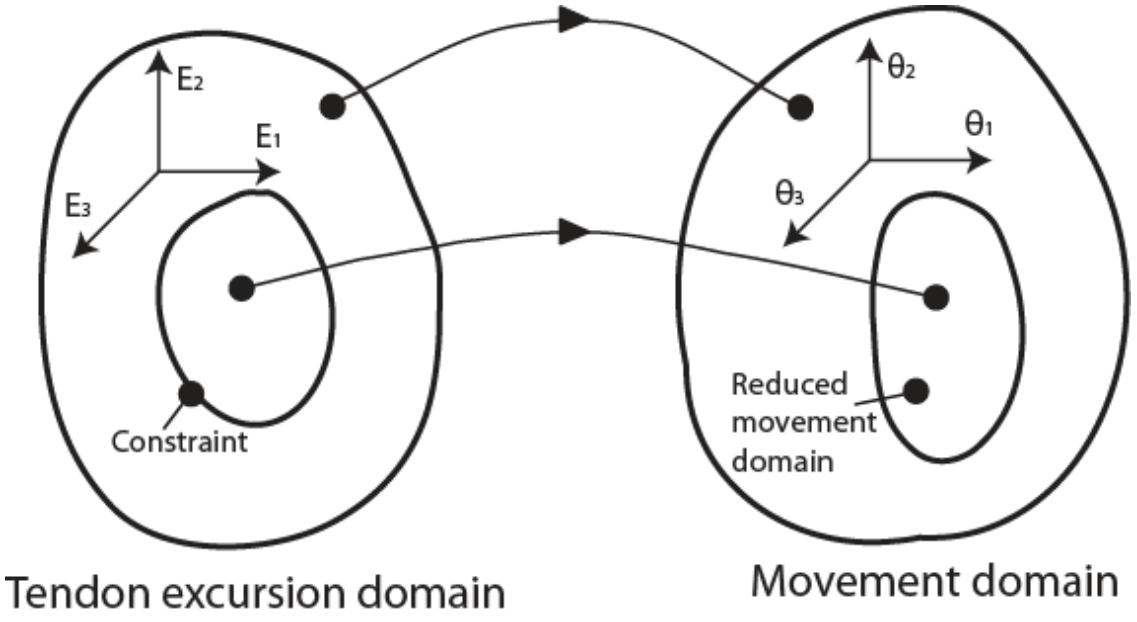

Figure 2.9. This illustrates how constraints in the tendon excursion domain result in reduced movement in the movement domain. Adapted from [17].

excursions and anatomically possible finger movements and positions. Leijnse et al. attempted to relate these domains with their 2D (flexion-extension only) model of a single finger. This model includes the FDP, FDS, ED and DI tendons (Figure 2.10).

The work of Leijnse et al. presented the first 2D displacement model of the free-moving unloaded finger:

$$d\varepsilon_P = r_{P1}d\theta_1 + r_{P2}d\theta_2 + r_{P3}d\theta_3 - d\sigma_P \quad (2.1)$$

$$d\varepsilon_s = r_{s1}d\theta_1 + r_{s2}d\theta_2 - d\sigma_s \quad (2.2)$$

$$d\varepsilon_E = -r_{E1}d\theta_1 - r_{M2}d\theta_2 \quad (2.3)$$

$$d\varepsilon_I = r_{I1}d\theta_1 - r_{M2}d\theta_2 \quad (2.4)$$

$$d\theta_3 = \frac{r_{M2}-r_{L2}}{r_{L3}}d\theta_2 - \frac{d\sigma_L}{r_{L3}} \quad (2.5)$$

$$\sigma_P * \sigma_S = 0 \quad (2.6)$$

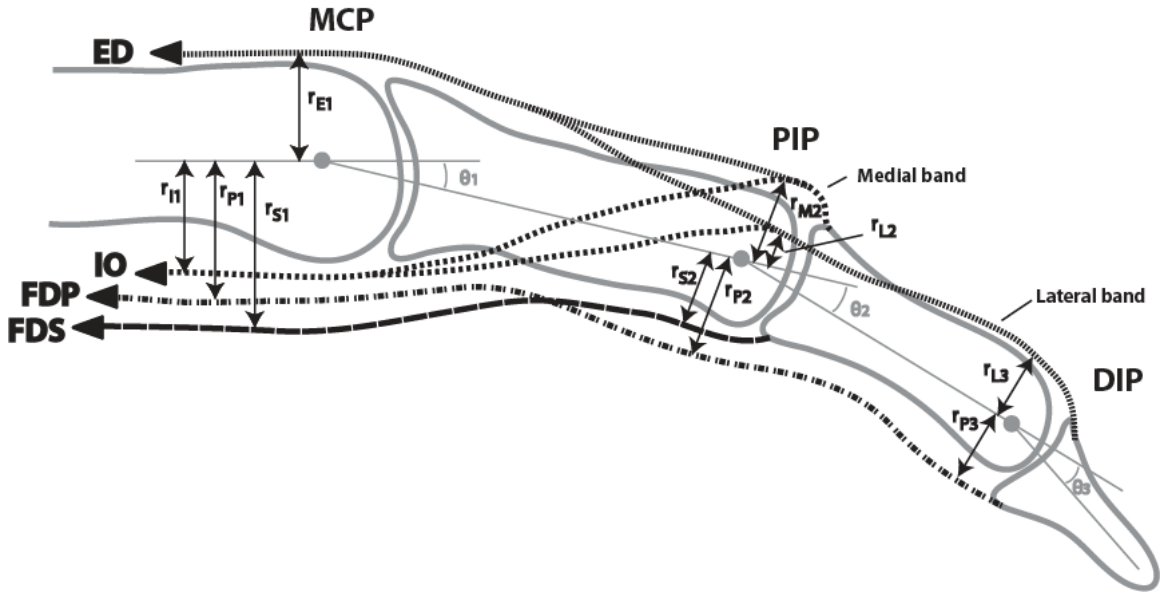

Figure 2.10. Tendon model of Leijnse et al. Adapted from [17]

where $d\varepsilon_i$ is the infinitesimal displacement of the tendon i, $d\theta_j$ is the infinitesimal change of joint j, $d\sigma_i$ is the infinitesimal accumulation of slack in tendon i, r_{ij} is the moment arm of the tendon i around joint j. *P* is for the FDP tendon, *S* is for the FDS tendon, E is for the ED tendon, *I* is for the PI tendon, *M* is for the medial band, *L* is for the lateral band, joint 1 is the MCP, joint 2 is the PIP and joint 3 is the DIP. Equations (1-4) show the change in tendon displacement as a function of joint angles, using Landmeer's Model I. Equation (5) is the coupling relationship between the PIP and DIP joints. Equation (6) is a mathematical constraint to impose the condition that one of the two flexion tendons (FDP or FDS) has to be under tension at all times. The Leijnse et al. 2D model only needs one interossei tendon (labeled IO), since a second interossei or LUM tendon is redundant with (ab-ad) motion. Leijnse et al. continued work on this 2D model and included the missing LUM tendon in later work [19]. The Leijnse et al. model, along with other early tendon models, indentified specific complexities associated with modeling the tendon system of the fingers and hand.

2.2.2.1 Tendon Modeling Complexities

The tendon complexities identified in the tendon modeling literature include the redundancy of tendons (multiple tendons actuating the same joint), tendons slacking (similar to the way a rope slackens), tendon interconnectivity, and changing tendon moment arms during joint motion [17-19, 33, 40, 41].

Early tendon models discussed the necessity of redundant tendons and considered the redundancy as a possible protective measure to ensure hand function in the event of injury [17, 28]. Researchers later identified that the apparent tendon redundancy does not imply robustness, and that very few tendons or muscles can be damaged without causing major motion limitations [42]. This redundancy of tendons complicates finger tendon models because there are more controllable inputs than the degrees of freedom of the system.

The concept of tendons slacking was introduced by Leijnse et al.; this slacking occurs when a tendon is no longer under tension [17]. An example of this is when the FDP tendon is pulled toward the foreman, due to muscle contraction of the FDP muscle, while the FDS muscle is not contracted. In this case, since the FDP tendon causes flexion on the same finger joints that the FDS tendon does, the FDS tendon would lose its tension and become slack. When a tendon becomes slack in the tendon system it does not contribute to the kinematics of the fingers and hand; this can become even more complicated as a tendon goes in and out of being slack during motion. Leijnse et al. specified situations where this complexity can occur based on finger posture and tendon configurations, but did not suggest their findings were comprehensive [17].

The extensor mechanism is a complex web of tendon interconnections, but there are also interconnectionss between the other tendons of the hand. This tendon interconnectivity

causes unique coupling kinematics between the connected tendons [18]. Additionally, not every hand has the same interconnections, though certain interconnections are common across all hands, such as the extensor mechanism's interconnections [25]. These tendon interconnections cause a single tendon to influence other tendons in the hand, which adds considerable complexity to a tendon model [10].

The tendons of the fingers are wrapped very closely to the MCP, PIP and DIP joints. However, during any motion of the finger, the tendons shift their position based on the angle of the joints [38]. This shift in tendon position around the joints changes the moment arm for each tendon. Previous research in this area has shown that this change in moment arm has a significant effect on the kinematics of the finger [23, 43].

2.2.2.2 Current Tendon Models

There are various models of the fingers and hand in the literature; however, many of these models are more interested in the general movement of the hand without regard to the underlying tendon system [20, 44-48]. Of the few models that are created with regard to the tendon system, almost all model a single central finger and have limited model validation [15-17, 19]. There is one tendon model of the thumb in the literature [49]. This section will describe tendon modeling improvements over the Leijnse et al. tendon model described above.

The Leijnse et al. model was improved by himself and other researchers over many years. The model developed from a 2D model with four tendons to a 2D model with five tendons. Leijnse et al. also attempted to include the tendon modeling complexities, presented in the previous section, with limited or varying success [17, 18, 33, 40, 41]. The next step in

kinematic tendon modeling was the addition of adduction and abduction. Brook et al. created a 3D model with six tendons, however, they did not include the tendon modeling complexities of tendons slacking, changing tendon moment arms or tendon interconnectivity [16]. Despite not including these complexities the Brook et al. model showed a fair correlation to electromyography based finger experiments. The most current tendon model is from Biggs et al.; they created a 3D model with six tendons and the tendon modeling complexities of redundant tendons and tendon slacking [15]. This model is one of the more complex 3D single finger tendon models currently in the literature; however, it is limited to finger motion only and does not attempt to include any tendon and joint stiffness parameters for estimating the effects of fingertip contact on the tendon system. Finger models after Biggs et al. shifted from analytical solutions of tendon kinematics to optimization programs designed to solve tendon kinematics by minimizing tendon parameters [50-52]. Literature reviews of single finger tendon modeling suggest that this area of research has stalled over the past decade, as the new optimization based models do not differ much from models developed before 2000 [9].

2.3 Modeling for Anatomical Accuracy

This dissertation defines modeling for anatomical accuracy as modeling all the anatomical features that contribute to the motion of the human body. The anatomical factors for a tendon model of the finger include the tendon modeling complexities presented above, along with several others. This section will present the additional anatomical factors needed for anatomical accuracy.

The factors that this dissertation identifies for anatomical accuracy in tendon modeling

are: including all finger tendons, tendons slacking, tendon interconnectivity, changing tendon moment arms during joint motion, accurate center of rotation of the finger joints, maximum Range of Motion (ROM) of the finger joints, stiffness of the finger joint's connective tissue, and stiffness of tendon tissue. The first four factors have been presented previously while the last four are presented here.

2.3.1 Accurate Center of Rotation of the Finger Joints

The center of rotation of the joints is the point around which the attached bones of a joint articulate. Previous researchers have shown that the center of rotation of a finger joint moves depending on joint angle [53]. However, this motion of the center of rotation is very small and it is common in tendon modeling to assume no motion of the center of rotation. Most researchers agree that using a hinge joint for the PIP and DIP is very close to being anatomically accurate [53]. The MCP joint can also be accurately modeled using two intersecting hinge joints for flex-ext and ab-ad [53, 54]. This anatomical feature is simple to implement into a model since most joint analysis techniques make a hinge joint assumption.

2.3.2 Maximum Range of Motion (ROM)

The maximum range of motion of a finger joint is an important anatomical factor, as it sets the maximum flex-ext and ab-ad of the joints. Previous models have not attempted to implement the maximum ROM of the finger's joints. Allowing a tendon model to find joint angle solutions outside the limits of the ROM of finger motion greatly reduces its anatomical accuracy.

2.3.3 Joint Connective Tissue Stiffness

The stiffness of the finger joint's connective tissues, all the ligaments and structures not responsible for kinematics, are an important factor in understanding how a finger will move during tendon excursion [55, 56]. There is limited work in the area of joint stiffness but changes in stiffness can have large effects on finger kinematics [55]. The connective tissue at the joints has also been shown to have nonlinear stiffness, which is dependent on the angle of the joint [56].

2.3.4 Tendon stiffness

The stiffness in the tissue of the tendon has similar importance to the tissue stiffness of the joints, as its value can affect kinematics [57, 58]. In addition to being an essential anatomical feature to include in modeling, adding stiffness into a tendon model allows for insight on estimating tension in anatomical structures during different activation configurations and motions. Tendon stiffness has been shown to be a function of tension in various tendons in the body, including the hand [15, 16, 19, 57-60].

2.4 Finger Kinematics Conclusions

Including the presented anatomical factors in a model will help to push tendon modeling towards the goal of accurately representing the human system. There are additional factors that can affect anatomical accuracy; however, the ones presented here are the most noteworthy.

Based on the review of previous tendon models, there are significant gaps between an anatomically accurate tendon model of the finger and the tendon models found in the

literature. The Leijnse et al. models never include all the tendons of the finger, nor address most of the features for anatomical accuracy. Both Brooks et al. and Biggs et al. began to address some tendon modeling complexities but never considered any of these additional features for anatomical accuracy. The most current finger models, employing optimization techniques, use best guess anatomical assumptions for how to optimize the parameters of the tendons and muscles, and all these models ignore several features for anatomical accuracy. No previous tendon models have successfully included the following features: tendon interconnectivity, changing tendon moment arms, limits on maximum finger joint angles, stiffness of joint connective tissue, or stiffness of the tendons. The following chapters will attempt to fill this gap in the tendon modeling literature by implementing the presented tendon modeling complexities and anatomical features into a new tendon model of the finger. This model also will be the first tendon model to allow for exploration of the effects of fingertip contact on the tendon system.

CHAPTER 3

A NEW TENDON MODEL FROM BOND GRAPH MODELING

This chapter is arranged into three sections. The first section will describe bond graph modeling and how its principles were applied in modeling the tendon system of the finger. The next section presents a custom GUI for visualizing the results of the tendon model. The last section presents comparisons between the new tendon model and the results from human tendon experiments from the literature.

3.1 Development of the Bond Graph Tendon Model

Bond graphs are a powerful graphical description of energy transfer through a system and are often used in modeling complex systems [61, 62]. Bond graphs represent the physical dynamics of a system and can seamlessly incorporate multiple energy domains (e.g., the domains of mechanical translation and mechanical rotation are incorporated into the tendon model.) Bond graph modeling has an advantage over previous tendon models because it uses junctions to model connections between elements in the system; this makes modeling the complexity of tendon interconnections more natural. Previous researchers have used bond graphs to model sections of tendons in a single finger [21]. The bond graph presented here includes all the anatomical features, as discussed in Chapter 2, of the index finger of the hand.

3.1.1 Anatomical Features of the Bond Graph Tendon Model

3.1.1.1 Finger Bones

The four bones that make up the structure of the index finger bond graph tendon model are the metacarpal, proximal phalanx, middle phalanx, and distal phalanx. The bones' length values used in the bond graph tendon model are from [3]. In addition to length, the shape of the bones is also an important factor in finger tendon modeling [36, 38]. The moment arm around each joint is dependent on the shape of the bone, and as the angles between the bones change, the moment arms can vary. The nonlinearity of changing moment arms is often ignored in previous tendon models [15, 16, 18, 19]. For the bond graph tendon model, the variable moment arm values from [23] are used, where each moment arm is a function of the joint angles of the finger. The bones do not explicitly show up in the bond graph, as their inertia is lumped into the rotational inertia around the joints. The bone lengths and the moment arm changes caused by the shape of the bones are used when solving the tendon model.

3.1.1.2 Finger Joints

The three joints of the index finger are the MCP, the PIP, and the DIP joint. The index finger has 4 degrees of freedom (DOF), ab-ad at the MCP joint and flex-ext at all joints. In the human hand, each joint is contained within a low friction joint capsule formed by fine ligaments that determine its DOF and ROM [63]. The joint capsules have very low friction, due to synovial fluid, and the stiffness of the MCP(flex-ext) DOF can range from 0 – 500 *Nmm/rad*, depending on joint angle [56]. The nonlinearity of variable joint stiffness is ignored in previous tendon models since the data on the MCP (ab-ad), PIP (flex-ext) and DIP

(flex-ext) are limited. Without variable joint stiffness values for the full ROM of the joints, the bond graph tendon model assumes constant stiffness values over the full ROM for all the joints, with values from [64]. The bond graph tendon model also assumes the MCP (flex-ext) and MCP (ab-ad) joint stiffness is the same, as they have been shown to be similar under equivalent loading conditions [65]. The joints are implemented into the bond graph tendon model with rotational springs to represent joint stiffness, rotational inertias that combine the inertia of the joints and the bones, and rotational linear viscous dampers to represent the friction in the joint capsules.

3.1.1.3 Finger Tendons and Muscles

There are seven muscles in the index finger. However, the EI muscle is combined with the ED in the bond graph tendon model; these tendons have similar routing and have been shown to be equivalent during single finger analysis [23]. The six tendons and muscles presented for the index finger are the FDP, the FDS, the ED, the LUM, the first DI, and the first PI.

Previous tendon models assume the tendons of the finger to be inextensible, i.e., infinite tendon stiffness, and unchanging [15, 16, 19]. Since the data for variable finger tendon stiffness are unrecorded, the bond graph tendon model implements an average tendon stiffness value of k = 100 *N/mm* for the input tendons (FDP, FDS, ED, LUM, DI, PI) over the whole ROM [58]. Tendon stiffness is implemented in the bond graph tendon model as a translational linear spring. Models to represent the muscles of the finger are not implemented into the bond graph tendon model; instead, tendon tensions or tendon excursions are used as direct input to the tendon model. In the bond graph, an effort source (input) prescribes the

desired tendon tension, while a flow source (input) prescribes the rate of tendon excursion.

3.1.2 Tendon Implementation into the Bond Graph Tendon Model

3.1.2.1 Flexor Tendons

The flexor tendons are one of the least complex structures of the bond graph tendon model. All the energy generated by the contracting flexor muscles is transferred through the flexor tendons to flex the joints of the finger; the FDP causes flexion on all joints while the FDS causes flexion on only the MCP and PIP joints. The energy transfer of the FDP is illustrated in Figure 3.1, where the energy from the translation domain flow source of the FDP tendon is transferred to the rotation domain elements of the finger joints. When using a flow source, tendon excursion, as input to the bond graph tendon model, a small amount of energy is stored, elongating the tendon (Figure 3.1); this is not the case when an effort source, tendon tension, is used. Due to the high stiffness of the tendons versus the low stiffness of the joints, very little energy is stored in the tendon as a majority is transferred to the rotational components of the bond graph.

The amount of energy transferred from the flexor tendons to the joints is governed by the rotational stiffness, inertia and friction parameters at each joint. The joint parameters vary depending on joint angles, as well as tension in the tendons [64]. There are no data currently available in the literature for joint rotational stiffness, inertia, and friction over the full ROM of the finger. The estimated average values for joint rotational stiffness and friction used in this model are from [64] (Table 3.1); the values used for rotational inertia are discussed in the GUI section. The joint parameters are the same for the extensor tendons as they are for the flexor tendons.

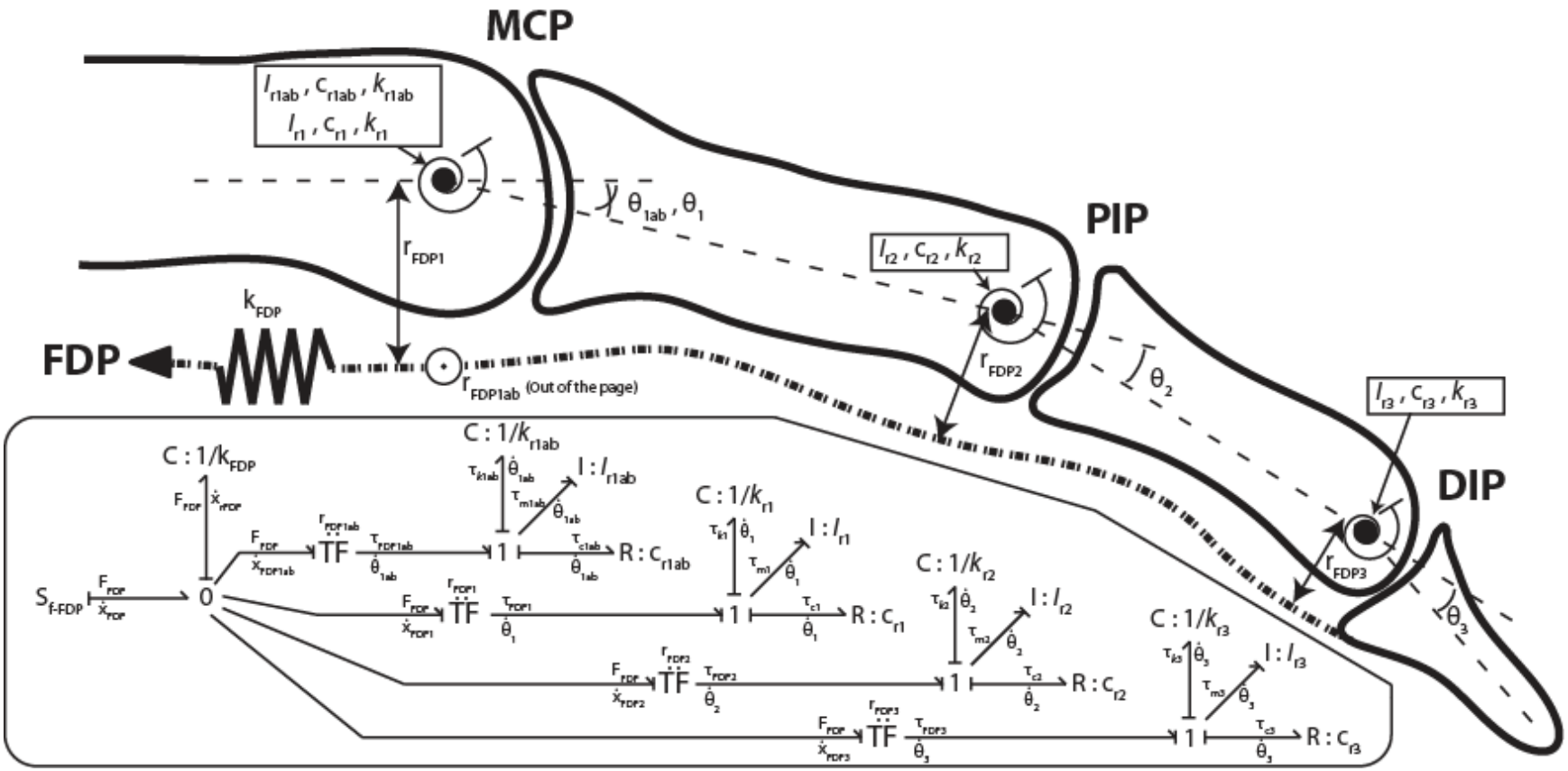

Figure 3.1. An example bond graph tendon model of the FDP tendon (see Appendix C for derivation).

Table 3.1 Resting angles, joint stiffness and joint damping values used in the bond graph tendon model. Data adapted from [64].

	MCP (ab-ad)	MCP (flex-ext)	PIP (flex-ext)	DIP (flex-ext)
Resting Angle (degrees)	0°	27°	26°	10°
k (N mm rad^{-1})	580	580	290	120
c (N mm s rad^{-1})	3.1	3.1	3.3	0.9

3.1.2.2 Extensor Tendons and the Extensor Mechanism

The bond graph tendon model mimics the anatomical tendon routing of the ED, LUM, DI and PI as well as the combination of the extensor tendons into the extensor mechanism. The extensor mechanism is oversimplified in previous tendon models, but [66] has shown that its complexity is essential for anatomical accuracy. When contracted, the ED muscle transfers a majority of its energy into extending the MCP, PIP, and DIP joints; it also causes a slight abduction or adduction of the MCP joint, depending on MCP(flex-ext) joint angle. In the index finger, the first PI muscle causes adduction and the first DI and LUM muscles cause abduction. The LUM, DI and PI muscles flex the MCP and extend the PIP and DIP finger joints. The extensor mechanism is commonly described by Winslow's Rhombus, and its unique interconnections are mimicked in the bond graph tendon model (Figure 3.2) [67]. Accurate representation of the extensor mechanism is important to retaining its unique role in tendon tension distribution and finger motion. The interconnections of the extensor mechanism change the tendon tension distribution throughout the extensor mechanism [66, 68, 69]. Previous researchers have looked at the effects of different tendon interconnection arrangements of extensor mechanisms [58, 66, 69]. This bond graph tendon model matches the extensor mechanism used in [69] (Winslow's Rhombus) with the addition of the LUM; this extensor mechanism architecture is the most common representation in the literature.

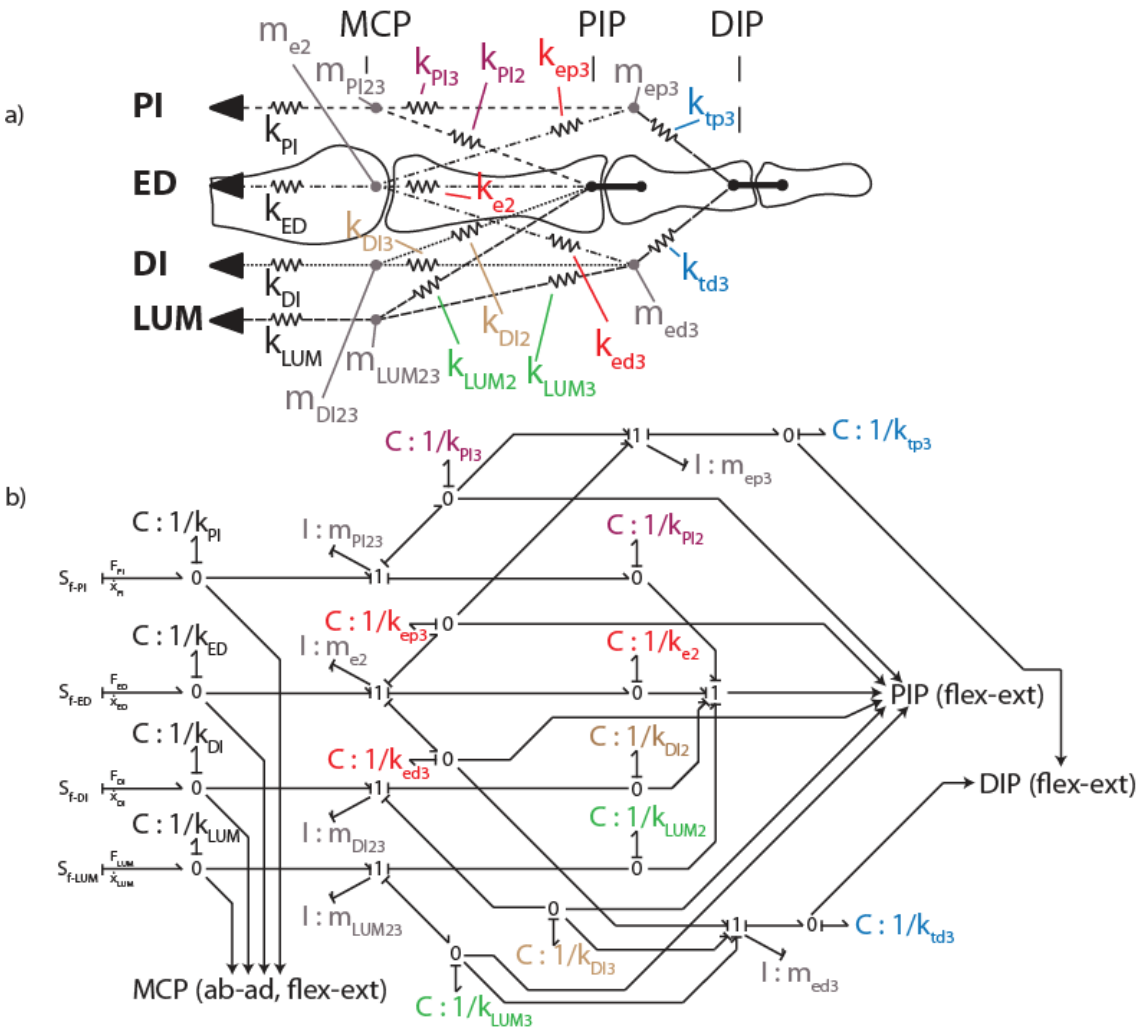

Figure 3.2. Extensor mechanism converted to bond graph model components. *(a)* The extensor mechanism in linear mechanical components. *(b)* Bond graph of the extensor mechanism in the linear mechanical domain.

Different interconnections of the extensor mechanism have different tension stiffness values, ranging from 40-120 N/mm. This variation in extensor mechanism interconnection stiffness is implemented into the bond graph tendon model using values from [58]. The bond graph tendon model's extensor mechanism also implements very small inertial masses at every tendon interconnection (Figure 3.2). The inertial masses are included to avoid algebraic loops during the derivation of state equations; without the inertial masses, the state equations

are a set of Differential Algebraic Equations (DAEs) instead of a set of Ordinary Differential Equations (ODEs). Solving the set of ODEs is preferable over the DAEs since the finger GUI (discussed later in this section) can solve ODEs much faster, which allows users a more interactive experience. The addition of inertia elements to the bond graph tendon model also gives the system the capability to simulate the dynamic motion of the finger; previous tendon models are incapable of simulating these dynamics. The value chosen for tendon interconnection masses is discussed in following section.

3.1.3 Solver Implementation and Tendon Modeling Complexities

The bond graph tendon model is used to determine the relationship between tendon excursion or tension (input) and final finger position in joint angles (output). A fourth order Runge-Kutta solver is used to solve the set of ODEs derived from the bond graph tendon model. Solving the bond graph tendon model's set of ODEs as quickly as possible, while retaining anatomical accuracy, is desirable for keeping the GUI interactive. Issues encountered when implementing the solver were assessed with the goal of maintaining quick computational speed and anatomical accuracy; these issues include selecting a moment arm model, choosing inertia values for joint rotation and tendon interconnection masses, and implementing tendon slack and maximum joint ROM.

The three main moment arm models for relating tendon excursion to changes in joint angle were discussed in Chapter 2: Landsmeer's Models I, II and III. Model I is used in the bond graph tendon model to represent the tendon excursion relationship for tendons that are wrapping over a joint during motion, and Model II is used to represent the tendon excursion relationship for tendons that bowstring during motion; bowstringing is defined in Chapter 2.

Both models are assumed to accurately estimate the anatomical relationship between tendon excursion and joint angle when provided with the anatomically accurate moment arm value. Selecting Model I and II over Model I and III also helps to minimize the computation time, since Model III is more computationally expensive. Computation time is also kept low by choosing small values for the inertial elements; this allows the dynamics of the bond graph tendon model to react quickly.

The bond graph tendon model is capable of simulating the dynamic motion of the finger; however, the transient response of the human finger is not being investigated in this work. The main focus of this work is exploring the final state of the finger given an input of tendon tension or excursion. The inertial elements in the bond graph tendon model do not represent their anatomical counterparts, but instead are only added to alleviate algebraic loops during state equation derivation. For this reason, the combined inertia of the bones and joints, and the tendon interconnection masses are chosen with consideration for the fastest computation time and minimal effect on system dynamics. A value of 0.029 g/mm^2 is used to represent the total rotational inertia at each joint. To keep the joints and tendon interconnection masses moving at close to the same velocity, a value of 1.0 *mg* is used for the mass at the tendon interconnections; this value is calculated based on the selected rotational inertia value above and the moment arm data for the finger joints. The low values of inertia decrease computation time but increase instability in the solver; the addition of the following tendon model complexities also moves the solver's solutions to unrealistic or unstable regions.

Only Leijnse et al. implemented tendon slacking in their tendon models, with limited success, while no researchers included maximum joint ROM in their tendon models [17-19]. These modeling complexities are inherently nonlinear, and there are no bond graph elements

that innately model nonlinearities; instead, nonlinearities are introduced into the constitutive laws of existing bond graph elements. The following two nonlinearities are defined in the system: joint angles cannot exceed values beyond maximum ROM of the index finger, from [27], and tendon tension values cannot go below 0 N (as a negative tension would imply compression of the tendon). However, tendon values of 0 N can cause the tendon system to become unsolvable or find unrealistic solutions. To alleviate this issue, the system assumes that all input tendons (FDP, FDS, ED, LUM, DI, and PI) always have a minimum tensile force of 1 mN; assumed to be unmodeled frictional forces that keep the tendons from moving when slacked. This is a small enough force to keep the system from deviating from its initial states while still removing the issues caused by 0 N tendon values. There is another nonlinearity of rerouting tendons in the extensor mechanism that is difficult to implement in the bond graph tendon model since there is limited literature to accurately describe it.

The nonlinearity of rerouting tendons in the extensor mechanism is discussed in great detail in [66]. The unique structure and interconnections of the extensor mechanism leads to "somatic logic," as described in [66], where input tendon tensions can preferentially propagate tension to the proximal and terminal slips by nonlinearly rerouting the distribution of tendon tensions (Figure 2.6). This nonlinearity is not implemented into the bond graph tendon model because there are no results in the literature that accurately describe how the extensor mechanism reroutes tension during loading.

The entire bond graph tendon model described in this section is presented in Figure 3.3.

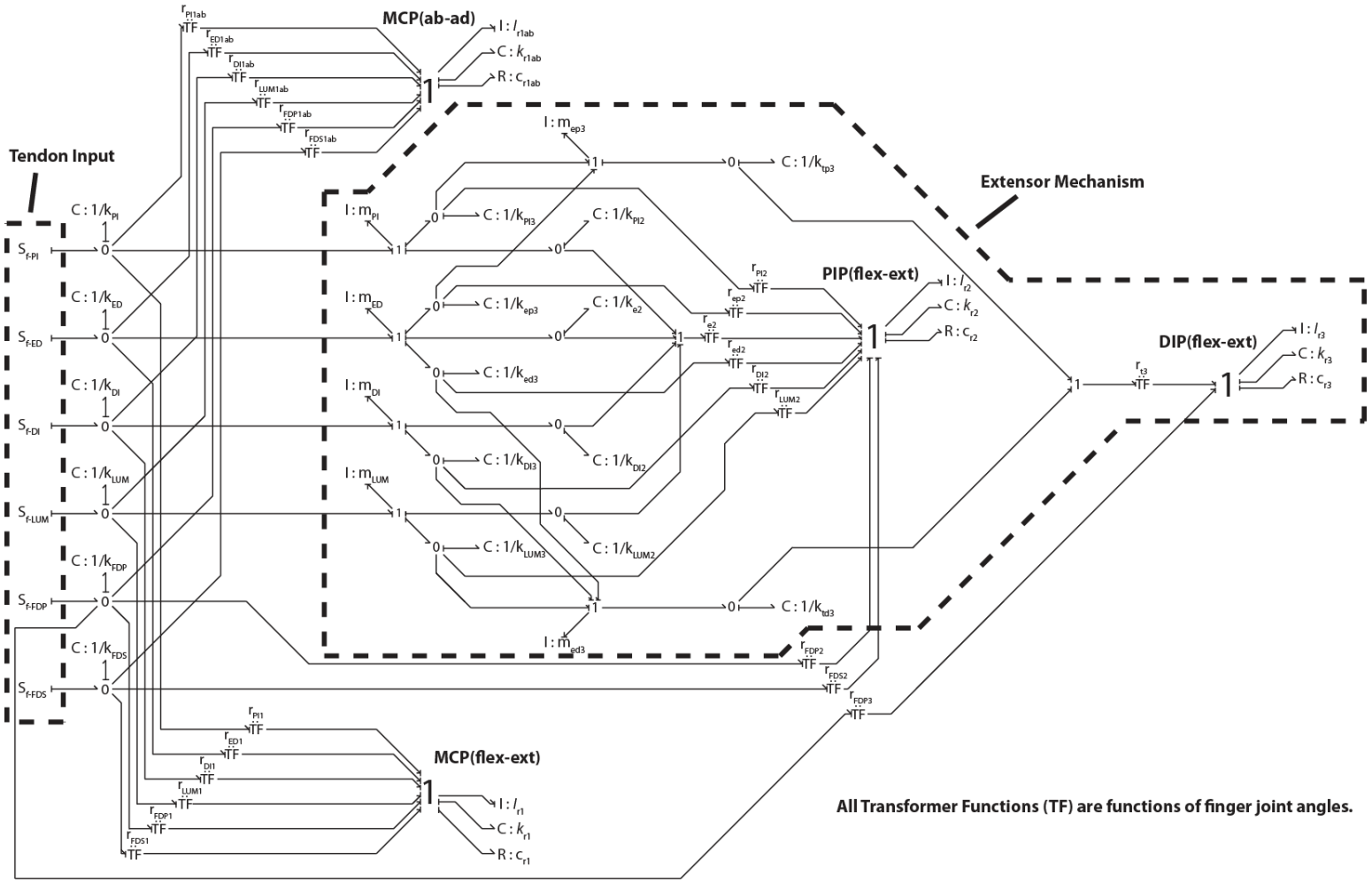

Figure 3.3. The bond graph tendon model of the finger.

3.2 Graphical User Interface (GUI) of the Finger

During development of the bond graph tendon model, the ability to visually define the input (tendon excursion or tension) and observe all the possible outputs (final joint angle, tendon tensions, etc.) became an important diagnostic tool for validating model accuracy (Figure 3.4). The GUI of the single finger was developed using Microsoft Visual Studio 2008 and Nokia's Qt software, and is capable of solving most all tendon inputs in less than a second on a single core 1.90 Ghz processor. All input and output values are relative to the initial states of the GUI, thus selecting an appropriate set of initial states is essential for anatomical accuracy.

The four possible input conditions for the tendons are "Active Pull," "Soft Attachment," "Hard Attachment," and "Hanging Weight" (Figure 3.5). An input type for each tendon must be selected before running the solver.

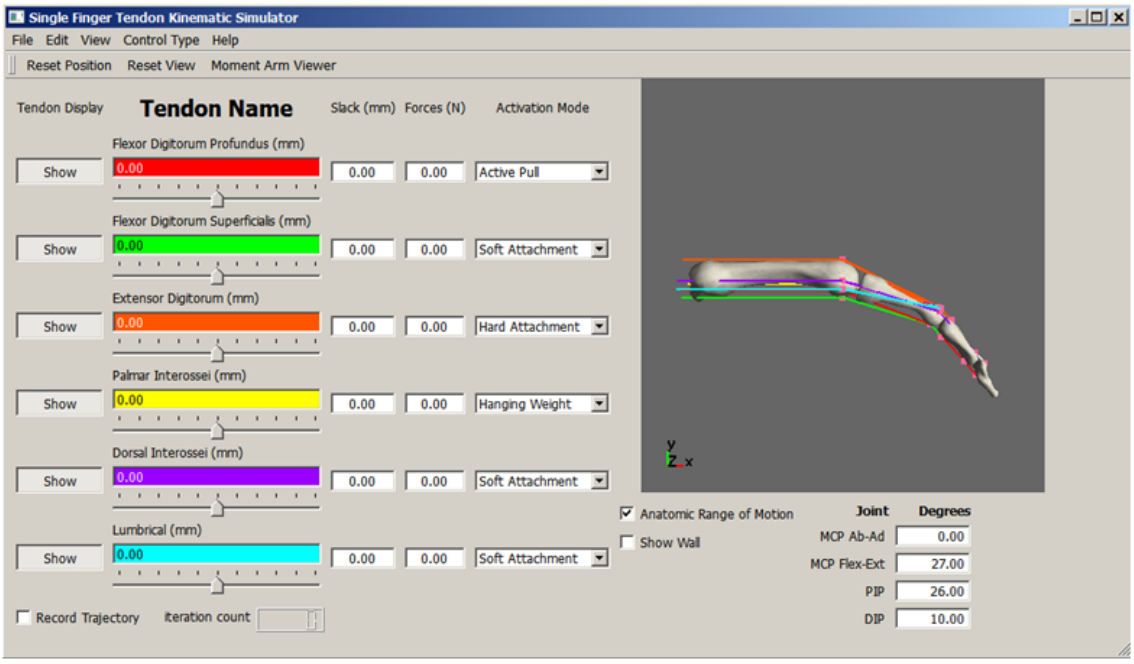

Figure 3.4. A Graphical User Interface (GUI) for controlling the index finger using either tendon excursions or tendon tension. All values are relative to the initial state of the finger.

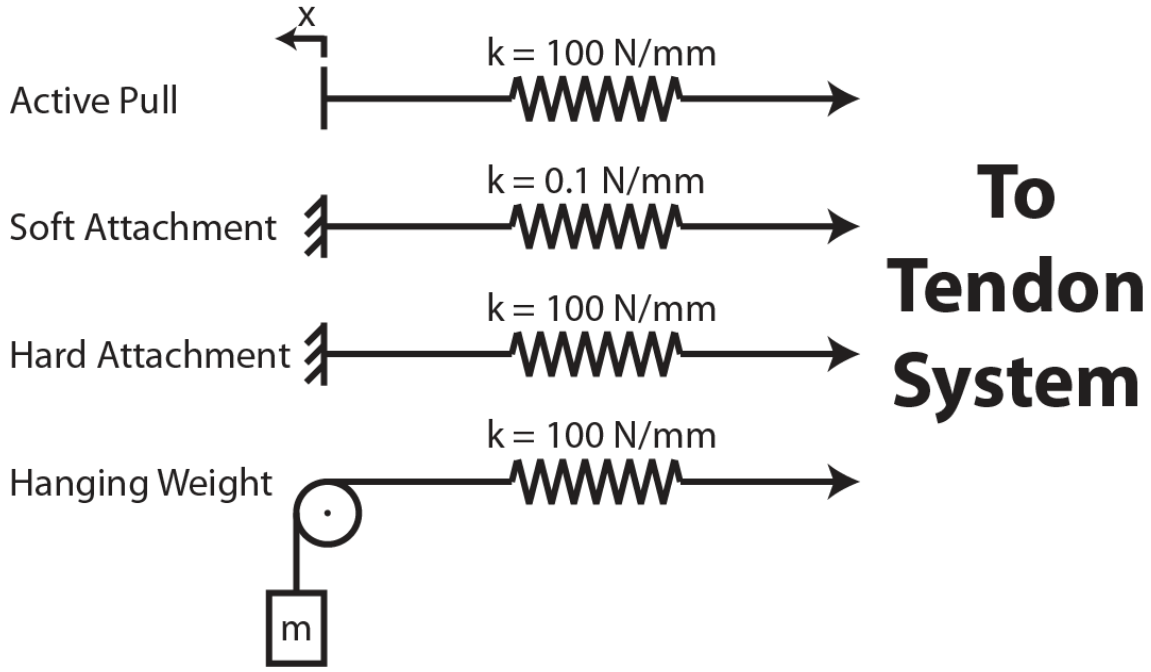

Figure 3.5. The four possible tendon input conditions to the GUI.

The Active Pull condition is used for setting a tendon's excursion as the input to the system; this condition sets the specified tendon in the bond graph tendon model as a flow source, equal to the desired tendon excursion with a corresponding tendon stiffness of 100 *N/mm* [58]. The Active Pull condition mimics a muscle contraction event, where the muscle shortens and pulls its attached tendon proximally.

The Soft Attachment condition is used for making a tendon passive, allowing it to be stretched by an Active Pull tendon. The Soft Attachment condition removes the tendon as a flow source and sets the associated tendon stiffness to a more malleable stiffness of 0.1 *N/mm*. The Soft Attachment mimics an antagonistic muscle being stretched by the active (protagonist) muscle.

The Hard Attachment condition is similar to the Soft Attachment condition except it maintains a tendon stiffness of 100 *N/mm*. The Hard Attachment mimics an antagonistic

muscle that is isometrically contracted (no change in muscle length) to oppose an active tendon.

The Hanging Weight condition replaces the flow source in the bond graph tendon model with an effort source; tendon stiffness is maintained at 100 *N/mm*. The Hanging Weight mimics an isotonic contraction (no change in muscle tension). Any combination of input conditions can be chosen for the tendons, all of which result in various outputs of the tendon model.

The main GUI outputs are the final joint angles, tendon tensions, tendon slacks, and positions of the moment arms. The joint angles are rendered in the 3D environment and also displayed numerically. The tendon tension and slack values are presented numerically in the center of the GUI. Since the positions of the moment arms vary based on joint angles, a second dialog box (not pictured in Figure 3.4) is used to present a selected moment arm's current distance to its corresponding joint's center of rotation. All the output values are relative to the initial state, except for the moment arm values which are calculated based on the current joint angles.

The initial state chosen for the GUI is based on the resting position of the index finger. It is assumed that an index finger set at its resting angles would have minimal tendon tension. With no data in the literature on finger tendon tensions at rest they are assumed to be at 0 *N* at the resting angles defined in Table 3.1, all tendon tensions calculated during simulation are relative to this initial value.

3.3 Comparisons between the Bond Graph Tendon Model and Literature Experiments

Comparisons to human cadaver and *in vivo* experiments from the literature are used to evaluate the anatomical accuracy of the bond graph tendon model. First, the tendon model's tension distribution in the extensor mechanism is compared to cadaver data from [66]. Second, the tendon model compares coupling of the PIP and DIP joints during motion to *in vivo* experimental data from [8]. These two mechanisms were chosen to be compared with the bond graph tendon model due to their unique function in the tendon system and their previous anatomical investigation in the literature.

3.3.1 Comparison of Extensor Mechanism Tension Distribution

An experimental apparatus used for measuring extensor mechanism tension distribution is described in [66]. The cadaver hand is mounted to the apparatus and the middle finger is configured at 0° MCP (ab-ad), 45° MCP (flex) and PIP (flex) and 10° DIP (flex). Two buckle transducers were used to measure tendon tension at the proximal and terminal slips of the extensor mechanism (Figure 2.5). To excite the unique properties of the extensor mechanism it was loaded with various levels of DI/PI and ED tension; ranging from DI/PI tensions twelve times greater than the ED tension (an interosseous to extensor (IO:ED) tension ratio of 12:1) to no DI/PI tension (an IO:ED of 0:1). All IO:ED tension ratios are calculated using (DI + PI : ED). The bond graph tendon model mimics this setup by matching the joint angles and loading conditions used in the experiment.

The bond graph tendon model is able to match the trend of the ratio of proximal slip to terminal slip tensions from the cadaver experiments (Figure 3.6, the proximal slip and

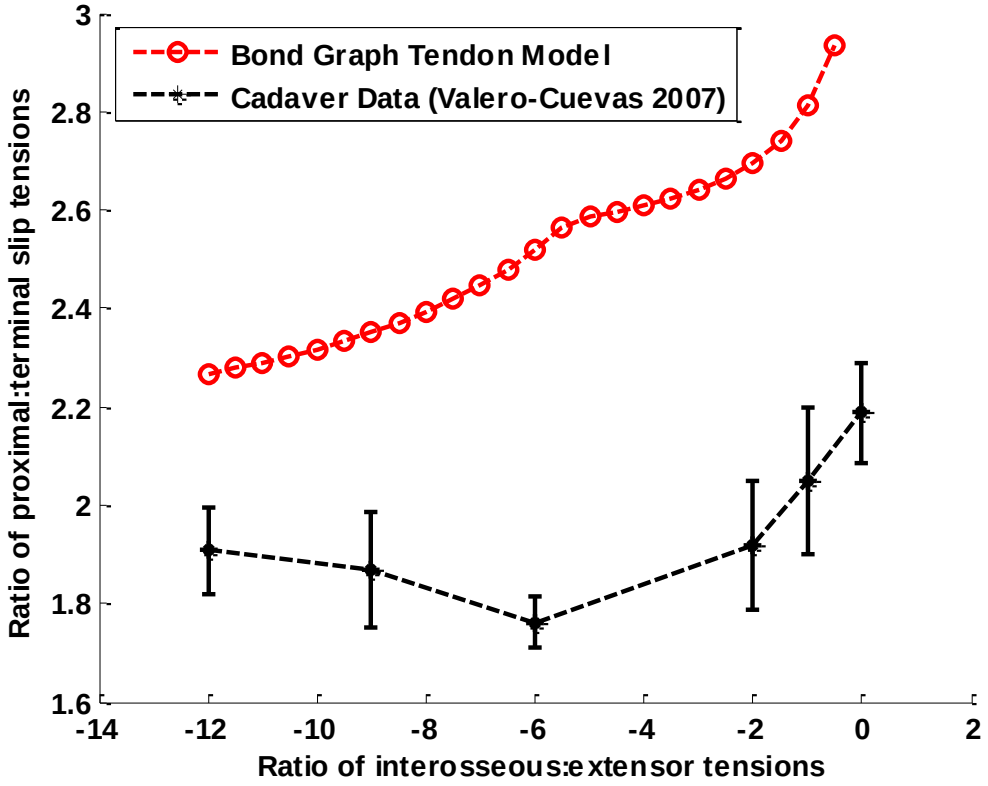

Figure 3.6. Comparison of the tension ratio between the proximal slip and terminal slip to the ratio of interosseous tension to extensor tension (DI + PI : ED) between the bond graph tendon model and cadaver experiments. Experimental data adapted from [66].

terminal slip are defined in Figure 2.6). The "switching behavior," described in [66], caused by the somatic logic of the extensor mechanism is not matched by the bond graph tendon model. The switching behavior of the extensor mechanism is visible in the cadaver experiments in Figure 3.6, as the IO:ED tension ratio goes from 0:1 to 12:1. Where the 6:1 IO:ED tension ratio shows a minimum proximal slip to terminal slip tension ratio before "switching" and increasing again as the IO:ED tension ratio goes to 12:1. Since little is understood about how this switch behavior occurs, the bond graph tendon model does not represent this anatomical characteristic of the extensor mechanism. However, the bond graph tendon model does show a different trend between the IO:ED tension ratio from 12:1-5:1

versus 5:1-0.5:1. This change in trend suggests that there is a switching behavior occurring in the bond graph tendon model but it does not match the cadaver experiments. No tension on the DI or PI tendon completely removes their effect from the extensor mechanism in the bond graph tendon model; this is not the case for the anatomical system, as there still would be some effect of the DI and PI even when unloaded.

The comparison of the cadaver experiment and the bond graph tendon model presents an encouraging validation for anatomical accuracy over the IO:ED tension ratios of 5:1-0.5:1. The difference in values of proximal slip to terminal slip tension between the bond graph tendon model and the cadaver experiment are most likely caused by their difference in internal parameters. The bond graph tendon model used the internal parameters (moment arms, tendon stiffness, joint stiffness) presented in the previous sections, while the internal parameters of the cadaver experiment were not reported. These differences in internal parameters cause the values of proximal slip to terminal slip tension not to match between the two systems, however, the trends of the two systems can still be compared for anatomical accuracy. The IO:ED tension ratios greater than 5:1 do not match the cadaver experiment trends, however, IO:ED tension ratios from 5:1-0.5:1 show excellent trend agreement. Overall the bond graph tendon model is capable of representing the trends of a large section of loading conditions of the extensor mechanism. However, more research on the human extensor mechanism is needed to improve the anatomical accuracy of the extensor mechanism of the bond graph tendon model.

3.3.2 Comparison of PIP:DIP Coupling

The *in vivo* finger experiment described in [8] collected motion capture data during normal unloaded motion of a single finger. The joint angles of 68 fingers were measured to obtain an average coupling relationship between the PIP and DIP [8]. The bond graph tendon model mimicked this experiment by flexing and extending the finger starting at the resting angles presented in Table 3.1.

The bond graph tendon model is able to match *in vivo* data of the relationship between the PIP and DIP joint (Figure 3.7). The *in vivo* experiment shows that there is large variability in the coupling between the PIP and DIP joint angles (Figure 3.7 dotted lines without asterisks). Since the internal parameters of the fingers used in the experiments were

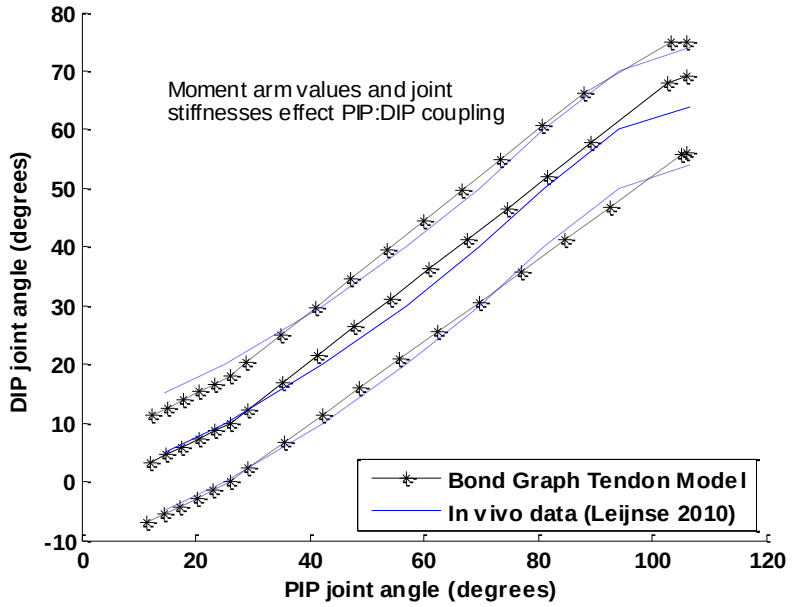

Figure 3.7. Comparing finger PIP: DIP coupling between the bond graph tendon model and *in vivo* data; positive joint angles represent flexion. The lines without asterisks are the average *in vivo* data (solid line), and the upper and lower bounds of the *in vivo* data (dashed lines). The lines with asterisks show that the bond graph model is versatile enough to match all ranges of PIP:DIP coupling.

not measured, additional bond graph tendon model trials with various values of moment arms (± 2 *cm* from [23] values) and joint stiffness (± 40 *Nmm/rad* from [64] values) were used. The bond graph tendon model shows that changing the stiffness and moment arms of the PIP and DIP joints can greatly affect the joint angle coupling relationship between these joints. This result may explain the large variability in PIP:DIP joint angle coupling in the *in vivo* data. The bond graph tendon model is capable of matching a range of these coupling relationships; this shows that not only is the model capable of accurately representing this coupling but also able to accommodate human variability.

CHAPTER 4

KINEMATIC VALIDATION OF THE BOND GRAPH TENDON MODEL USING THE ACT HAND

In this chapter, the ACT Hand will be introduced and justification of its use presented. A bond graph tendon model validation experiment involving the motion of the ACT Hand's index finger is described and performed. Lastly, the results from the ACT Hand's index finger's motion experiments are compared to the bond graph tendon model.

4.1 Anatomically Correct Testbed (ACT) Hand

The ACT Hand focuses on mimicking the intrinsic biomechanics, actuation and control behavior of the human hand to achieve human-like dynamic motions, and has been under development for over a decade [3, 23, 24, 43, 70, 71]. The ACT Hand consists of biologically inspired bone structures, joints, and tendons, and has been shown to accurately represent several features of the human hand through experimentation [23, 24, 43]. The ACT Hand was chosen for validating the bond graph tendon model because the ACT Hand's anatomical parameters are precisely measurable and it does not degrade from prolonged experimentation, both of which are complications with *in vivo* and cadaver experimentation. A full description of all the mechanisms of the ACT Hand can be found in [3].

The ACT hand consists of all the fingers of the hand, however, only the index finger of

the ACT hand is described and used in the experimental analysis in this dissertation (Figure 4.1). The ACT index finger consists of the four 3D printed bones that match the shape of the metacarpal bone, the proximal phalanx, the middle phalanx and the distal phalanx. These bones are connected by three hinge joints at the MCP, PIP and DIP joint. These hinge joints allow for the MCP joint to have ab-ad and flex-ext motion while the PIP and DIP joints only have flex-ext motion. The ACT index finger is controlled by six tendons, the FDP, the FDS, ED, LUM, DI, and PI. Similar to the bond graph tendon model, the EI and ED are combined into only the ED tendon since they are mechanically equivalent in a single finger system. The ACT Hand is always being improved to better represent the human hand; for this work the extensor mechanism was modified and validated for its anatomical accuracy [72]. The current extensor mechanism more closely resembles Winslow's Rhombus.

The previous ACT index finger's extensor mechanism had static attachment points at the MCP and PIP joints (Figure 4.2), leading to the inability of the extensor mechanism to translate along the bones during flex-ext of the finger. The changes made to the extensor mechanism help to more closely match the anatomical behavior of the human finger's

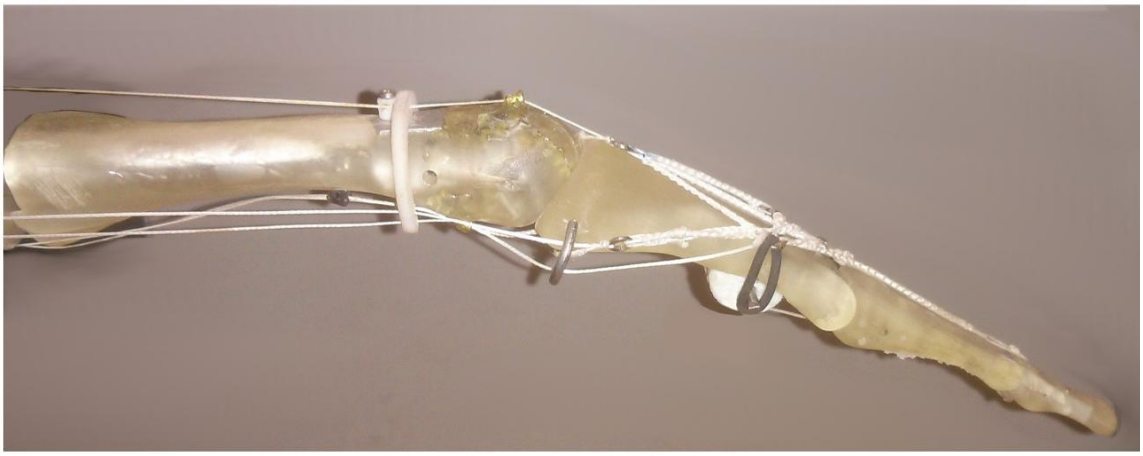

Figure 4.1. The index finger of the ACT Hand.

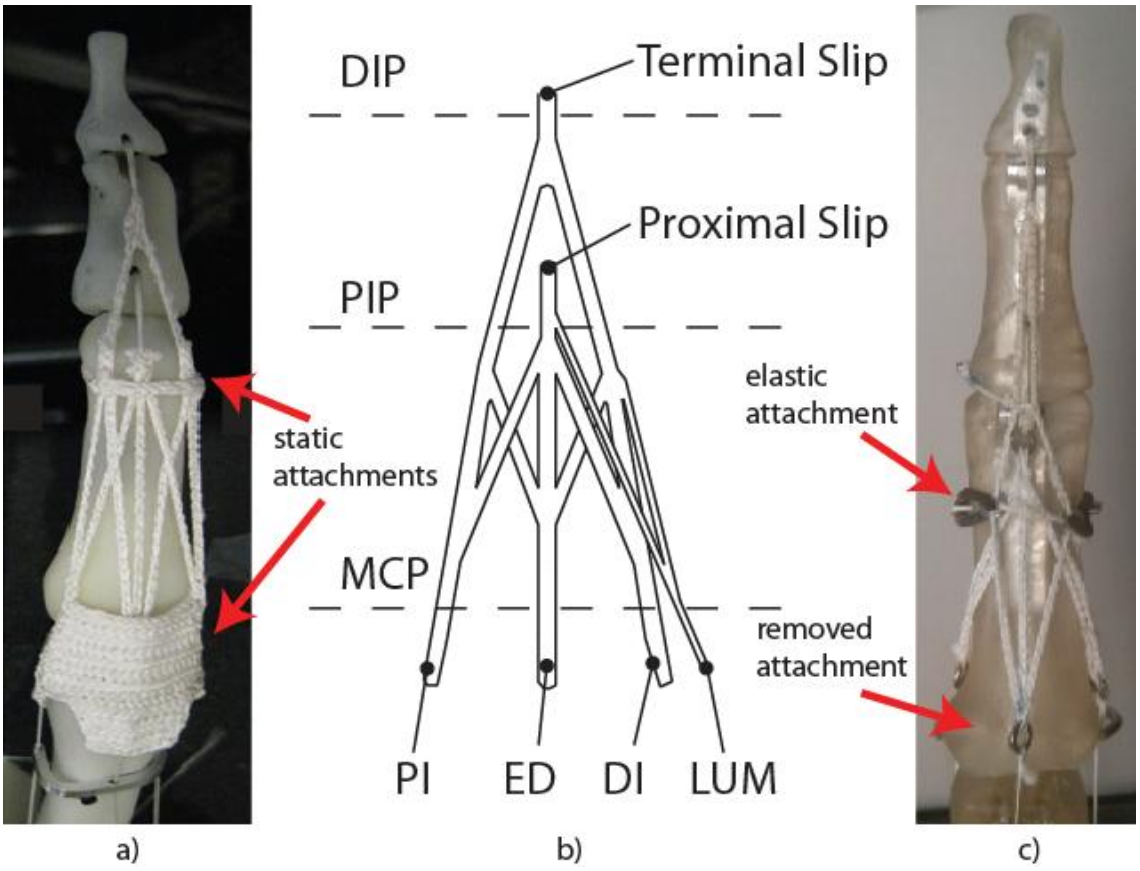

Figure 4.2. Different versions of the ACT index finger's extensor mechanism. *(a)* Previous extensor mechanism design with static attachments at the MCP and PIP joints. *(b)* Winslow's Rhombus as described in [30] with the addition of the LUM tendon. *(c)* The extensor mechanism design used in this work, removal of static attachments allows for more anatomically accurate translation of the extensor mechanism.

extensor mechanism [30, 66, 69].

A unique benefit of mimicking the bone structure and tendon system of the index finger is the preservation of the anatomical moment arms at the joints of the finger [23]. The biological shape of the finger bones cause the moment arms of the tendons to vary with joint angle and tendon arrangement. Since the tendon arrangement of the extensor mechanism in the ACT index finger was changed, previously collected variable moment arm data cannot be used. New tendon excursion and joint angle data were collected using a motion capture

system to find new variable moment arm functions for the ACT index finger; the methods used for collecting these data are fully described in [23]. After data were collected, a feed forward neural network [73] was used to learn the new variable moment arm functions in the new tendon arrangement of the ACT index finger. A neural network was used in place of the Gaussian process regression used in [23] due to a neural networks' simple training process and lower computational cost. These moment arm functions are used in the bond graph tendon model when performing experiments with the ACT index finger. In addition to changes in the moment arm functions in the bond graph tendon model, a new element of joint friction was needed for the tendon model to account for the presence of friction in the physical system of the ACT index finger.

4.2 Implementation of Joint Friction into the Bond Graph Tendon Model

The ACT index finger has observable friction in all its joints, and this friction needs to be considered for the bond graph tendon model to match the ACT index finger. The friction at each joint of the ACT index finger increases as tendon tension around the joint increases. A friction model is added into the joints of the bond graph tendon model to mimic both the friction and stiction of the ACT index finger's joints. The following friction model was used to calculate joint angle velocity at all finger joints:

$$\dot{\theta}_{joint} = \begin{cases} 0 & if \ \sum \tau_{joint} < \tau_s \\ \frac{1}{I}\left(\tau_{joint} - \tau_k - b * \dot{\theta}\right) & if \ \sum \tau_{joint} \geq \tau_s \end{cases} \quad (4.1)$$

$$\tau_s = f_c + \mu_s * \sum F_t \quad (4.2)$$

$$\tau_k = f_c + \mu_k * \sum F_t \quad (4.3)$$

where τ_s is the static friction torque, f_c is the constant friction, μ_s is the static coefficient of friction, F_t is the tendon tension, τ_k is the kinetic friction torque, μ_k is the kinetic coefficient of friction, τ_{joint} is the torque at the joint, $\dot{\theta}_{joint}$ is the velocity of the joint, I is the inertia of the joint and b is the damping coefficient of the joint. The constant friction, static coefficient of friction, and kinetic coefficient of friction at each joint is different, due to the different tendon arrangement at each joint and the individual friction of each joint of the ACT index finger. The values used for constant friction and the coefficients of friction were experimentally found during the ACT index finger experiments.

4.3 ACT Index Finger Motion Experimental Setup

An experiment was designed to compare the joint angles of the ACT index finger to the estimated joint angles of the bond graph tendon model given the same tendon excursions. The ACT index finger was mounted on a tabletop with each tendon attached to a motor through an extension spring (Figure 4.3). Before each trial, the finger was placed in an initial finger posture of neutral abduction, 27° flexion at the MCP and PIP joints, and 10° flexion at the DIP joint. Motion capture markers (PhaseSpace Inc., San Leandro, CA) were placed at the MCP joint, the PIP joint, the DIP joint and the fingertip. High tension kite string (WSK Premium Spectra, Windstar Kites of Greater Pittsburgh North, Baden, PA) was used as the tendon material for the ACT index finger and the tendon connections to the servo motors (Dynamixel, Robotis Inc., Irvine, CA). Six servo motors were used to give tendon excursion inputs to the system. An extension spring was placed in series with the tendons for estimating the tension in the tendons, and also to protect the ACT index finger from high tendon tensions. Potentiometers (3382 Model, Bourns, Inc., Riverside, CA) were used to

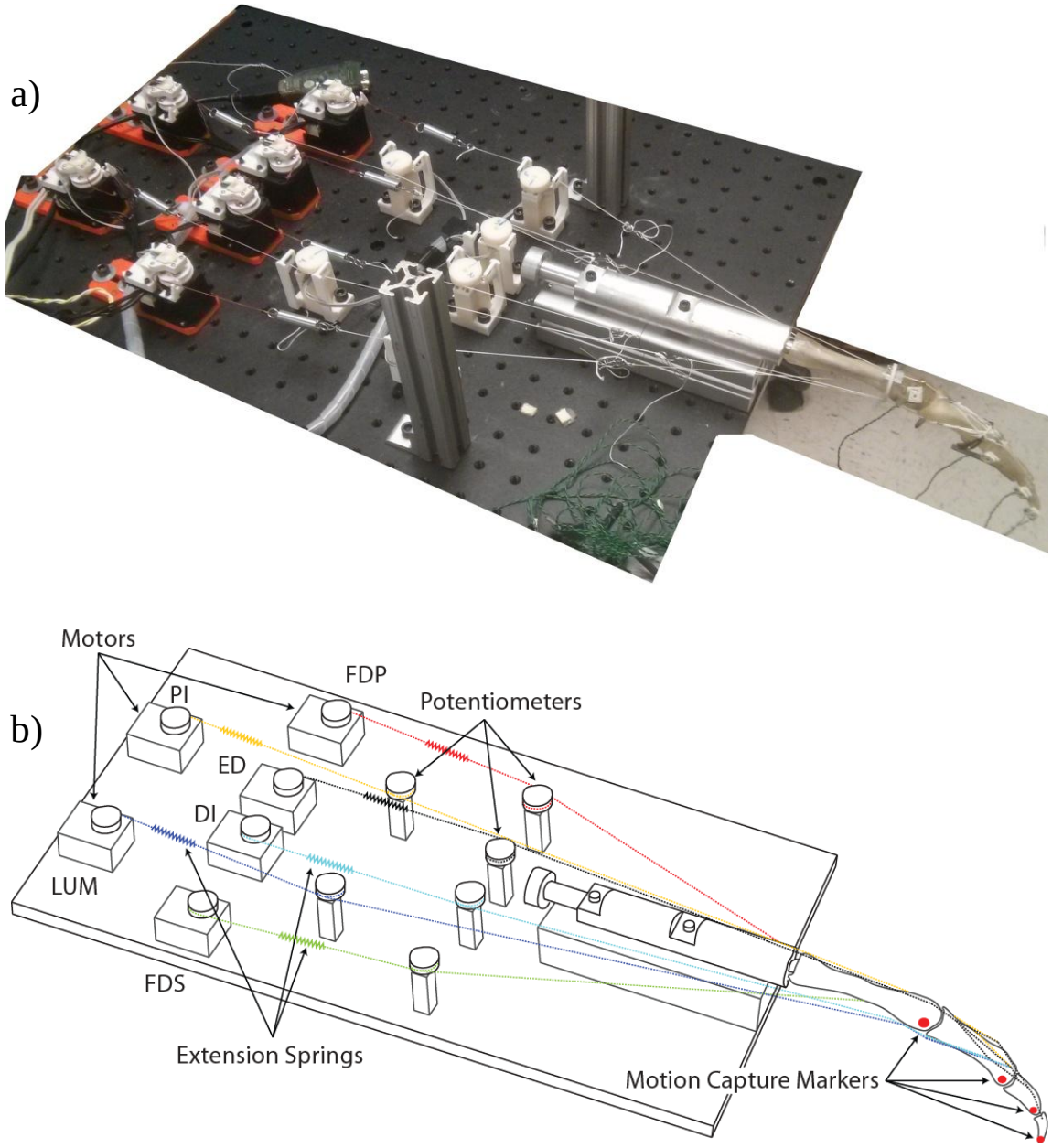

Figure 4.3. Experimental setup for the finger motion experiments, *(a)* is a photo of the setup, *(b)* is a schematic. The ACT index finger is suspended off the edge of the setup to allow for unhindered motion.

measure the stretch in the extension springs for estimating tendon tension. A Matlab (MathWorks, Inc., Natick, MA) program running on a laptop (ASUS K55N, ASUSTeK Computer Inc., Taipei, Taiwan) with data acquisition hardware (NI USB-6356, National Instruments, Austin, TX) was used to command tendon excursions and record tendon tension at 30 Hz. A Linux-RTAI (RealTime Application Interface) platform was used on a separate computer (Dell Precision 1650, Dell Inc., Round Rock, TX) to collect the motion capture data at 480 Hz. Tendon tension for each tendon was recorded for all trials but is not presented in this work. This setup was used for both single tendon excursion experiments and the multitendon excursion experiments.

4.3.1 Single Tendon Excursion Experiments

For the single tendon excursion experiments, six discrete levels of tendon excursion were tested for each tendon over four trials. Each tendon was tested individually starting at 0 *mm* and increasing to 18 *mm* in increments of 3 *mm*. All excursion levels were maintained long enough to ensure quasistatic equilibrium at each excursion level. The extension spring was removed during testing of the active tendon to ensure all tendon excursion was transferred to the ACT index finger; this spring was then replaced before testing the next tendon. This experimental setup is mirrored in the bond graph tendon model. The motion capture position data collected from each trial were used to calculate the joint angles of the finger.

4.3.2 Multitendon Excursion Experiments

For the multitendon excursion experiments, three tendons were selected to be displaced in varying activation orders. It was concluded that activating three tendons would cause the

most motion of the ACT index finger with minimal joint stiffness, as activating more than three tendons increases co-contraction around the joints and results in an increase of joint stiffness and reduction of finger motion. Three sets of three tendons were chosen to represent the multitendon excursion of the ACT index finger. Each set was chosen to have one flexor (FDP or FDS) and two tendons that are part of the extensor mechanism (ED, LUM, DI, or PI); the three sets chosen were: [FDP, ED, DI], [FDS, ED, PI], [FDS, LUM, PI]. Of the six possible permutations in each tendon set only three were tested; three trials of each permutation were performed. Each multitendon excursion trial displaced the selected tendons in sequence by 3 *mm* before displacing each tendon another 3 *mm* in the same sequence (e.g., in the [FDS, ED, PI] trial, the FDS is displaced 3 *mm*, then ED by 3 *mm*, then PI by 3 *mm*, and then this sequence was repeated once more). Each trial had a total of six different levels of excursion; maintained long enough to ensure quasistatic equilibrium between excursions. The motion capture position data collected from each trial were used to calculate the joint angles of the finger.

4.4 Finger Motion Experiment Results

Two sets of experimental data were collected during these experiments, single tendon excursions and multitendon excursions. The single tendon excursion data are compared to the bond graph tendon model both with and without the addition of joint friction. The multi-tendon excursion data are compared only to the bond graph tendon model with joint friction. The analysis of the motion experiments is discussed after the results are presented.

The bond graph tendon model struggles to match the motion of the ACT index finger without the addition of joint friction during the single tendon excursion experiment (Figure

4.4). With the addition of joint friction, the bond graph tendon model is able to better represent the motion of the ACT index finger (Figure 4.5). The results of the FDP, ED, and DI tendons are representative of all the tendons for the single tendon excursion experiments. All tendon excursion experiments show agreement between the bond graph tendon model with friction and the ACT index finger. The average joint angle errors between the bond graph tendon model without friction and the ACT index finger over all tendons and trials are 12.3°, 6.4°, 9.1°, and 4.1° for MCP(ab-ad), MCP(flex-ext), PIP(flex-ext), and DIP(flex-ext), respectively. The average joint angle errors for the bond graph tendon model with friction are 8.3°, 7.0°, 2.6°, and 2.3° for MCP(ab-ad), MCP(flex-ext), PIP(flex-ext), and DIP(flex-ext), respectively. The addition of friction into the bond graph tendon model is necessary to better represent the ACT index finger. Only the bond graph tendon model with friction is used for the multitendon excursion experiments.

The bond graph tendon model with friction is able to match the trends and directions of the ACT index finger during multitendon excursion experiments (Figure 4.6). The results of the [ED, FDS, PI] are representative of all the multitendon excursion experiments. The average joint angle errors between the bond graph tendon model with friction and the ACT index finger for all [ED, FDS, PI] excursion experiments are 1.8°, 3.5°, 4.3°, and 2.3° for MCP(ab-ad), MCP(flex-ext), PIP(flex-ext), and DIP(flex-ext), respectively. The multi-tendon excursion data also show that the final joint angles are dependent on both the set of tendons activated and the order in which the tendons are activated. The bond graph tendon model is able to replicate this aspect and match the final joint angle posture of the ACT index finger within 8° for all tendon activation orders in all joints. A 3D comparison between the bond graph tendon model and the motion of the ACT index finger is also presented

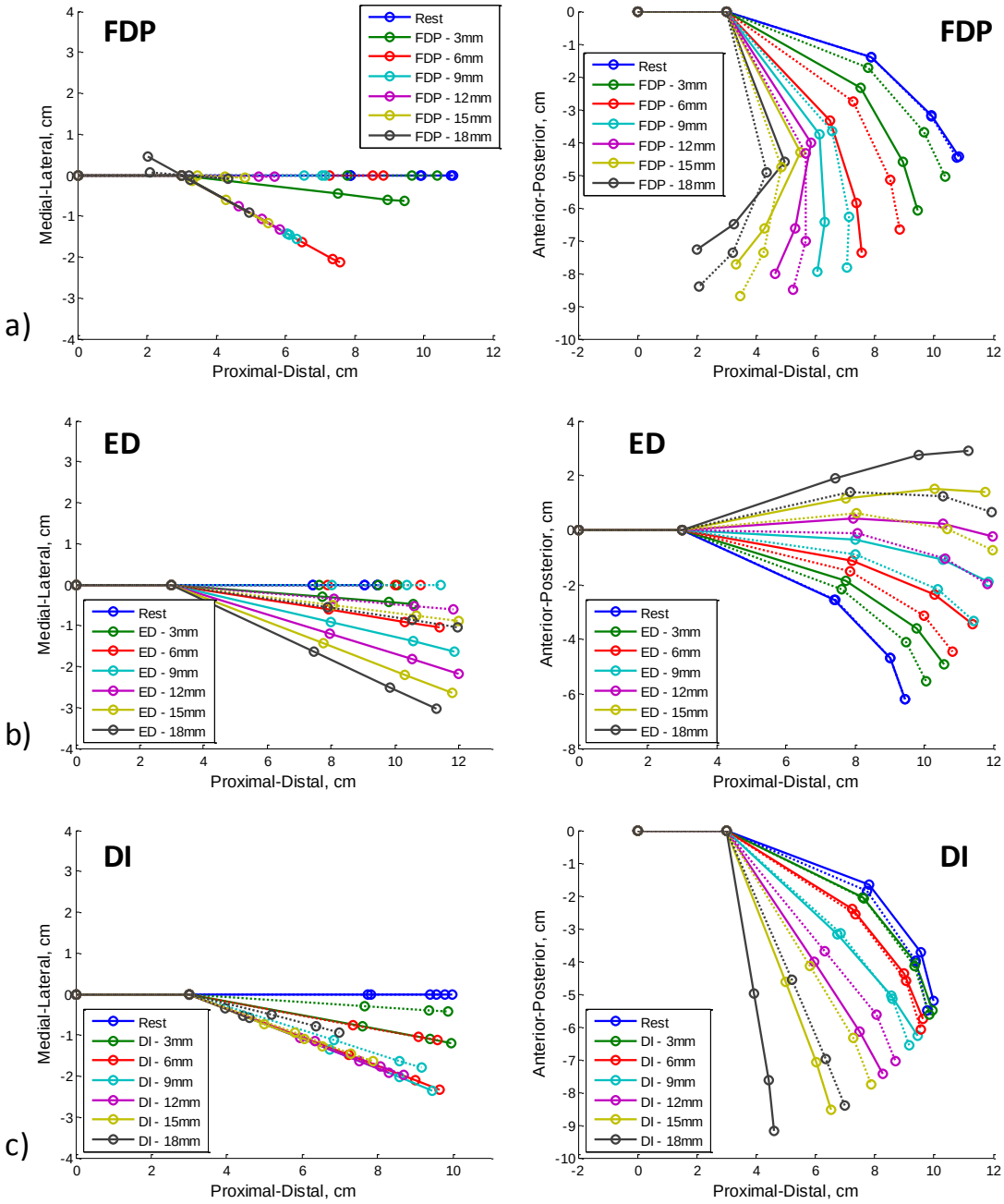

Figure 4.4. Results for the single tendon excursion experiments with the frictionless bond graph tendon model, positive angles represent extension and abduction. *(a)* is the FDP tendon experiment, *(b)* is the ED tendon experiment, *(c)* is the DI tendon experiment. Lines of the same color represent the same tendon activation, solid lines are the bond graph tendon model and the dotted lines are the ACT index finger.

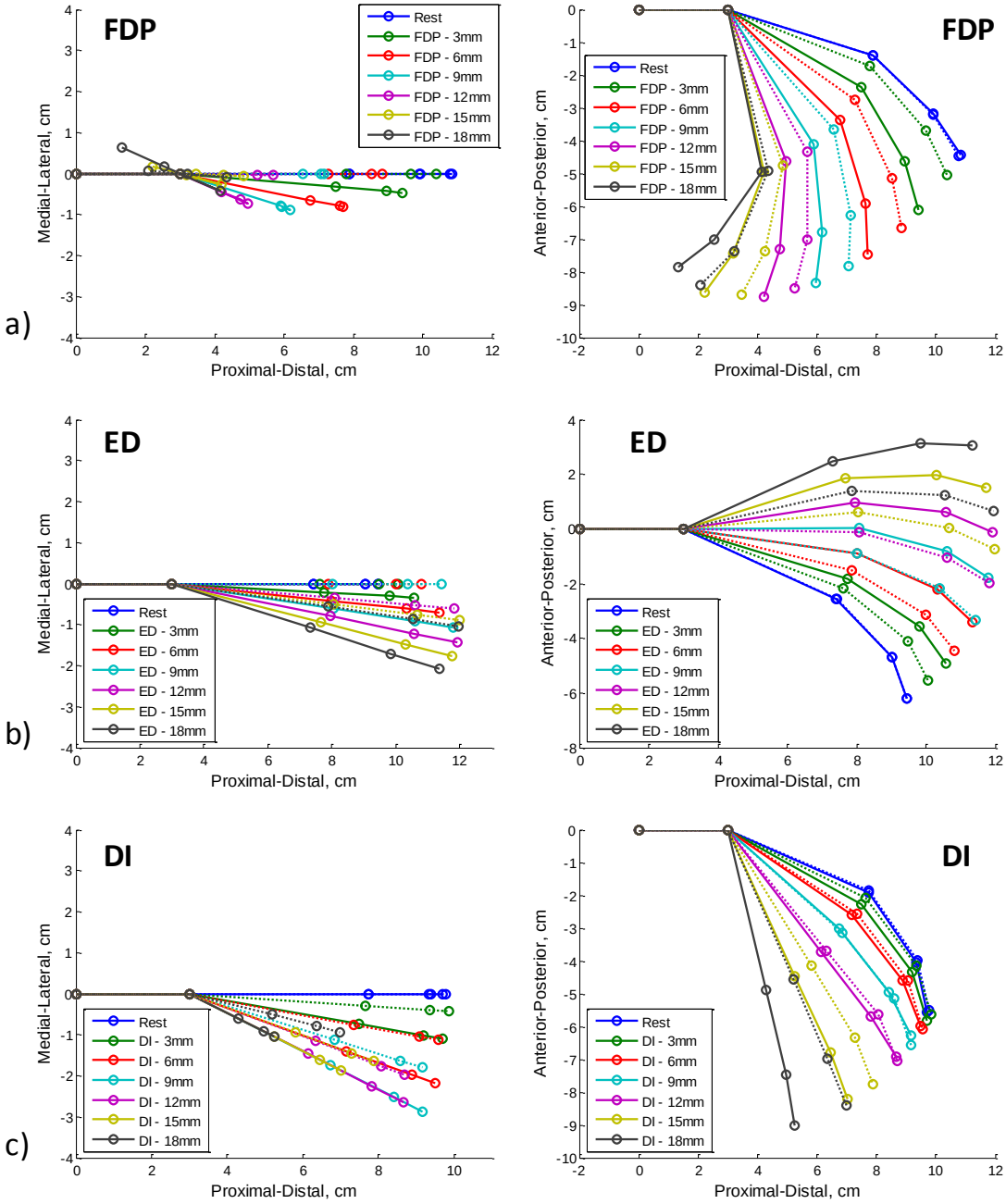

Figure 4.5. Results for the single tendon excursion experiments with the bond graph tendon model including friction; *(a)* is the FDP tendon experiment, *(b)* is the ED tendon experiment, *(c)* is the DI tendon experiment. Lines of the same color represent the same tendon activation, solid lines are the bond graph tendon model and the dotted lines are the ACT index finger.

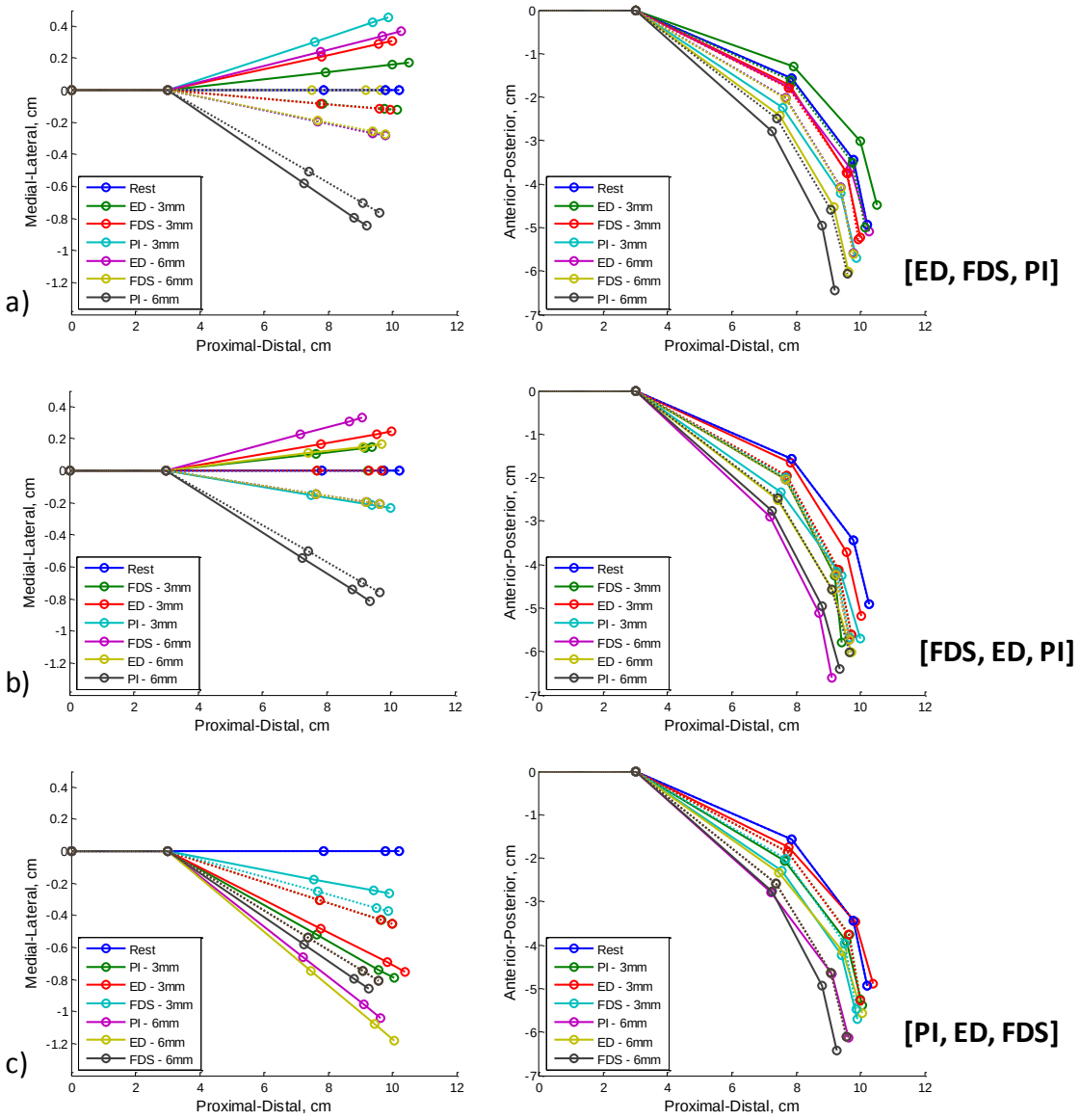

Figure 4.6. Results for the [ED, FDS, PI] multitendon excursion experiments. The tendon activation order for this experiment was: *(a)* - [ED, FDS, PI], *(b)* - [FDS, ED, PI], *(c)* - [PI, ED, FDS]. Lines of the same color represent the same tendon activation, solid lines are the bond graph tendon model and the dotted lines are the ACT index finger.

(Figure 4.7).

The bond graph tendon model with joint friction is able to accurately represent the complex tendon-based system of the ACT index finger during motion. A few limitations and assumptions lead to notable discrepancies between the bond graph tendon model and the ACT index finger, including: possible differences in variable moment arm functions, an incomplete joint friction model, and unmodeled characteristics of the ACT index finger. These limitations are presented and discussed along with the analysis of the experimental results below.

One limitation of the bond graph tendon model in relation to the ACT index finger is possible inaccuracies in the variable moment arm functions. The bond graph tendon model is only as accurate as the variable moment arm functions that were found from ACT index finger motion data. Any errors during the neural network fitting of the kinematic data could lead to unanticipated differences in moment arm values between the two systems. It is unknown how much this limitation contributed to the error between the two systems. However, based on the good agreement between the bond graph tendon model and the ACT index finger, and qualitative observations between the variable moment arm functions and the ACT index finger, these errors are assumed to be minimal. The incomplete model of ACT index finger's joint friction has a much greater effect on the differences between the two systems during the motion experiments.

The friction model implemented into the bond graph tendon model does not accurately represent the friction in the joints of the ACT index finger. The errors caused by the inaccurate joint friction model are most notable during the multitendon excursion experiments (Figure 4.6). In several instances during the multitendon excursion

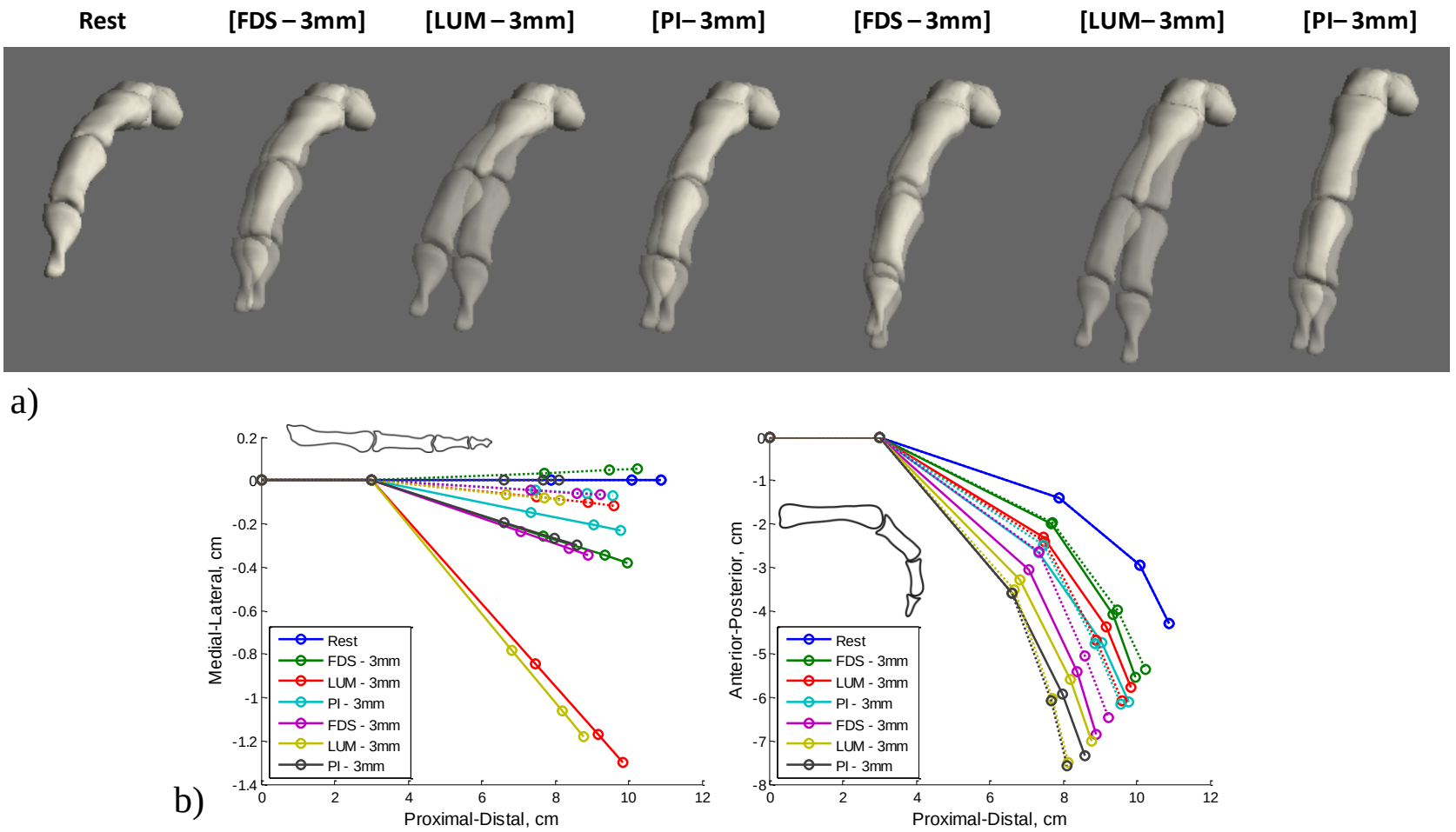

Figure 4.7. Comparison between the ACT index finger and the bond graph tendon model with friction for each discrete tendon activation [FDS, LUM, PI] trial. *(a)* A 3D motion comparison. *(b)* 2D motion comparison, where lines of the same color represent the same tendon activation, solid lines are the bond graph tendon model and the dotted lines are the ACT index finger.

experiments, the bond graph tendon model inaccurately predicts a large change in joint angle that does not occur in the ACT index finger. Currently, the ACT Hand's joint friction is significantly larger than the joint friction of the human hand [27]. Since the ACT index finger does not match the anatomical joint friction of the human finger, only a simple model of friction was implemented into the bond graph tendon model to avoid spending extensive time and effort matching joint friction that is not anatomically accurate to the human system. However, the results show that even the addition of a simple model of joint friction is able to reduce the average joint angle error between the bond graph tendon model and the ACT index finger. The limitation of an incomplete model of the ACT index finger's joint friction is the reason for most of the discrepancies between the bond graph tendon model and the ACT index finger during the motion experiments; this was discerned from observation of the ACT index finger motion.

The last limitation is a mechanical difference between the bond graph tendon model and the ACT index finger. At large flexion angles (over 50°) of the ACT index finger's MCP joint the maximum angle for ab-ad is reduced; this is not the case in the bond graph tendon model. This mechanical discrepancy can be seen in Figure 4.5c, where the DI tendon's MCP (ab-ab) angle is reduced near the end of the trial as the flexion angle of the MCP joint increases past 50°. This reduction of ab-ad motion in the ACT index finger is anatomically correct to the human index finger, however, the relationship between MCP (flex-ext) angle and MCP (ab-ad) angle has yet to be fully explored. Future work will implement this relationship into the bond graph tendon model. Currently, this is a limitation between the two systems that causes angle errors during large MCP (flex) and MCP (ab-ad) angles. The effect of this limitation is only apparent in the single tendon excursion experiments of the PI, DI

and LUM tendons; the multitendon excursion experiments are not affected by this limitation since they do not achieve large MCP (flex) or MCP (ab-ad) angles.

Despite the presented limitations, the bond graph tendon model can accurately represent the complex tendon-based system of the ACT index finger. The bond graph tendon model has been shown to represent the motion of the ACT index finger during both single tendon excursion and multitendon excursion experiments within a range of 1.8°-8.3°. The bond graph tendon model is the first fully interconnected tendon system model to be validated through the use of the ACT index finger; this shows great potential for the tendon model to accurately represent the human finger system.

CHAPTER 5

FINGERTIP FORCE VALIDATION OF BOND GRAPH TENDON MODEL

This chapter is arranged into the following sections: implementation of the fingertip force to the bond graph tendon model, comparison of the bond graph tendon model to fingertip force experiments in the literature, and a fingertip force experiment using the ACT index finger. Additional elements are added to the bond graph tendon model to illustrate the relationship between input tendon tension and fingertip force. This relationship is validated using both literature and ACT index finger experiments; both are presented and discussed individually.

5.1 Implementation of Fingertip Force into the Bond Graph Tendon Model

An external fingertip force was implemented into the bond graph tendon model as a means to simulate contact with an environmental surface. The external fingertip force is implemented in the bond graph model using the Jacobian transpose as a multiport transformer. The Jacobian transpose, generated from the Denavit-Hartenberg (D-H) parameters of the finger (Figure 5.1), is used to relate the external fingertip force to the torque in the joints of the finger. The fingertip force is calculated by specifying the

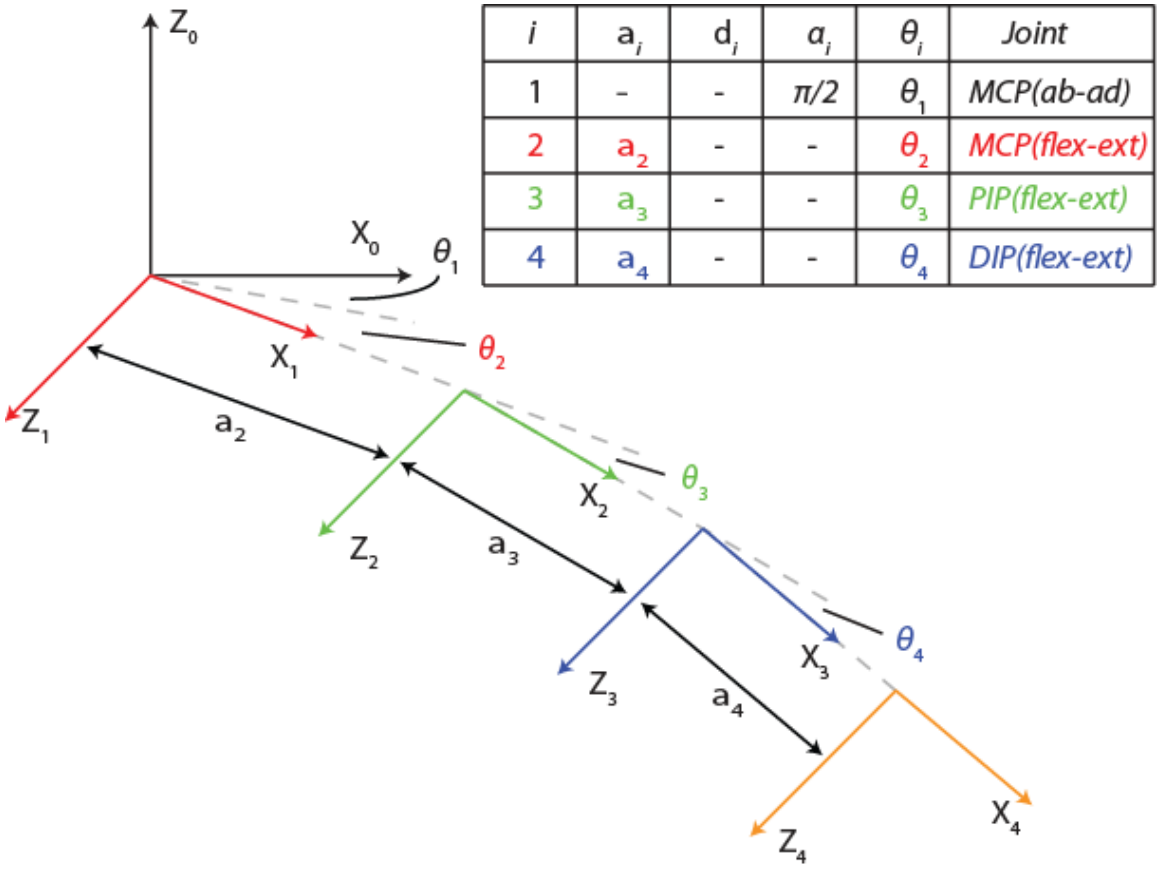

i	a_i	d_i	α_i	θ_i	Joint
1	-	-	$\pi/2$	θ_1	MCP(ab-ad)
2	a_2	-	-	θ_2	MCP(flex-ext)
3	a_3	-	-	θ_3	PIP(flex-ext)
4	a_4	-	-	θ_4	DIP(flex-ext)

Figure 5.1. The Denavit-Hartenberg (D-H) parameters of the finger.

environmental surface stiffness and identifying the depth that the fingertip has penetrated this environmental surface. Figure 5.2 shows the implementation of the external fingertip force into the bond graph tendon model.

5.2 Fingertip Force Comparison between the Bond Graph Tendon Model and Literature Experiments

An *in vivo* fingertip force experiment from the literature is used to evaluate the anatomical accuracy of the bond graph tendon model's fingertip force. Nine subjects undergoing open carpal tunnel release surgery participated in exploring the relationship

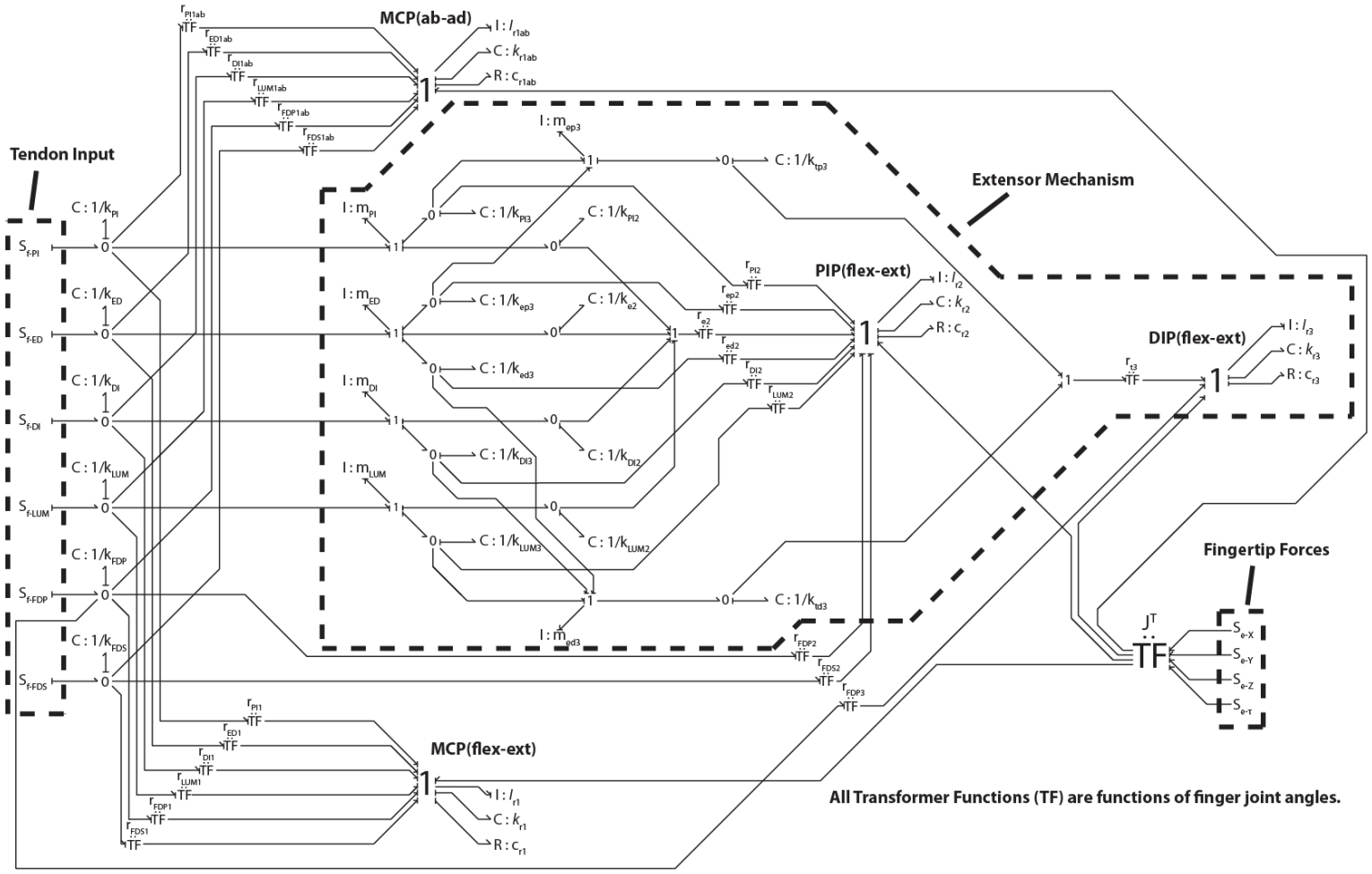

Figure 5.2. The bond graph tendon model of the finger with the addition of fingertip force.

between *in vivo* FDS tendon tension and fingertip force [11]. During the surgery, a force transducer was mounted to the FDS tendon and measured tendon tension, while a single axis load cell measured middle finger fingertip force. The authors in [11] do not directly measure the moment arms of their subjects, but instead presented the average joint thickness of their subjects' middle fingers; which ranged from the 60th to 93rd percentile of data presented in [74, 75]. The result for one of the subjects in the *in vivo* experiment is presented along with the fingertip force vs. FDS tendon force generated using the bond graph tendon model for three different values for FDS moment arm (Figure 5.3). Three different moment arm values are used to match the presented subject's FDS moment arms, estimated from the 60th, 76th, and 93rd percentile data in [74, 75]. Smaller FDS moment arm values result in a steeper

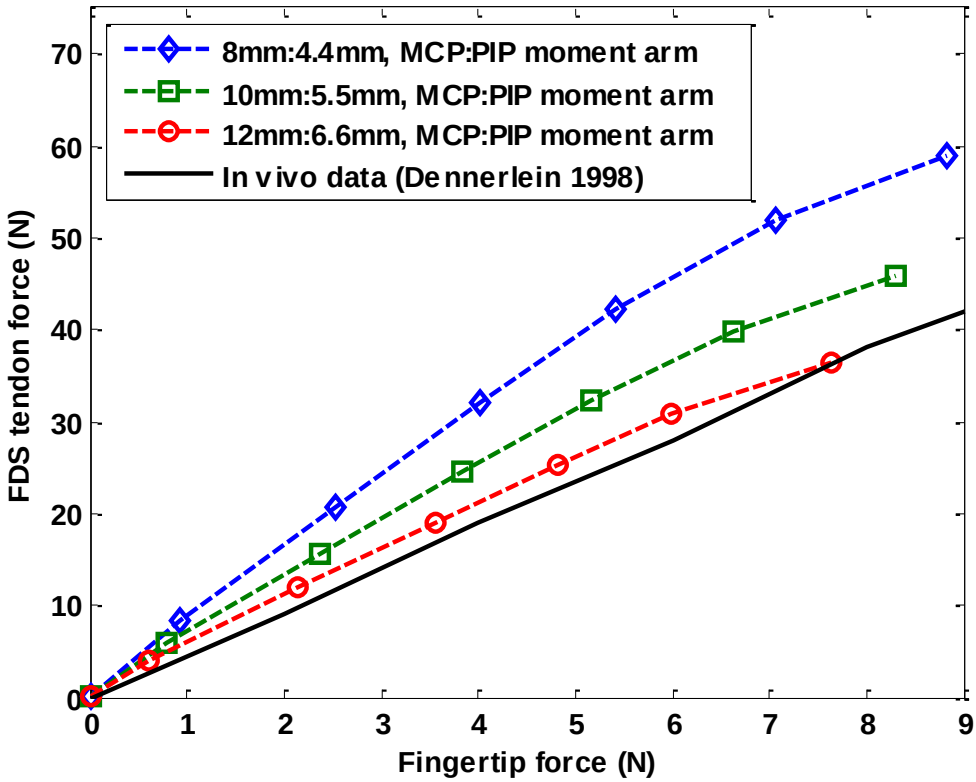

Figure 5.3. The relationship between FDS tendon tension and fingertip force during pinching for different bond graph model FDS moment arms and *in vivo* experimental data.

relationship between FDS tendon tension and fingertip force, whereas larger moment arm values result in a more gradual relationship. The largest FDS moment arm value used in the bond graph tendon model matches closely with the *in vivo* data collected. This result shows the presented bond graph model can accurately represent the *in vivo* FDS tendon tension to fingertip force relationship.

5.3 ACT Index Fingertip Force Experiment Setup

An experiment was designed to compare the fingertip forces of the ACT index finger to the estimated fingertip forces of the bond graph tendon model given the same tendon tensions. The ACT index finger was mounted on a tabletop and the distal phalanx was fixed to a six-axis force/torque transducer (Figure 5.4). The finger was fixed in two different postures during testing: a flexed posture of neutral abduction, 45° flexion at the MCP and PIP joints, and 10° flexion at the DIP joint, and an extended hook posture of neutral abduction, 30° extension at the MCP joint, 95° flexion at the PIP joint, and 10° flexion at the DIP joint. The six-axis force/torque transducer (F/T Nano25 SI-250-6, ATI Industrial Automation, Garner, NC) was mounted to the table and kept stationary during all trials. High tension kite string (WSK Premium Spectra, Windstar Kites of Greater Pittsburgh North, Baden, PA) was used to hang different masses from the tendons. Fingertip forces were measured with a resolution of 0.2 *N* in the Z-direction and 0.05 *N* in the X and Y-directions. For both the single tendon loading and multitendon extensor mechanism loading experiments a computer (Optiplex 990, Dell Inc., Round Rock, TX) with data acquisition hardware/software (NI PCIe-6321, NI SCB-68 and LabView, National Instruments, Austin, TX) recorded the force output from the transducer at 100 Hz.

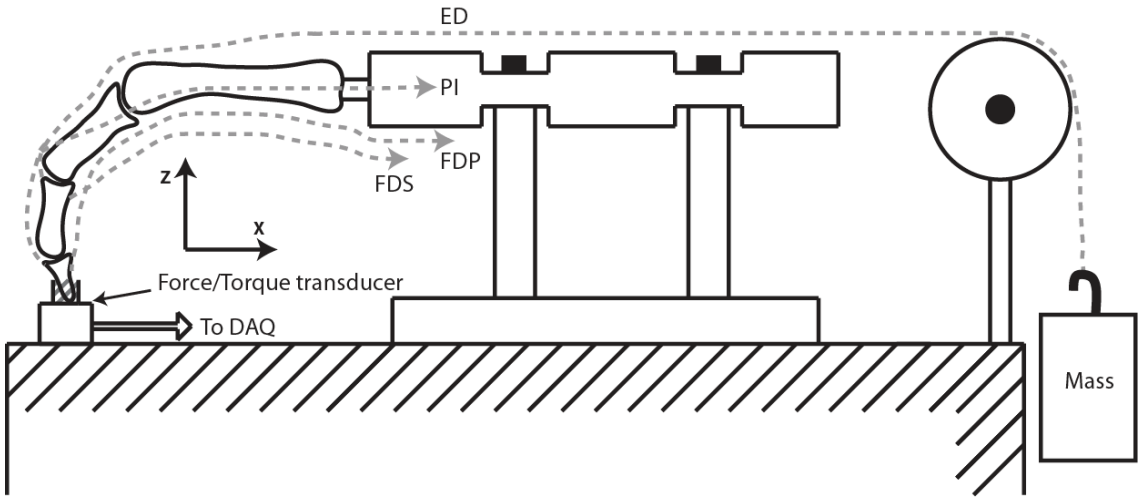

Figure 5.4. Experimental setup for the fingertip force experiments. In this figure the ED tendon is loaded with a mass while the other tendons are disconnected from loading. The maximum mass used in the experiment was 3 kg, as weight above this amount posed possible damage to the ACT index finger.

5.3.1 Single Tendon Loading Experiments

For the single tendon loading experiments, five discrete levels of tendon loading were tested for each individual tendon over three trials in both finger postures. The FDP, FDS, DI, and PI tendons were loaded starting at 1 *kg* and increased to 3 *kg* in increments of 0.5 *kg*. The ED tendon was loaded starting at 1 *kg* and increased to 2.5 *kg* in increments of 0.5 *kg*, and the LUM tendon was loaded starting at 0.2 *kg* and increased to 0.6 *kg* in increments of 0.1 *kg*. The ED and LUM tendons were loaded lighter than the FDP, FDS, DI and PI tendons to reflect their lower maximal muscle output [76]. During loading of a single tendon, all other tendons were disconnected to ensure only the tendon being tested was contributing to fingertip force. The validation for anatomical accuracy between the ACT finger and cadaver data, using this experimental setup, are presented in [72].

5.3.2 Multitendon Extensor Mechanism Loading Experiments

For the multitendon extensor mechanism loading experiments, the ED, DI and PI tendons were loaded at discrete tension levels in both finger postures; three trials were conducted for each different extensor mechanism loading scheme. The ED, DI, and PI tendons were all loaded to 0.5 *kg*, and then each was individually loaded to 1.0 *kg* to represent increased muscle contraction of the different extensor mechanism tendons. It was decided not to include the LUM tendon during the extensor mechanism loading experiments because of its lower maximal muscle output compared to the similarly routed DI tendon. The FDP and FDS were disconnected during this experiment to ensure fingertip force contribution from the extensor mechanism only.

5.4 Fingertip Force Experiment Results

Four sets of experimental data were collected over the single tendon loading and multi-tendon loading experiments. The single tendon loading data are compared to the bond graph tendon model in both flexed and extended hook postures. The multitendon extensor mechanism loading data are also compared to the bond graph tendon model in both flexed and extended hook postures. Analyses of the fingertip force experiments are discussed after the results are presented.

The bond graph tendon model presents good directional agreement with the fingertip forces of the ACT index finger during single tendon loading in flexed and extended hook postures (Figure 5.5, Table 5.1, Table 5.2). The fingertip force vector of the ED tendon in the flexed posture, and the ED and FDP tendons in the extended hook posture, match closely in direction and magnitude between the bond graph tendon model and ACT index finger. The

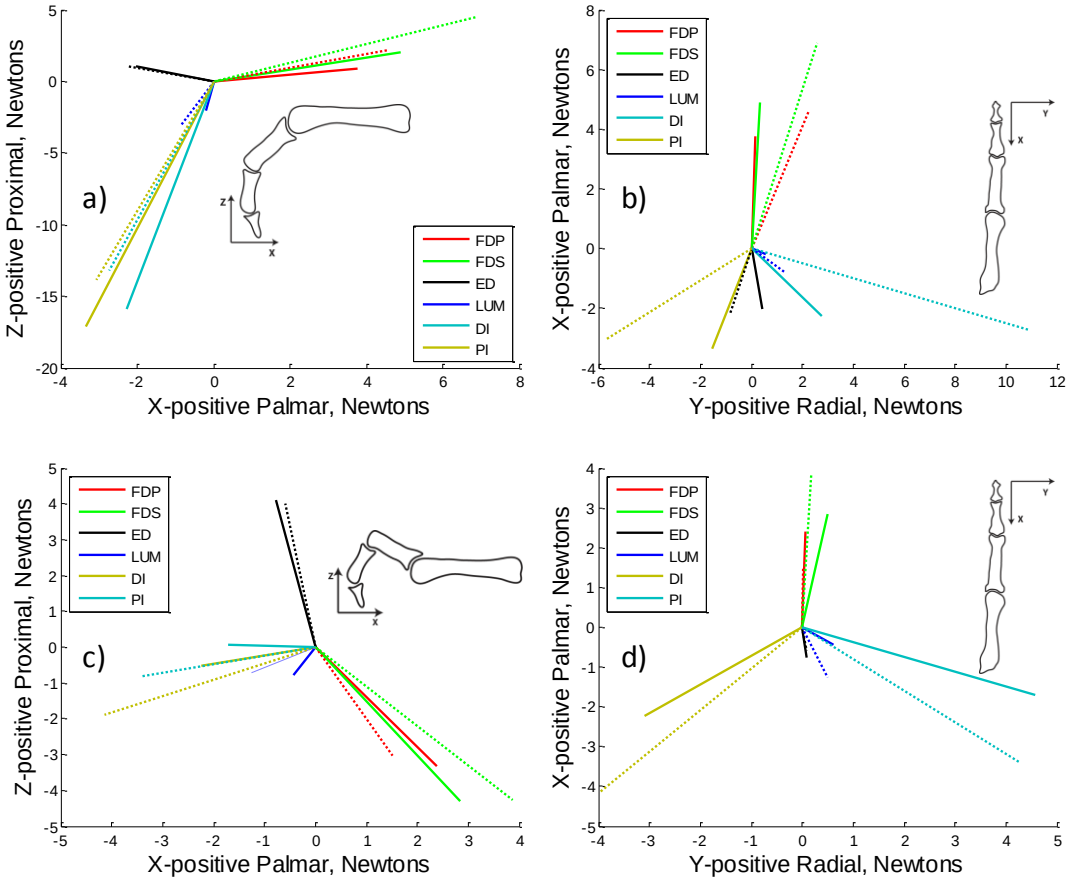

Figure 5.5. The fingertip force vectors for the single tendon loading experiments in the flexed *(a-b)* and extended hook *(c-d)* postures. The solid lines represent the fingertip force vectors of the ACT index finger and the dotted lines represent the bond graph tendon model force vectors. FDP, FDS, DI and PI tendons represent fingertip force values loaded with 3 kg. The ED is loaded with 2.5 kg and the LUM is loaded with 0.6 kg.

Table 5.1 Fingertip force values during single tendon loading for the flexed posture.

Tendon (weight)	**Force, Newton (SD)**					
	ACT finger			**Bond Graph Model**		
	X	***Y***	***Z***	***X***	***Y***	***Z***
FDP (3kg)	3.76 (0.4)	0.16 (0.2)	0.91 (0.8)	4.61	2.28	2.15
FDS (3kg)	4.89 (0.6)	0.36 (0.2)	2.03 (0.9)	6.87	2.58	4.43
ED (2.5kg)	-2.02 (0.4)	0.42 (0.3)	1.03 (0.8)	-2.24	-0.83	1.09
PI (3kg)	-3.34 (0.5)	-1.53 (0.4)	-17.11 (1.7)	-3.06	-5.68	-13.82
DI (3kg)	-2.28 (0.4)	2.79 (0.5)	-15.89 (1.2)	-2.72	10.94	-13.18
LUM (0.6kg)	-0.2 (0.2)	0.57 (0.2)	-2.02 (0.9)	-0.83	1.37	-3.02

Table 5.2 Fingertip force values during single tendon loading for extended hook posture.

Tendon (weight)	**Force, N (SD)**					
	ACT finger			**Bond Graph Model**		
	X	***Y***	***Z***	***X***	***Y***	***Z***
FDP (3kg)	2.39 (0.5)	0.06 (0.3)	-3.31 (0.7)	1.52	0.03	-3.04
FDS (3kg)	2.84 (0.4)	0.50 (0.4)	-4.31 (0.8)	3.88	0.18	-4.27
ED (2.5kg)	-0.77 (0.4)	0.09 (0.2)	4.11 (0.9)	-0.59	0.09	4.02
PI (3kg)	-2.23 (0.4)	-3.09 (0.5)	-0.52 (0.7)	-4.13	-3.97	-1.89
DI (3kg)	-1.71 (0.3)	4.58 (0.5)	0.06 (0.6)	-3.40	4.29	-0.80
LUM (0.6kg)	-0.44 (0.2)	0.62 (0.2)	-0.78 (0.6)	-1.25	0.50	-0.71

force vectors of the FDP, FDS, and LUM in the flexed posture, and the FDS, LUM, DI and PI in the extended hook posture, agree in vector direction but the bond graph tendon model slightly overestimates the magnitude of force when compared to the ACT index finger. The DI and PI fingertip force vectors in the flexed posture match magnitude and direction in the X and Z directions, but have a noticeable difference in vector magnitude and direction in the Y direction (Figure 5.5b). In the flexed posture the average fingertip force direction error between the bond graph tendon model and the ACT index finger is 24.3° in the X-Y direction and 6.2° in the X-Z direction, with an overall fingertip force magnitude error of 42.4%. In the extended hook posture, the average fingertip force direction error is 11.7° in X-Y and 12.2° in X-Z, with an overall fingertip force magnitude error of 22.9%. The bond graph tendon model matches the fingertip force of the ACT index finger closer in the extended hook posture than the flexed posture during single tendon loading experiments.

The bond graph tendon model closely estimates the fingertip force of the ACT index finger during multitendon loading of the extensor mechanism, in both the flexed and extended hook postures. All the fingertip force vectors from the four different ACT index finger tendon loading schemes match closely with the bond graph tendon model (Figure 5.6). In the flexed posture, the average fingertip force direction error between the bond graph tendon model and the ACT index finger is 8.5° in the X-Y direction and 1.5° in the X-Z direction. In extended hook posture, the average fingertip force direction error is 4.9° in the X-Y direction and 2.2° in the X-Z direction. The average fingertip force magnitude error between the bond graph tendon model and the ACT index finger is 8.4% in the flexed posture and 16.8% in the extended hook posture. The fingertip force vectors match more closely between the bond graph tendon model and the ACT index finger during the

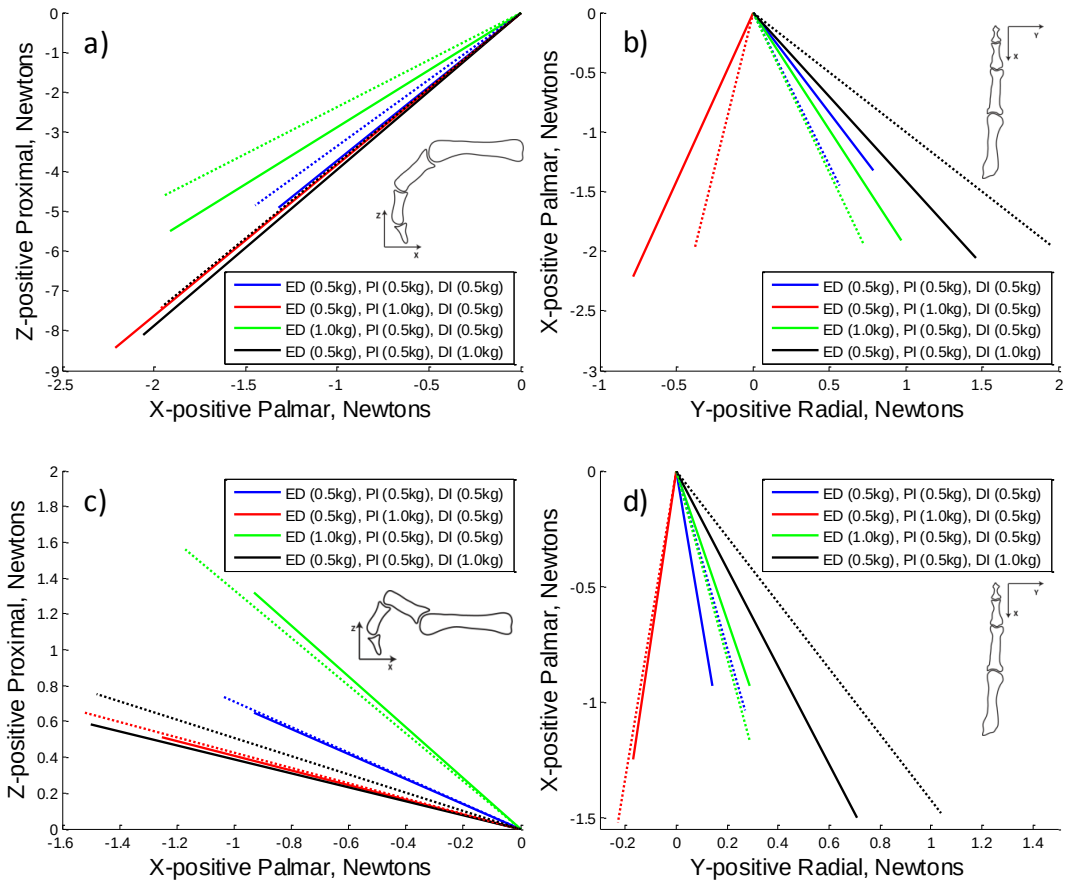

Figure 5.6. The fingertip force vectors for the multitendon extensor mechanism loading experiments, in the flexed *(a-b)* and extended hook *(c-d)* postures. The solid lines represent the fingertip force vector of the ACT index finger and the dotted lines represent the bond graph tendon model.

multitendon extensor mechanism loading experiments than the single tendon loading experiments.

The bond graph tendon model is able to accurately represent the fingertip force of the ACT index finger during tendon loading experiments. These results demonstrate that the bond graph tendon model could accurately represent fingertip force produced by the tendon system of the human finger. Similar to the results of the motion experiments in Chapter 4, two possible limitations lead to notable discrepancies between the bond graph tendon model and the ACT index finger: possible differences in moment arm values between the two systems, and deformation and movement of the extensor mechanism. Limitations of an incomplete joint friction model and unmodeled ACT index finger characteristics do not affect the results of the fingertip force experiments because the ACT index finger's joints did not move during these experiments. The effects of these limitations are presented and discussed along with the analysis of the experimental results below.

Different values of moment arms have been shown to cause the fingertip force to notably change (Figure 5.3). These results demonstrate that the bond graph tendon model is only as accurate as the variable moment arm functions, similar to the motion experiments. It is unknown how much this limitation contributed to the error between the two systems. However, based on the good agreement between the two systems during the motion experiments, it is assumed that only small or negligible differences in moment arm values exist between the two systems. The most likely cause of discrepancy between the two systems is the deformation and movement of the extensor mechanism.

Uneven tension on the extensor mechanism can cause unmodeled deformation and movement of the extensor mechanism; the result of which is most noticeable in the Y-

direction of the single tendon loading in the flexed posture experiment (Figure 5.5b). In the ACT index finger, individual tendon loading of the tendons that make up the extensor mechanism (ED, PI, DI and LUM) can cause it to shift and deform towards the direction of the loaded tendon. This effect is most obvious on the tendons that have larger ab-ad moment arms (PI, DI and LUM), where tension from these tendons deform and shift the extensor mechanism first before being transferred to the fingertip. The deformation and movement of the extensor mechanism is not currently modeled in the bond graph tendon model, since the equations to fully describe the human extensor mechanism's deformation and movement have not been investigated. This deformation and motion may have caused the high average fingertip force direction error of 24.3% in the X-Y direction during single tendon loading in the flexed posture. This analysis is also consistent when considering the improved average fingertip force direction error of 11.7% in the X-Y direction during single tendon loading in the extended hook posture. During experiments involving the extended hook posture, the extensor mechanism is pulled taut because of the large flexion angle of the PIP joint. This pretensions the extensor mechanism and reduces its deformation and movement under uneven tension; this allows more tension from the ED, PI, DI or LUM tendons to transfer directly to the fingertip. The deformation and motion of the extensor mechanism may have also caused the larger overall fingertip force magnitude error in the flexed posture of 42.4%, versus the magnitude error of only 22.9% in the extended hook posture. The effect of extensor mechanism deformation and movement is mostly prevalent in the single tendon loading experiments, since the extensor mechanism is loaded more evenly in the multi-tendon loading experiments and all previous tendon excursion experiments. The incomplete model of the ACT index finger's joint friction and the reduction of ab-ad motion at large

MCP flexion angles in the ACT index finger have negligible effect on the fingertip force experiments because the ACT index finger's joint angles are fixed.

The results from the fingertip force experiments validate that the bond graph tendon model can accurately represent fingertip forces of the complex tendon-based system of the ACT index finger. The bond graph tendon model has been shown to match fingertip force vector directions of the ACT index finger in a flexed posture and fingertip force vector magnitudes and directions in an extended hook posture. This is the second successful validation of the bond graph tendon model through the use of the ACT index finger. This supports the bond graph tendon model as an accurate representation of the human finger tendon system, and is the first tendon model to explore the effects of fingertip contact on the tendon system.

CHAPTER 6

CONCLUSIONS AND FUTURE WORK

This work presents the complex nature of the human hand's tendon system and the challenges of modeling this system. Through the help of previous tendon models, the ACT Hand, and bond graph modeling, important steps toward modeling the complexity of tendon systems have been achieved. This final chapter summarizes the major contributes of this work and provides suggestions on possible extensions and future work.

6.1 Summary of Contributions

The major contributions of this dissertation are:

- A new finger tendon model developed using bond graph modeling

  This bond graph tendon model is the first model to contain all the anatomical tendon characteristics of: six tendons, tendons slacking, tendon interconnectivity, variable moment arms, joint ROM limits, joint stiffness, tendon stiffness, and joint friction. This model is also the first to explore the effects of fingertip contact on the tendon system. The model is flexible to allow inputs of either tendon tension or tendon excursion. The bond graph tendon model uses its anatomical parameters and interconnected tendon system to transfer tendon input into estimations of finger joint angles and motion, and

fingertip force.

- A GUI of the tendon system of the finger for visualizing the tendon model

  A user friendly GUI was presented to visually explore the relationship between tendon input and the resulting finger posture. The main GUI outputs are the final joint angles, tendon tensions, tendon slack values, and 3D position of the moment arms. The tendons and posture of the finger are rendered in a 3D environment and also displayed numerically. All the output values are relative to the user defined initial state.

- Validation of the bond graph tendon model with cadaver and *in vivo* experiments.

  The bond graph tendon model is compared to two *in vivo* experiments and one cadaver study to validate its anatomical accuracy. The tendon model demonstrated the ability to match the *in vivo* data, presented for PIP:DIP coupling and FDS fingertip pinch force. The bond graph tendon model was also able to represent the somatic logic presented in the cadaver study of the extensor mechanism. Though it did not match directly, the model was able to show a change in tension distribution under different loading conditions.

- Validation of the bond graph tendon model with the ACT Hand's index finger during motion experiments.

  The bond graph tendon model's ability to accurately represent human finger motion was explored using the ACT index finger. The ACT index finger represents the most anatomically correct physical system of the human finger and its internal kinematic parameters are more accessible than cadaver or *in vivo*

specimens. Two different experiments were performed to compare the motion of the ACT index finger to the bond graph tendon model. Results show good agreement between the two systems after a joint friction model was added to the bond graph tendon model; this experiment demonstrates the bond graph tendon model's ability to represent the complex tendon system of the ACT index finger.

- Validation of the bond graph tendon model with the ACT Hand's index finger during fingertip force experiments.

  The bond graph tendon model was validated against the ACT index finger for fingertip force production under different tendon loading conditions. This experiment showed close agreement between fingertip force vectors for the two systems in two different finger postures, though one finger posture was shown to match closer between the two systems; this is assumed to be caused by the different pretension on the extensor mechanism. This experiment continued to demonstrate the bond graph tendon model's ability to represent the complex tendon system of the ACT index finger.

6.2 Future Work

The bond graph tendon model presented in this dissertation was shown to match both human and ACT Hand finger experiments. However, there are some important improvements before the tendon model can be considered anatomically accurate, including: the correct routing of the LUM tendon, better modeling of the extensor mechanism, and addition of more fingers. The importance of these improvements and how they would be implemented into the current bond graph tendon model are discussed.

6.2.1 Anatomical Routing of the LUM Tendon

Currently the bond graph tendon model includes the LUM tendon and muscle as a separate tendon not connected to the FDP tendon. In Chapter 2, the LUM was described to have an origin on the FDP tendon and an insertion on the extensor mechanism, the bond graph tendon model does not reflect this anatomical configuration. This discrepancy between the human finger tendon system and the bond graph tendon model was decided upon to allow the model to better match the current ACT index finger and cadaver studies. Since the LUM muscle is attached at both ends to tendons, it is difficult to replicate in a physical system (e.g., the ACT Hand) and cadaver experiments when excursions of the LUM tendon are needed. Detaching the LUM tendon from the origin of the FDP allowed the bond graph to better model the ACT Hand and cadaver experiments, however, to make the bond graph tendon model more anatomically accurate, the origin of the LUM needs to be connected to the FDP tendon.

6.2.2 Improved Modeling of the Extensor Mechanism

The extensor mechanism is one of the unique tendon structures responsible for the dexterity and functionality of the human hand. Previous researchers have explored the different aspects of the extensor mechanism, including identifying the differing tendon stiffnesses in different areas of the extensor mechanism, theorizing different functional aspects, and attempting to design equivalent physical systems [58, 66, 71]. However, a comprehensive model, physical or simulation, has never been created to match the unique capabilities of the extensor mechanism. This makes improving the extensor mechanism of the bond graph tendon model challenging because more work needs to be done on fully

identifying all the functionally of the human extensor mechanism. Future work on improving the extensor mechanism of the ACT index finger to be more anatomically accurate will also help to enhance the extensor mechanism of the bond graph tendon model through future comparison studies.

6.2.3 Multiple Finger Bond Graph Tendon Model

The long-term goal of this project is to create a tendon model of the entire hand system as a way to improve understanding of the human hand's tendon system. To achieve this long-term goal, additional fingers need to be added to the bond graph tendon model to investigate their effects on the system. The extrinsic muscles of the hand all connect to each of the individual fingers (e.g., all the fingers share one FDP muscle); this poses interesting questions about how these interconnections work together. The tendon interconnection between fingers has yet to be explored in the literature. The addition of the thumb to the bond graph tendon model is also part of future work, and will be a new challenge since the thumb has a much different tendon arrangement than the fingers.

A multiple finger bond graph tendon model could be used to better understand the human tendon system and help create exoskeleton hand robotic systems.

6.3 Conclusion

This dissertation has presented and validated a new tendon model, created using bond graph modeling, for accurately representing the kinematics of the human hand's tendon system. The bond graph tendon model is the first model to implement several anatomical characteristics that have not been addressed in previous tendon models. This tendon model

has been shown to accurately represent both human and ACT Hand motion and fingertip forces through a variety of experiments and comparisons. This work also introduces an interactive GUI, powered by the bond graph tendon model, for simulating motion of the human finger.

Modeling the finger tendon system is a complex problem with few advances in the past decade and this work takes important steps towards creating a more anatomically accurate tendon model of the finger. This work will eventually lead to the creation of an anatomically accurate tendon model of the entire hand, which can be use to help create a better understanding of tendon kinematics, future robotic systems and surgical procedures.

APPENDIX A

STATE EQUATIONS OF THE BOND GRAPH

TENDON MODEL

The bond graph tendon model consisted of seventeen tendon springs, four rotation springs, six translations inertias, and four rotational inertias. These means there are 31 state equations for the bond graph tendon model of the single finger. However, because the values of joint angles were of interest, four additional state equations were added to allowed easier identification of joint angles. The following are the state equations:

$$\frac{dF_p}{dt} = K_p * \left(\dot{X}_p - \left(r_{p1}\dot{\theta}_1\right) - \left(r_{p1ab}\dot{\theta}_{1ab}\right) - \left(r_{p2}\dot{\theta}_2\right) - \left(r_{p3}\dot{\theta}_3\right)\right) \quad \text{(A.1)}$$

$$\frac{dF_s}{dt} = K_s * \left(\dot{X}_s - r_{s1}\dot{\theta}_1 - r_{s1ab}\dot{\theta}_{1ab} - r_{s2}\dot{\theta}_2\right) \quad \text{(A.2)}$$

$$\frac{dF_e}{dt} = K_e * \left(\dot{X}_e - \left(r_{e1}\dot{\theta}_1\right) - \left(r_{e1ab}\dot{\theta}_{1ab}\right) - \dot{X}_t\right) \quad \text{(A.3)}$$

$$\frac{dF_{e2}}{dt} = K_{e2} * \left(\dot{X}_t - \left(r_{e2}\dot{\theta}_2\right)\right) \quad \text{(A.4)}$$

$$\frac{dF_{ep3}}{dt} = K_{ep3} * \left(\dot{X}_t - \left(r_{mp2}\dot{\theta}_2\right) - \dot{X}_{ep3}\right) \quad \text{(A.5)}$$

$$\frac{dF_{ed3}}{dt} = K_{ed3} * \left(\dot{X}_t - \left(r_{md2}\dot{\theta}_2\right) - \dot{X}_{ed3}\right) \quad \text{(A.6)}$$

$$\frac{dF_{tp3}}{dt} = K_{tp3} * \left(\dot{X}_{ep3} - \left(r_{t3}\dot{\theta}_3\right)\right) \quad \text{(A.7)}$$

$$\frac{dF_{td3}}{dt} = K_{td3} * \left(\dot{X}_{ed3} - \left(r_{t3}\dot{\theta}_3\right)\right) \quad \text{(A.8)}$$

$$\frac{dF_{ip}}{dt} = K_{ip} * \left(\dot{X}_{ip} - r_{ip1}\dot{\theta}_1 - r_{ip1ab}\dot{\theta}_{1ab} - \dot{X}_{ip23}\right) \quad \text{(A.9)}$$

$$\frac{dF_{ip2}}{dt} = K_{ip2} * \left(\dot{X}_{ip23} - \left(r_{e2}\dot{\theta}_2\right)\right) \quad \text{(A.10)}$$

$$\frac{dF_{ip3}}{dt} = K_{ip3} * \left(\dot{X}_{ip23} - \dot{X}_{ep3} - \left(r_{ip2}\dot{\theta}_2\right)\right) \quad \text{(A.11)}$$

$$\frac{dF_{id}}{dt} = K_{id} * \left(\dot{X}_{id} - r_{id1}\dot{\theta}_1 - \left(r_{id1ab}\dot{\theta}_{1ab}\right) - \dot{X}_{id23}\right) \quad \text{(A.12)}$$

$$\frac{dF_{id2}}{dt} = K_{id2} * \left(\dot{X}_{id23} - \left(r_{e2}\dot{\theta}_2\right)\right) \quad \text{(A.13)}$$

$$\frac{dF_{id3}}{dt} = K_{id3} * \left(\dot{X}_{id23} - \left(r_{id2}\dot{\theta}_2\right) - \dot{X}_{ed3}\right) \quad \text{(A.14)}$$

$$\frac{dF_{L}}{dt} = K_{L} * \left(\dot{X}_{L} - r_{L1}\dot{\theta}_1 - \left(r_{L1ab}\dot{\theta}_{1ab}\right) - \dot{X}_{L23}\right) \quad \text{(A.15)}$$

$$\frac{dF_{L2}}{dt} = K_{L2} * \left(\dot{X}_{L23} - \left(r_{e2}\dot{\theta}_2\right)\right) \quad \text{(A.16)}$$

$$\frac{dF_{L3}}{dt} = K_{L3} * \left(\dot{X}_{L23} - \dot{X}_{ed3} - \left(r_{L2}\dot{\theta}_2\right)\right) \quad \text{(A.17)}$$

$$\frac{d\tau_1}{dt} = K_{r1}\,\dot{\theta}_1 \quad \text{(A.18)}$$

$$\frac{d\tau_{1ab}}{dt} = K_{r1ab}\,\dot{\theta}_{1ab} \quad \text{(A.19)}$$

$$\frac{d\tau_2}{dt} = K_{r2}\,\dot{\theta}_2 \tag{A.20}$$

$$\frac{d\tau_3}{dt} = K_{r3}\,\dot{\theta}_3 \tag{A.21}$$

$$\frac{d\dot{X}_t}{dt} = \frac{1}{m_t}\left(F_e - F_{e2} - F_{ep3} - F_{ed3}\right) \tag{A.22}$$

$$\frac{d\dot{X}_{ip23}}{dt} = \frac{1}{m_{ip23}}\left(F_{ip} - F_{ip2} - F_{ip3}\right) \tag{A.23}$$

$$\frac{dX_{id23}}{dt} = \frac{1}{m_{id23}}\left(F_{id} - F_{id2} - F_{id3}\right) \tag{A.24}$$

$$\frac{d\dot{X}_{L23}}{dt} = \frac{1}{m_{L23}}\left(F_L - F_{L2} - F_{L3}\right) \tag{A.25}$$

$$\frac{d\dot{X}_{ep3}}{dt} = \frac{1}{m_{ep3}}\left(F_{ep3} + F_{ip3} - F_{tp3}\right) \tag{A.26}$$

$$\frac{d\dot{X}_{ed3}}{dt} = \frac{1}{m_{ed3}}\left(F_{ed3} + F_{id3} + F_{L3} - F_{td3}\right) \tag{A.27}$$

$$\frac{d\dot{\theta}_1}{dt} = \frac{1}{I_1}\left(r_{p1}F_p + r_{s1}F_s + r_{e1}F_e + r_{ip1}F_{ip} + r_{id1}F_{id} + r_{L1}F_L - \tau_1 - b_1\dot{\theta}_1\right) \tag{A.28}$$

$$\frac{d\dot{\theta}_{1ab}}{dt} = \frac{1}{I_{1ab}}\left(r_{p1ab}F_p + r_{s1ab}F_s + r_{e1ab}F_e + r_{ip1ab}F_{ip} + r_{id1ab}F_{id} + r_{L1ab}F_L - \tau_{1ab} - b_{1ab}\dot{\theta}_{1ab}\right) \tag{A.29}$$

$$\frac{d\dot{\theta}_2}{dt} = \frac{1}{I_2}\left(r_{p2}F_p + r_{s2}F_s + r_{e2}\left(F_{e2} + F_{ip2} + F_{id2} + F_{L2}\right) + r_{ip2}F_{ip3} + r_{id2}F_{id3} + r_{L2}F_{L3} + r_{md2}F_{ed3} + r_{mp2}F_{ep3} - \tau_2 - b_2\dot{\theta}_2\right) \tag{A.30}$$

$$\frac{d\dot{\theta}_3}{dt} = \frac{1}{I_3}\left(r_{p3}F_p + r_{t3}\left(F_{tp3} + F_{td3}\right) - \tau_3 - b_3\dot{\theta}_3\right) \tag{A.31}$$

$$\frac{d\theta_1}{dt} = \dot{\theta}_1 \tag{A.32}$$

$$\frac{d\theta_{1ab}}{dt} = \dot{\theta}_{1ab} \tag{A.33}$$

$$\frac{d\theta_2}{dt} = \dot{\theta}_2 \tag{A.34}$$

$$\frac{d\theta_3}{dt} = \dot{\theta}_3 \tag{A.35}$$

where F_i is the tension in tendon i, K_i is the stiffness of tendon i, r_{ij} is the moment arm of tendon i at joint j (all are functions of joint angle), θ_j is the joint angle of joint j, $\dot{X}_i$ is the velocity of either flow source i or tendon mass i, m_i is the mass of connection i, I_j is the rotation inertia of joint j, τ_j is the torque at joint j, K_{rj} is the rotational stiffness of joint j, and b_j is the damping at joint j. The terms here match those used in Figure 3.2a, while the values used can be found in the C++ visual basic code.

APPENDIX B

REMAINING MOTION EXPERIMENT RESULTS

The results for all the motion experiments using the ACT index finger were not presented in the main document; they are presented and briefly discussed here for completeness. The following figures include the single tendon motion data for the FDS, LUM and PI trials, and the all the trials for the [FDP, ED, RI] and [FDS, LUM, PI] multitendon experiments. All presented figures are using the bond graph tendon model with friction.

The FDS and LUM single tendon excursion experiments match closely with the motion of the ACT index finger and agree with the FDP, ED, and DI tendons presented in Chapter 4 (Figure B.1). However, the PI tendon diverges significantly in comparison to the other tendons. This divergence is caused by the mechanical difference between the bond graph tendon model and the ACT index finger limitation discussed in Chapter 4. Similar to the FDP tendon, the FDS tendon trials (Figure B.1*a*) have significant noise in the MCP ab-ad ACT index finger data after 6 *s*, this occurs because the motion capture marker of the fingertip is directly below the MCP joint's motion capture marker causing a numerical singularity during joint angle calculation. This motion was not observed during the FDS tendon experiment trials, it is assumed that the MCP ab-ad value remains around 0° for the remainder of these trials.

The [FDS, LUM, PI] and [ED, FDP, DI] multitendon excursion experiments match the

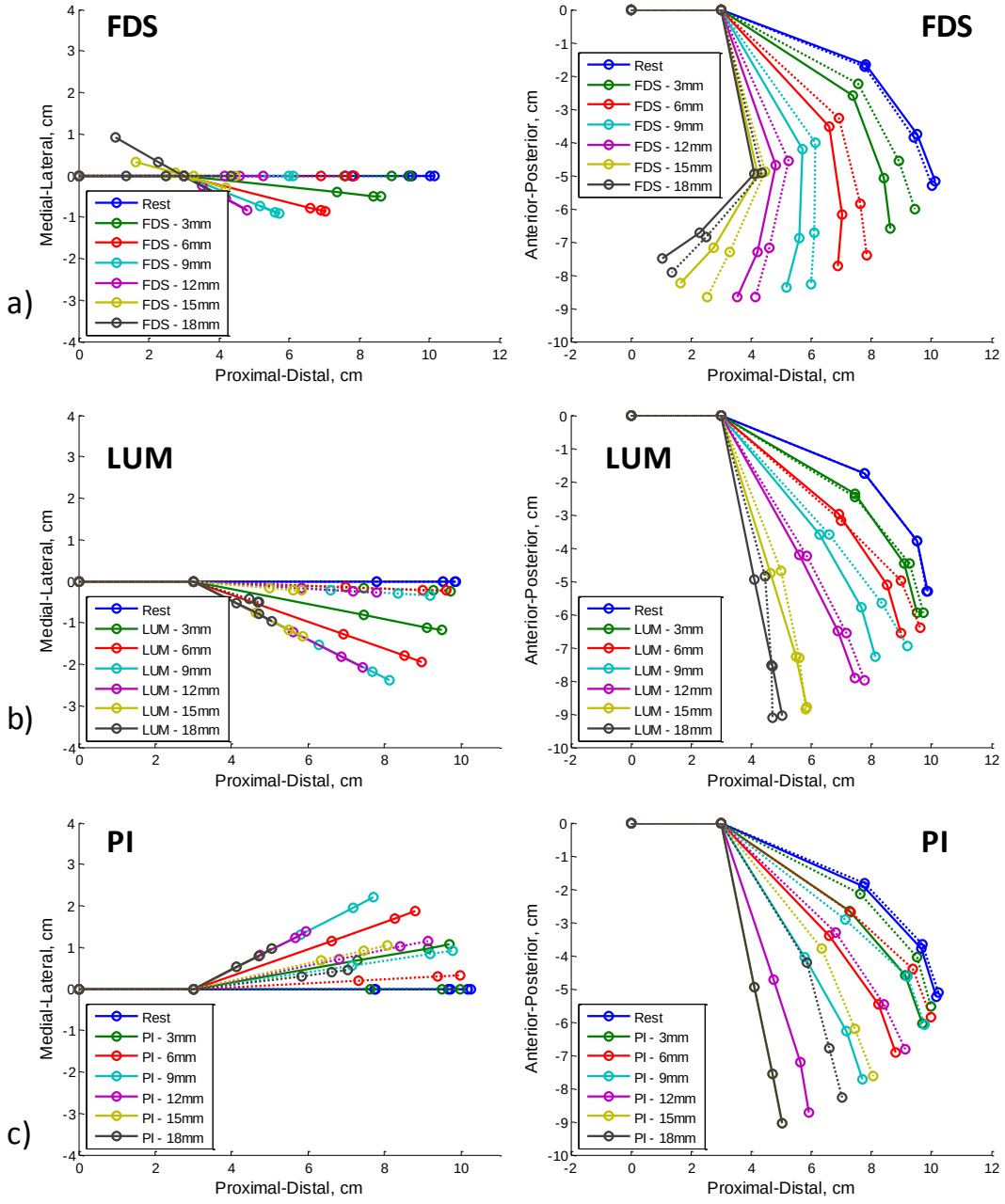

Figure B.1. Results for the single tendon excursion experiments with the bond graph tendon model including friction; *(a)* is the FDS tendon experiment, *(b)* is the LUM tendon experiment, *(c)* is the PI tendon experiment. Lines of the same color represent the same tendon activation, solid lines are the bond graph tendon model and the dotted lines are the ACT index finger.

trends and directions of the ACT index finger (Figure B.2 and Figure B.3). However, similar to the [ED, FDS, PI] multitendon excursion presented in Chapter 4, the errors caused by the inaccurate joint friction model are notable, and in several instances there are large joint angle discrepancies between the bond graph tendon model and the ACT index finger.

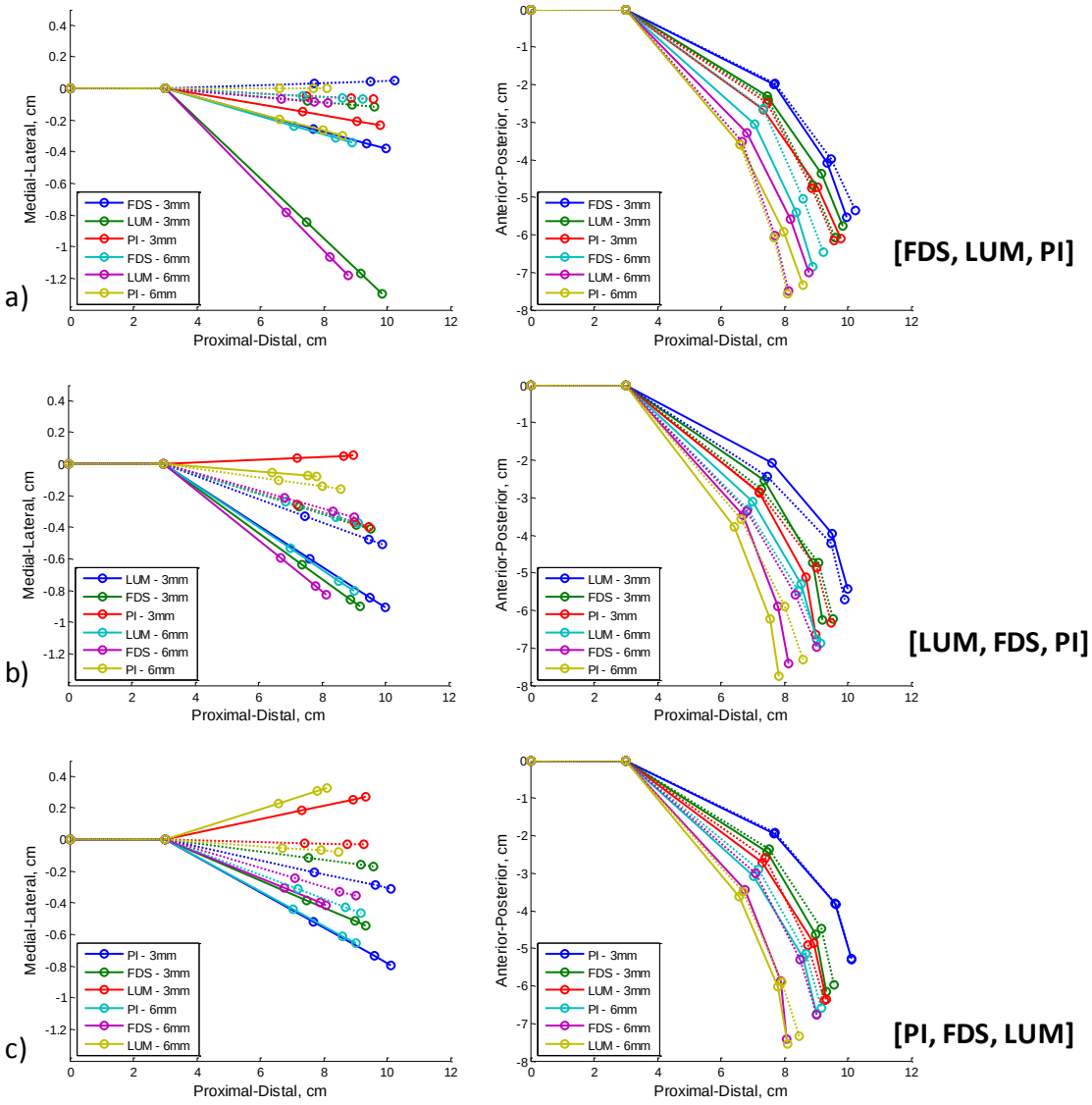

Figure B.2. Results for the [FDS, LUM, PI] multitendon excursion experiments. The tendon activation order for this experiment was: *(a)* - [FDS, LUM, PI], *(b)* - [LUM, FDS, PI], *(c)* - [PI, FDS, LUM]. Lines of the same color represent the same tendon activation, solid lines are the bond graph tendon model and the dotted lines are the ACT index finger.

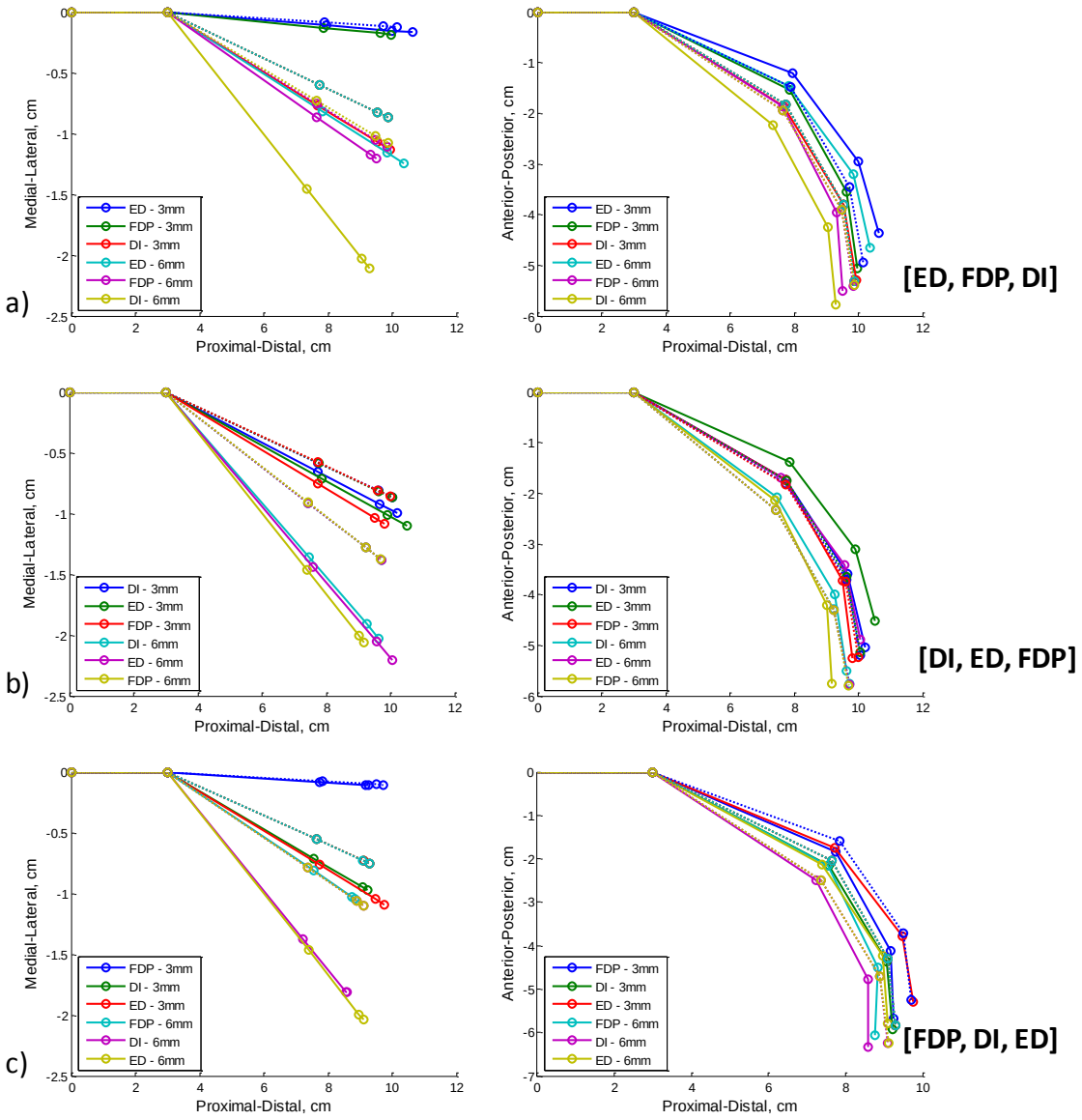

Figure B.3. Results for the [ED, FDP, DI] multitendon excursion experiments. The tendon activation order for this experiment was: *(a)* - [ED, FDP, DI], *(b)* - [DI, ED, FDP], *(c)* - [FDP, DI, ED]. Lines of the same color represent the same tendon activation, solid lines are the bond graph tendon model and the dotted lines are the ACT index finger.

APPENDIX C

DERIVATION EXAMPLE FOR BOND GRAPH TENDON MODEL

This appendix shows the steps for developing a bond graph based on the tendon system of the finger. The first section describes the two energy-conserving junctions used in bond graph modeling in the context of tendon modeling. Next, a bond graph tendon model of the FDP tendon is described. Last, a section on how the interconnections of the ED, LUM, DI, and PI tendons were handled in the extensor mechanism is presented.

C.1 Energy Conserving Junctions

There are two types of energy-conserving junctions used in bond graph models, 0-junctions and 1-junctions. A 0-junction is an energy-conserving junction that has the same effort (tendon tension) value on all its bonds, but different flow values (tendon velocities). In the bond graph tendon model a 0-junction is used to represent a tendon that has the same tendon tension throughout, while also representing the different resulting tendon velocities to other elements of the bond graph; the tendon velocities around a 0-junction must sum to zero. A 1-junction is an energy-conserving junction that has the same flow value on all its bonds, but different effort values. 1-junctions in the bond graph tendon model are used to model both the physical attachments of tendons and the rotational velocity of the joints; the

tendon tension (or joint torques) bonds around a 1-junction must sum to zero in a free-body diagram sense.

C.2 FDP Tendon Bond Graph Model

Starting from the left side of Figure C.1 the FDP bond graph model begins at an energy source; either a flow source (tendon velocity is prescribed) or an effort source (tendon tension is prescribed) can be chosen (for Figure C.1 a flow source is chosen, $S_{f\text{-}FDP}$). The arrows on the bonds of the graph show how the energy flows into and out of the different elements of the bond graph model. The $S_{f\text{-}FDP}$ flow source is the only input to the FDP model and energy from the $S_{f\text{-}FDP}$ flows to the first bond graph junction, which is a 0-junction. For the first 0-junction, the energy from $S_{f\text{-}FDP}$ flows into the 0-junction and then flows out to all the other bonds surrounding the junction. The amount of tendon velocity each bond receives is based on the elements further down the graph; however, the total flow value into a 0-junction always equal the total flow out to satisfy conservation of energy. The first 0-junction represents how the tension in the FDP tendon is the same throughout the tendon, but different values of tendon velocity are distributed to the joints based on the FDP tendon's stiffness and the stiffness of all the joints.

The tendon velocity is split between stretching the FDP tendon and changing the joint angles of the MCP (ab-ad), MCP (flex-ext), PIP and DIP. The amount of tendon velocity that goes to stretching the FDP tendon is based on the stiffness of the tendon (represented by a Capacitance (C) element around the 0-junction); the tendon input cases of Active Pull, Hard Attachment and Hanging Weight allow minimal tendon stretch during system simulation, while the input case of Soft Attachment allows the tendon to stretch and mimic a

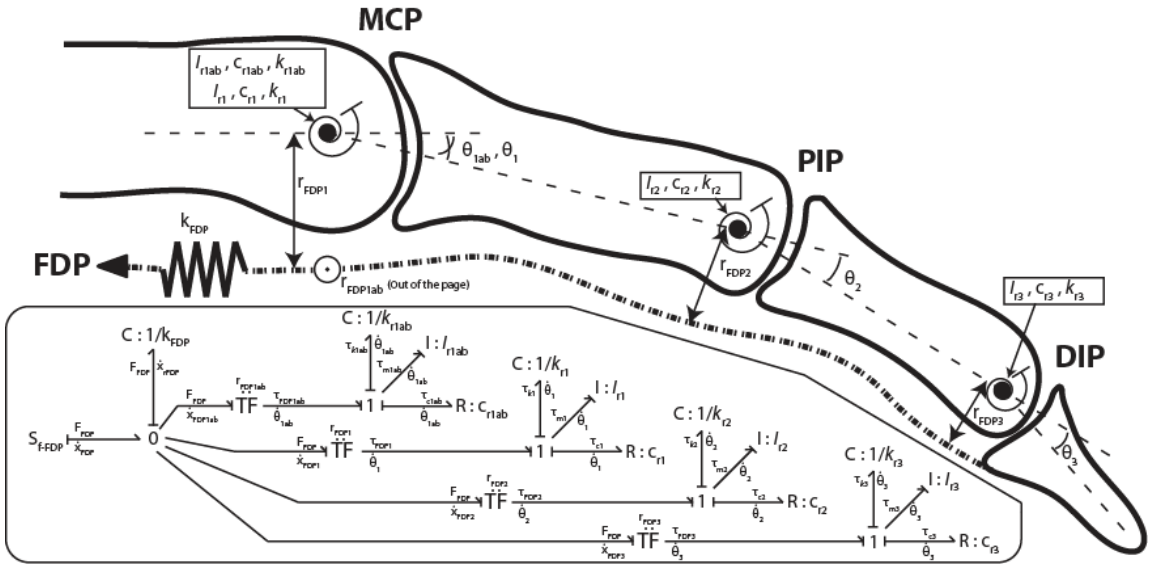

Figure C.1. Bond graph tendon model of the FDP tendon.

passive muscle. The remaining tendon velocity that does not go to stretching the FDP tendon goes on to the finger joints through four separate TF (Transfer Function) elements. In this example, the TF elements convert the linear tendon velocity to rotational joint velocity through the moment arm equations from the ACT finger. Each degree of freedom's rotational velocity then enters a 1-juncition. There are three elements at each 1-junction for all the degrees of freedom: a Capacitance (C) element, a Resistive (R) element and an Inertial (I) element. The C element represents the stiffness of the joint, the R element represents the damping of the joint, and the I element represents the combined inertia of the joint. Changing the values of these elements changes the dynamics of the system. For example, high stiffness values in the PIP joint may cause little to no change in joint angle to the PIP, but instead cause larger changes in the other joints; since the energy from tendon input velocity has to equal the total amount of stretch in the tendon plus the total change in joint angles. All bond graph element values are presented in Chapter 3.

C.3 Extensor Mechanism Tendon Bond Graph Model

The complex connections of the extensor mechanism are reproduced in the bond graph tendon model. Figure C.2 shows a reduced version of the full bond graph tendon model that highlights only the extensor mechanism's tendon interconnections. Based on the bond graph element explanations from the FDP tendon example (S_f, 0-junction, 1-junction, C elements and I elements) the bond graph tendon for the extensor mechanism can be explained more easily. In the extensor mechanism bond graph, every 1-junction is connected to an I element and represents both a tendon interconnection and the inertial mass of that connection. Every 0-junction connected to only a C element represents a tendon between interconnections with the ability stretch based on tendon stiffness. The values used for the I and C elements are presented in Chapter 3.

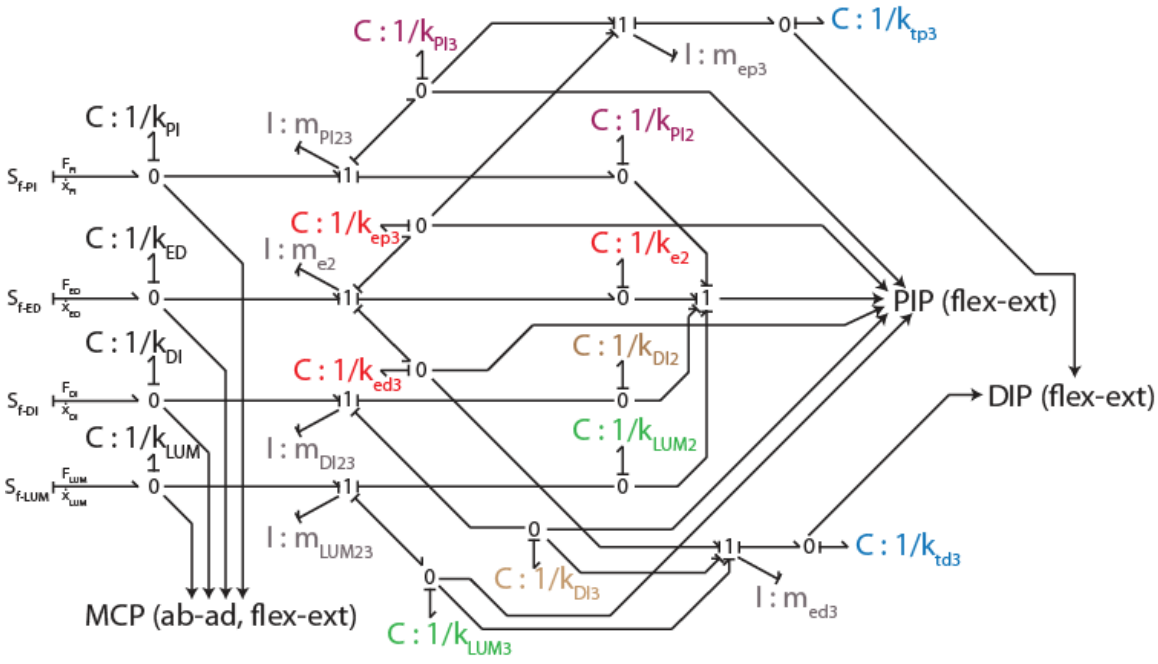

Figure C.2. Bond graph tendon model of the extensor mechanism.

REFERENCES

[1] V. Bundhoo, *et al.*, "A shape memory alloy-based tendon-driven actuation system for biomimetic artificial fingers, part I: design and evaluation," *Robotica,* vol. 27, pp. 131-146, 2009.

[2] A. Chiri, *et al.*, "HANDEXOS: towards an exoskeleton device for the rehabilitation of the hand," presented at the IEEE/RSJ International Conference on Intelligent Robots and Systems, 2009.

[3] A. D. Deshpande, *et al.*, "Mechanisms of the Anatomically Correct Testbed Hand," *Mechatronics, IEEE/ASME Transactions on,* vol. 18, pp. 238-250, 2013.

[4] M. Grebenstein, *et al.*, "The DLR hand arm system," in *Robotics and Automation (ICRA), 2011 IEEE International Conference on*, 2011, pp. 3175-3182.

[5] F. Lotti, *et al.*, "Development of UB Hand 3: early results," in *Robotics and Automation, 2005. ICRA 2005. Proceedings of the 2005 IEEE International Conference on*, 2005, pp. 4488-4493.

[6] J. Yang, *et al.*, "A multi-fingered hand prosthesis," *Mechanism and Machine Theory,* vol. 39, pp. 555-581, 2004.

[7] M. U. Kurse, *et al.*, "Extrapolatable analytical functions for tendon excursions and moment arms from sparse datasets," *Biomedical Engineering, IEEE Transactions on,* vol. 59, pp. 1572-1582, 2012.

[8] J. N. A. L. Leijnse, *et al.*, "Kinematic evaluation of the finger's interphalangeal joints coupling mechanism - variability, flexion-extension differences, triggers, locking swanneck deformities, anthropometric correlations," *J. Biomechanics,* vol. 43, pp. 2381-93, 2010.

[9] J. L. Sancho-Bru, *et al.*, *Towards a Realistic and Self-Contained Biomechanical Model of the Hand, Theorectical Biomechanics,* Dr Vaclav Klika (Ed.), InTech, 2011.

[10] F. J. Valero-Cuevas, "An integrative approach to the biomechancial function and neuromuscular control of fingers," *Journal of Biomechanics,* vol. 38, pp. 673-684, 2005.

[11] J. T. Dennerlein, *et al.*, "Tensions of flexor digitorum superficialis are higher than a current model predicts," *J. Biomechanics,* vol. 31, pp. 295-301, 1998.

[12] A. Esteki and J. M. Mansour, "A dynamic model of the hand with application in functional neuromuscular stimulation," *Annals of Biomedical Engineering,* vol. 25, pp. 440-451, 1997.

[13] J. L. Sancho-Bru, *et al.*, "A 3D biomechanical model of the hand for power grip," *Journal of Biomechanical Engineering,* vol. 125, pp. 78-83, 2003.

[14] S. Sueda, *et al.*, "Musculotendon simulation for hand animation," *ACM Trans. Graph.,* vol. 27, pp. 1-8, 2008.

[15] J. Biggs and K. Horch, "A three-dimensional kinematic model of the human long finer and the muscles that actuate it," *Medical Engineering & Physics,* vol. 21, pp. 625-639, 1999.

[16] N. Brook, *et al.*, "A biomechanical model of index finger dynamics," *Med. Eng. Phys.,* vol. 17, pp. 54-63, 1995.

[17] J. N. A. L. Leijnse, *et al.*, "Biomechanics of the finger with anatomical restrictions - the significance for the exercising hand of the musician," *J. Biomechanics,* vol. 25, pp. 1253-1264, 1992.

[18] J. N. A. L. Leijnse, *et al.*, "The hand of the musician: the kinematics of the bidigital finger system with anatomical restrictions," *J. Biomechanics,* vol. 26, pp. 1169-1179, 1993.

[19] J. N. A. L. Leijnse and J. J. Kalker, "A two-dimensional kinematic model of the lumbrical in the human finger," *Journal of Biomechanics,* vol. 28, pp. 237-249, 1995.

[20] J. L. Sancho-Bru, *et al.*, "A 3-D dynamic model of human finger for studying free movements," *Journal of Biomechanics,* vol. 34, pp. 1491-1500, 2001.

[21] A. Vaz and K. Singh, "A bond graph model for the extensor mechanism of human finger," in *14th National Conference on Machines and Mechanisms*, Durgapur, India, 2009, pp. 139-145.

[22] R. Balasubramanian and Y. Matsuoka, "Biological stiffness control strategies for the Anatomically Correct Testbed (ACT) hand," in *Robotics and Automation, 2008. ICRA 2008. IEEE International Conference on*, 2008, pp. 737-742.

[23] A. D. Deshpande, *et al.*, "Acquiring variable moment arms for index finger using a robotic testbed," *Biomedical Engineering, IEEE Transactions on,* vol. 57, pp. 2034-2044, 2010.

[24] X. Zhe, *et al.*, "Design of an anthropomorphic robotic finger system with biomimetic artificial joints," in *Biomedical Robotics and Biomechatronics (BioRob), 2012 4th IEEE RAS & EMBS International Conference on*, 2012, pp. 568-574.

[25] H. Gray, *Anatomy of the Human Body. 20th ed.* Philadelphia: Lea & Febiger, 1918.

[26] 2014, *Bones of the human hand*. Available: http://en.wikipedia.org/wiki/Hand

[27] F. H. Netter, *Atlas of Human Anatomy, Second Edition.* Teterboro, New Jersey: Icon Learning Systems, 1997.

[28] J. Landsmeer, "The anatomy of the dorsal aponeurosis of the human finger and its functional significance," *Anat Rec.*, vol. 104, pp. 31-44, 1949.

[29] D. Ranney and R. Wells, "Lumbrical muscle function as revealed by a new and physiological approach," *Anat Rec.*, vol. 222, pp. 110-114, 1988.

[30] J. B. Winslow, *Exposition Anatomique de la Structure du corps Humain*. Paris, France: Chez Guillaume Desprez et Jean Desessartz, 1732.

[31] I. Kapandji, *The Physiology of the Joints, Vol. I, Upper Limb*. Edinburg, UK: Churchill Livingstone, 1982.

[32] W. L. Buford, *et al.*, "Analysis of intrinsic-extrinsic muslce function through interactive 3-dimensional kinematic simulation and cadaver studies," *The Journal of Hand Surgery*, vol. 30A, 2005.

[33] J. N. A. L. Leijnse, "Why the lumbrical muscle should not be bigger - a force model of the lumbrical in the unloaded human finger," *J. Biomechanics*, vol. 11/12, 1997.

[34] J. Landsmeer, "Anatomical and functional investigations on the articulation of the human fingers," *Acta anatomica. Supplementum*, vol. 25, pp. 1-69, 1955.

[35] J. Landsmeer, "Studies in the anatomy of articulation. I. The equilibrium of the 'intercalated' bone," *Acta Morphol Neerl Scand.*, vol. 3, pp. 287-303, 1961a.

[36] K. N. An, *et al.*, "Tendon excursion and moment arm of index finger muscles," *J. Biomechanics*, vol. 16, pp. 419-425, 1983.

[37] K. N. An, *et al.*, "Normative model of human hand for biomechanical analysis," *J. Biomechanics*, vol. 12, pp. 775-788, 1979.

[38] A. D. Deshpande, *et al.*, "Understanding variable moment arms for the index finger MCP joints through the ACT hand," in *Biomedical Robotics and*

Biomechatronics, 2008. BioRob 2008. 2nd IEEE RAS & EMBS International Conference on, 2008, pp. 776-782.

[39] D. Thompson and D. Giurintano, "A kinematic model of the flexor tendons of the hand," *J. Biomechanics,* vol. 22, pp. 327-334, 1989.

[40] J. N. A. L. Leijnse, "A graphic analysis of the biomechanics of the massless bi-articular chain. Application to the proximal bi-articular chain of the human finger," *J. Biomechanics,* vol. 29, pp. 355-366, 1996.

[41] J. N. A. L. Leijnse, "The controllability of the unloaded human finger with superficial or deep flexor," *J. Biomechanics,* vol. 30, pp. 1087-1093, 1997a.

[42] J. J. Kutch and F. J. Valero-Cuevas, "Muscle redundancy does not imply robustness to muscle dysfunction," *J. Biomechanics,* vol. 44, pp. 1264-70, 2011.

[43] A. D. Deshpande, *et al.*, "Anatomically correct testbed hand control: muscle and joint control strategies," in *Robotics and Automation, 2009. ICRA '09. IEEE International Conference on*, 2009, pp. 4416-4422.

[44] B. Buchholz, "A kinematic model of the human hand to evaluate its prehensile capabilities," *J. Biomechanics,* vol. 25, pp. 149-162, 1992.

[45] W. L. Buford, *et al.*, "A modelling and simulation system for the human hand," *Journal of Clinical Engineering,* vol. 15, pp. 445-451, 1990.

[46] N. W. William, "The virtual hand: the pulvertaft prize essay for 1996," *J Hand Surg.,* vol. 22, p. 560, 1997.

[47] J. Z. Wu, *et al.*, "A practical biomechanical model of the index finger simulating the kinematics of the muscle/tendon excursions," *Biomedical Materials and Engineering,* vol. 20, pp. 89-97, 2010.

[48] B. Yi, *et al.*, "vHand: a human hand simulation system," in *Proceedings of the 21st International Conference on Computers and Their Applications (CATA 2006),* 2006, pp. 192-199.

[49] F. J. Valero-Cuevas, *et al.*, "Towards a realistic biomechanical model of the thumb: the choice of kinematic description may be more critical than the solution method or the variability/uncertainty of musculoskeletal parameters," *J. Biomechanics,* vol. 36, pp. 1019-1030, 2003.

[50] Y. Kurita, *et al.*, "Biomechanical analysis of subjective pinching effort based on tendon-skeletal model," in *Engineering in Medicine and Biology Society, 2009. EMBC 2009. Annual International Conference of the IEEE*, 2009, pp. 5231-5234.

[51] D. G. Kamper, *et al.*, "Impact of finger posture on mapping from muscle activation to joint torque," *Clincial Biomechanics,* vol. 21, pp. 361-369, 2006.

[52] K. S. Fok and S. M. Chou, "Development of a finger biomechanical model and its considerations," *J. Biomechanics,* vol. 43, pp. 701-713, 2010.

[53] O. A. van Nierop, *et al.*, "A natural human hand model," *The Visual Computer,* vol. 24, pp. 31-44, 2008/01/01 2008.

[54] F. J. Valero-Cuevas, "Applying principles of robotics to understanding the biomechanics, neuromuscular control and clinical rehabilitaion of human digits," in *Proceeings of the 2000 IEEE International Conference on Robotics & Automation*, San Francisco, CA, 2000.

[55] P.-H. Kuo and A. D. Deshpande, "Contribution of passive properties of muscle-tendon units to the metacarpophalangeal joint torque of the index finger," in *Biomedical Robotics and Biomechatronics (BioRob), 2010 3rd IEEE RAS and EMBS International Conference on*, 2010, pp. 288-294.

[56] P. H. Kuo and A. D. Deshpande, "Muscle-tendon units provide limited contributions to the passive stiffness of the index finger metacarpophalangeal joint," *J. Biomechanics,* vol. 45, pp. 2531-8, 2012.

[57] C. N. Maganaris and J. P. Paul, "In vivo human tendon mechanical properties," *Journal of Physiology,* vol. 521, pp. 307-313, 1999.

[58] M. Garcia-Elias, *et al.*, "Extensor mechanism of the fingers. II: tensile properties of components," *J. Hand Surg.*, vol. 16A, pp. 1136-1140, 1991.

[59] S. W. Lee, *et al.*, "Estimation of the effective static moment arms of the tendons in the index finger extensor mechanism," *Journal of Biomechanics,* pp. 1567-1573, 2008.

[60] F. Schuind, *et al.*, "Flexor tendon forces: in vivo measurements," *Journal of Hand Surgery,* vol. 17, pp. 291-298, 1992.

[61] D. C. Karnopp, *et al.*, *System Dynamics: Modeling and Simulation of Mechatronic Systems*. NJ, USA: John Wiley & Sons, Inc., 2006.

[62] R. C. Rosenberg, "Reflections on engineering systems and bond graphs," *Journal of Dynamic Systems, Measurement, and Control,* vol. 115, pp. 242-251, 1993.

[63] P. W. Brand, *et al.*, "Tendon and pulleys at the metacarpophalangeal joint of the finger," *J Bone Joint Surg. Am.*, vol. 57, pp. 779-84, 1975.

[64] D. L. Jindrich, *et al.*, "Finger joint impedance during tapping on a computer keyswitch.," *J. Biomechanics,* vol. 37, pp. 1589-96, 2004.

[65] A. Z. Hajian and R. D. Howe, "Identification of the mechanical impedance at the human finger tip," *J Biomech Eng.*, vol. 119, pp. 109-14, 1997.

[66] F. J. Valero-Cuevas, *et al.*, "The tendon network of the fingers performs anatomical computation at a macroscopic scale," *IEEE Transactions on Biomedical Engineering,* vol. 54, 2007.

[67] E. Zancolli, *Structural and Dynamic Bases of Hand Surgery*, 2nd ed. Philadelphia, PA: Lippincott, 1979.

[68] S. W. Lee, *et al.*, "Effect of finger posture on the tendon force distribution within the finger extensor mechanism," *J Biomech Eng.*, vol. 130, 2008.

[69] F. J. Valero-Cuevas, *et al.*, "Beyond parameter estimation: extending biomechanical modeling by the explicit exploration of model topology," *IEEE Transactions on Biomedical Engineering,* vol. 54, pp. 1951-64, 2007.

[70] M. VandeWeghe, *et al.*, "The ACT hand: design of the skeletal structure," in *Proceedings of the 2004 IEEE International Conference on Robotics and Automation*, 2004.

[71] D. D. Wilkinson, *et al.*, "An extensor mechanism for an anatomical robotic hand," presented at the *Proceedings of 2003 IEEE International Conference on Robotics and Automation*, 2003.

[72] R. J. King, *et al.*, "Validation of fingertip force in the ACT hand index finger and bond graph tendon model," in *IEEE International Conference on Robotics and Automation*, Seattle, WA - In review, 2015.

[73] W. McCulloch and W. Pitts, "A logical calculus of the ideas immanent in nervous activity," *The Bulletin of Mathematical Biophysics,* vol. 5, pp. 115-133, 1943/12/01 1943.

[74] J. W. Garrett, "Anthropometry of the hands of female air force flight personnel (Report AMRL-TR-69=26)," ed. Wright-Patterson Air Force Base, OH: Aerospace Medical Research Laboratory, Aerospace Medical Division, Air Force Systems Command, 1970a.

[75] J. W. Garrett, "Anthropometry of the hands of male air force flight personnal (Report AMRL-TR-69-42)," ed. Wright-Patterson Air Force Base, OH: Aerospace Medical Research Laboratory, Aerospace Medical Division, Air Force Systems Command, 1970b.

[76] F. J. Valero-Cuevas, *et al.*, "Quantification of fingertip force reduction in the forefinger following simulated paralysis of extensor and intrinsic muscles," *J Biomech*, vol. 33, pp. 1601-9, 2000.